THE UNIVERSITY OF QUEENSLAND

AUSTRALIA

Highly functional green materials platform:

Starch-ionic liquid-carbon nanotube polymer melt nanocomposites

Zhixue Liu

Bachelor of Material Engineering

A thesis submitted for the degree of Doctor of Philosophy at

The University of Queensland in 2016

School of Chemical Engineering

ABSTRACT

Starch is a promising biodegradable polymer material which has attracted attention recently. A renewable and biodegradable resource can potentially address the shortage of conventional petroleum-based polymers and help solve the problem of environmental pollution from the use of these polymers. To use starch in polymer processing, gelatinisation, which is the process to disrupt the native starch structure, must happen to turn the starch in to an amorphous thermoplastic starch (TPS). However, water, the conventional gelatinisation agent and plasticiser, is extremely volatile and will evaporate during thermal processing. This leads to high melt viscosities, processing difficulties and hence poor product quality. In addition the mechanical properties of the resulting TPS products are not as high as that of the currently used petroleum-based polymers that they seek to replace.

Therefore, potential solutions for TPS processing and application development is to use other plasticisers to aid processing and/or to reinforce TPS with nano-particles. One of the key tasks of this project was to understand the plasticizing effects of ionic liquids (ILs) in TPS processing and interpreting these in terms of the molecular interactions between the components. In addition the role of adding nano-particles, in the form of carbon nanotubes, in an attempt to strengthen TPS was investigated. The ultimate aim was to provide design guidelines to produce high value added biodegradable nanocomposites.

Three types of ionic liquids (ILs) were considered: 1-ethyl-3-methylimidazolium acetate ([Emim][OAc]), 1-allyl-3-methylimidazolium chloride ([Amim]Cl) and 1-butyl-3-methylimidazolium chloride ([Bmim]Cl). They were processed in batches of 150g by thermal mixing. Their behaviours were compared to glycerol as plasticisers of TPS, and their effects on TPS processing, water uptake during conditioning, mechanical properties, thermal stabilities, crystallisation behaviour and molecular interaction were studied. Both spectroscopic and X-ray analysis techniques were used to investigate the interactions that occurred, and these were related to the material characteristics. Then, multi-walled carbon nanotubes (MWCNTs) were introduced to the TPS matrix to investigate their behaviour as a strengthening agent and also to potentially create a functional material with useful electrical properties.

The results demonstrated that the ILs were effective plasticisers for TPS. However, whilst their use improved the flexibility of TPS, mechanical strength and thermal stability were decreased. The molecular interactions between TPS and ILs were found to differ between TPS and glycerol. This led to differences in the crystalline structures formed, 2% to 4% more water

uptake during conditioning and hence up to a 90% decrease in Young's modulus. In particular the effect of water uptake during conditioning was identified as the key contributor to the ultimate mechanical properties. The IL plasticised TPS were also found to be less thermally stable.

In order to improve these poorer mechanical properties, the introduction of MWCNTs was investigated. Whilst it was possible to introduce MWCNTs to the TPS matrix, the loading achieved was not sufficient to make a significant effect on the material and electrical properties. Experiment results have shown that the CNTs did however have an effect on the crystallisation behaviour, resulting in a reduction of the differences observed between different ILs.

Overall, this fundamental study on starch/ILs/carbon nanotubes composites has provided a better understanding of the interaction mechanisms and their impacts on material properties. This knowledge can be a guide and applied to further optimizing studies of starch/ILs/carbon nanotubes composites and eventually industrial applications in the future.

Declaration by author

This thesis is composed of my original work, and contains no material previously published or written by another person except where due reference has been made in the text. I have clearly stated the contribution by others to jointly-authored works that I have included in my thesis.

I have clearly stated the contribution of others to my thesis as a whole, including statistical assistance, survey design, data analysis, significant technical procedures, professional editorial advice, and any other original research work used or reported in my thesis. The content of my thesis is the result of work I have carried out since the commencement of my research higher degree candidature and does not include a substantial part of work that has been submitted to qualify for the award of any other degree or diploma in any university or other tertiary institution. I have clearly stated which parts of my thesis, if any, have been submitted to qualify for another award.

I acknowledge that an electronic copy of my thesis must be lodged with the University Library and, subject to the policy and procedures of The University of Queensland, the thesis be made available for research and study in accordance with the Copyright Act 1968 unless a period of embargo has been approved by the Dean of the Graduate School.

I acknowledge that copyright of all material contained in my thesis resides with the copyright holder(s) of that material. Where appropriate I have obtained copyright permission from the copyright holder to reproduce material in this thesis.

Publications during candidature

No publications

Publications included in this thesis

No publications included

Contributions by others to the thesis

Chapter 4 Regular maize starch mixing, water uptake measurement and tensile testing were partly assisted by Jonathan Nair who was an undergraduate project student working under my supervision.

Chapter 4 & Chapter 5 Regular maize starch mixing data recording was performed by A/Prof. Rowan Truss during his visit to the University of Warwick. Part of the samples used for these chapters was also supported by his work.

Chapter 5 Tensile testing and water uptake measurement were carried out by Meiling Mo who was an undergraduate project student working under my supervision.

All the XRD and TEM results were obtained by Centre for Microscopy and Microanalysis at the University of Queensland.

The original experimental idea, editing and reviewing of this thesis were contributed by Dr. Timothy Nicholson, Prof. Peter Halley and Dr. Fengwei Xie.

Statement of parts of the thesis submitted to qualify for the award of another degree

None

Acknowledgements

Words cannot express how much I appreciate everything I have encountered in these 4 years. This has been the most inspiring, interesting, thought provoking life experience which is completely different from my previous experience.

First of all, I would like to sincerely acknowledge my principle advisor Dr. Timothy Nicholson who offered me such a life-changing opportunity. From his critical thinking and rigorousness in science, I can eventually learn and understand the meaning of scientific spirit. Also, I am truly appreciative of his supportive attitude and action during these 4 years which helped me a lot in scientific research and academic issues.

My academic works would have not been performed well without a supportive research group. Hence, hereby I must thank my co-advisors Prof. Peter Halley, Dr. Fengwei Xie and A/Prof. Rowan Truss for helping me to improve my research plans and details all the way. Also I would like show appreciations to my colleagues who also are my dear friends, David Konigsberg, Enrico Hadde, Donna Capararo, Cindy September, Aarti Tobin and Sainimili Mateyawa. They were not only extremely supportive to my daily work, even very trivial, but also have introduced me to this very different multi-cultural society which is an absolutely beauty. In the meanwhile, I am appreciated for all the help given by every staff in the laboratories as well.

I thank Prof. Tony McNally very much for supporting my work and study during my visit to the University of Warwick in 2015. Thanks to his generosity in sharing his abundant knowledge of polymer nano-composites, I have been greatly inspired. Specifically, I would like to thank Mulan Mu who assisted me a lot in experimental issues.

In terms of the financial support, I represent my appreciation to the Chinese Guangzhou city government who offered me living allowance scholarship, the University of Queensland who offered me full tuition fee scholarship and 3M Australia who provides me extra living allowance scholarship as well as an internship opportunity in 3M Singapore.

Finally, I would like to thank my parents for supporting me all the way, my previous teachers and friends who support me and all the friends I have encountered in Australia. Especially, I thank my precious friend Paul Ivory who keeps improving my English speaking skills and expanding my knowledge in other subjects and his family, as well as my housemate Neil Ross who helped me significantly during my stay.

Keywords

Starch, glycerol, ionic liquids, carbon nanotubes, nano-composites, processing

Australian and New Zealand Standard Research Classifications (ANZSRC)

091209 Polymers and Plastics (100%)

Fields of Research (FoR) Classification

0912 Materials Engineering (100%)

TABLE OF CONTENTS

LIST OF TABLES

LIST OF FIGURES

NOMENCLATURE

[Amim]Cl	1-allyl-3-methylimidazolium chloride
[Bmim]Cl	1-butyl-3-methylimidazolium chloride
[Bmim][OAc]	1-butyl-3-methylimidazolium acetate
[Bmim]PF_6	1-butyl-3-methylimidazolium hexafluorophosphate
CNTs	carbon nanotubes
DSC	differential scanning calorimetry
[Emim][OAc]	1-ethyl-3-methylimidazolium acetate
FTIR	Fourier-transformed infrared
HDPE	high density polyethylene
[Hmim]PF_6	1-hexyl-3-methylimidazolium hexafluorophosphate
ILs	ionic liquids
MWCNTs	multi-walled carbon nanotubes
PMMA	poly(methyl methacrylate)
PP	polypropylene
PS	polystyrene
PVC	polyvinyl chloride
RH	relative humidity
RMS	regular maize starch
RMS-A	RMS samples plasticized by [Amim]Cl
RMS-B	RMS samples plasticized by [Bmim]Cl
RMS-CNT	RMS samples with added CNTs
RMS-E	RMS samples plasticized by [Emim][OAc]
RMS-G	RMS samples plasticized by glycerol
SWCNTs	single-wall carbon nanotubes
TEM	transmission electron microscopy
T_g	glass transition temperature
TGA	thermal gravimetric analysis
TPS	thermoplastic starch
XRD	X-ray diffraction

1 INTRODUCTION

1.1 Project Background

Starch is widely known as a biodegradable polymer material which has the potential to be used in place of conventional plastics. Though petrochemical-based polymers have brought us great convenience in last over 100 years, the resulting non-biodegradable plastic waste has a profoundly adverse effect on the environment. For example, marine ecosystems are severely threatened by the pollution of non-biodegradable plastic waste (Jambeck et al., 2015, Chris et al., 2015). Furthermore, with an increasing shortage of petroleum, conventional plastics will become scarce as well. It is, thus, an urgent undertaking to develop plastics from renewable sources. Starch polymers are an advantageous alternative as they are low cost with biodegradable properties. Contained in an array of staple foods, starch is a renewable resource, and can hence be regarded as "green": renewable, recyclable, and biodegradable. However, the characteristics of starch-based polymers, particularly the mechanical properties and thermal stability, are not as suitable as their petrochemical-based counterparts in many applications. In order to enhance the starch properties, composites have been explored. In particular, the use of nano-materials such as nanoclays have been demonstrated to be effective (Sadegh-Hassani and Mohammadi Nafchi, 2014). Therefore, developing nano-composites has the potential to expand the application of these green materials and make them promising alternatives to conventional plastics.

Starch processing raises issues that are not present in conventional plastics due to the biological multi-scale structure of starch granules. Starch granules are complicated structures consisting of both amorphous regions and crystalline regions. Both of these regions contain amylose and amylopectin, which have linear and branched microstructures respectively, and so the processing characteristics will vary as the ratios between amylose and amylopectin changes, since molecular interactions and steric effects have an influence on their properties. The consequence of these interactions are difficulties in processing, as the processing temperature for raw starch is higher than the material degradation temperature.

Gelatinisation is one of the most fundamental factors in starch processing. It is a process that involves disordering the natural crystalline structure of starch granules, and turning them into an amorphous-state polymer known as thermoplastic starch (TPS). To enable such a process, plasticisers which can lower the processing temperature and affect the final material properties

need to be added in as gelatinisation agents, which disrupt the starch granules. However, the most common plasticiser used, water, gives rise to problems due to its volatility, which results in unstable processing and inhomogeneous outcomes. So a better gelatinisation agent, which can also act as a plasticiser, is needed. Glycerol has been used as it does not readily evaporate during starch processing. Its use, however, gives rise to some other problems such as an increase in the gelatinisation temperature compared to water, and hence the potential for low processing efficiency. Therefore, there is a need to find alternative gelatinisation agents which are also non-volatile and effective plasticisers. Recently there has been an interest in the use of Ionic Liquids (ILs) for this purpose. For example, 1-ethyl-3-methylimidazolium acetate ([Emim][OAc]) has been suggested because of its strong interaction potential and non-toxic nature (Mateyawa et al., 2013).

A review has shown that TPS generally has a tensile strength of less than 22 MPa which has limited its applications (Zhang et al., 2014). Generally, the Young's modulus of starch is lower than 50% of the value of PP (polypropylene) or PS (polystyrene). Hence, exploring means of improving mechanical properties is considered significant to the increased application of TPS.

Nano-materials such as phyllosilicates, polysaccharide nanofillers and carbonaceous nanofillers have been investigated as TPS strengthening materials previously (Xie et al., 2013). These generally show improvement in some of their properties such as mechanical properties, thermal stability and moisture resistance. For example, it has been found that by using MWCNTs, the T_g of TPS formed from pea starch increased from 16.5 to 25.3°C, ultimate tensile strength increased from 2.85 MPa to 4.73 MPa, Young's modulus increased from 20.7 MPa to 39.2 MPa and moisture uptake decreased from 65% to 56% at 98% relative humidity (Cao et al., 2007). Carbon nanotubes (CNTs) have the potential to be very effective as a strengthening material due to their high physical properties and unique microstructures (Hussain et al., 2006, Xie et al., 2013).

In addition, the highly conductive nature of CNTs and metallic to semiconductor electrical conductivity of ILs might together enhance the electrical conductivity of TPS/IL/CNT composite materials. Such a characteristic might enable the TPS/ILs/CNTs nano-composites to be a cheap, biodegradable and conductive or semi-conductive material that can be used in sensors, for example. Thus, the creation of a nano-composite material can broaden the use of TPS from an engineering material to functional material.

1.2 Thesis Outline

The overall objective of this project is to give a clear understanding of starch-based nanocomposite processing and enable development of novel high performance green polymers which could be applied in high value added fields like aerospace, engineering structure material, sports equipment, etc.

The key aim of this study is to understand the material processing and characterisation of TPS systems plasticised with ILs, both with and without using CNTs as strengthening agents. In particular the thesis focuses on the molecular interactions between different components and thus their effects on material characteristics such as crystallinity, thermal stability and mechanical properties.

In this project, the basic interaction between TPS and ILs was initially investigated. Regular maize starch (RMS) was used because this generally has approximately 26-28% amylose content which makes it easier to process compared to higher amylose content starches (Li et al., 2011). Then in the following study, CNTs were introduced into the matrix. Subsequently, these results will provide a framework that can be applied to other maize starches with different amylose content.

The properties of the starch during and after processing have been investigated by a wide variety of techniques. Tensile testing has been applied to obtain Young's modulus, tensile strength and elongation at break. X-Ray Diffraction (XRD) as well as transmission electron microscopy (TEM) have been utilised to study the crystal structure and morphology of starch and the dispersion of CNTs in the matrix. Fourier-transformed Infrared (FTIR) and Raman spectroscopy have been used to characterize the molecular interactions between starch/plasticisers/CNTs.

1.2.1 Thesis Objectives

The key objectives in this project are as follows:

1. To study and understand the molecular interaction mechanism of an IL (1-ethyl-3-methylimidazolium acetate, [Emim][OAc]) plasticized RMS and to reveal its influences on RMS processing and material properties by comparing to glycerol (Chapter 4).

2. To investigate the molecular interaction and crystallisation behaviour of plasticized RMS, thus understand and compare the plasticizing effects of two further ILs 1-Allyl-3-methylimidazolium chloride ([Amim]Cl) and 1-Butyl-3-methylimidazolium chloride ([Bmim]Cl) on RMS processing and material properties. This will lead to guidelines for choosing an appropriate IL (Chapter 5).

3. To investigate the molecular interaction and crystallisation behaviour of glycerol/IL plasticized TPS material with added CNTs and hence understand the mechanisms that underlie the changes in TPS mechanical properties caused by this addition (Chapter 6). Also, to investigate the electrical conductivity of TPS/CNT nanocomposites and understand the relevant factors which affect the electrical conductivity of these materials. (Chapter 7)

By achieving these objectives, a clear understanding of the molecular interaction mechanism between different ingredients can be obtained. Hence, factors which are relevant to material properties variation can be identified, and hence provide fundamental knowledge which could be applied to guide material properties optimisation in the future.

2 LITERATURE REVIEW

This literature review explores the natural structure of starch and the mechanism of TPS processing. Fundamental knowledge of ILs and CNTs, their applications to TPS processing and research trend seen in others studies are also reviewed.

2.1 Starch Structure

Starch commonly exists in various types of botanical products such as cereal, legumes and tubers (table 2-1) (Avérous, 2004). Native starch granules can be isolated from these resources with dimensions from 0.5μm to 175μm (Eliasson, 2004). These have a complex concentric three dimensional structure (figure 2-1) with both amorphous and crystalline regions (Xie et al., 2013). Chemically, starch is a polysaccharide consisting of D-glucose units, referred to as homoglucan or glucopyranose. Starch is composed of two macromolecules, amylose and amylopectin.

Table 2-1 Amylose content of different types of starches

Starches	Amylose content (%)	Reference
Long-grain rice	27.2±0.3	(Chung et al., 2011)
Arborio rice	18.8±0.1	
Calrose rice	15.4±0.9	
Glutinous rice	4.2±0.1	
Waxy maize	<0.5	(Buckow et al., 2009)
Regular maize	26	
Gelose 50	50	
Gelose 80	80	

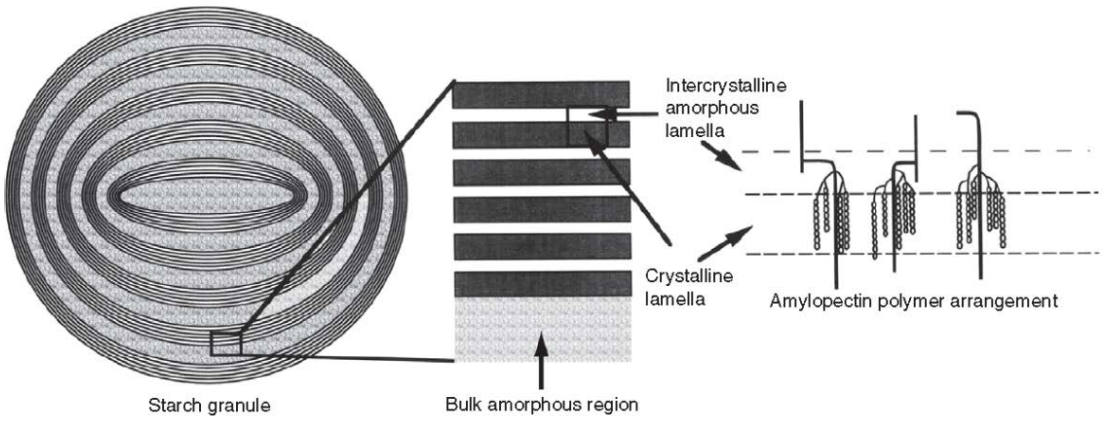

Figure 2-1 Schematic diagram of starch granule structure (Ratnayake and Jackson, 2008)

Amylose is a helical and linear or sparsely branched carbohydrate based mainly on α-1,4 bonds, with a molecular weight of 10^5-10^6 g mol^{-1}. In contrast, amylopectin is a highly branched

polymer with a higher molecular weight of 10^7-10^9 g mol^{-1}. Amylopectin is based on α-1,4 (approximately 95%), with α-1,6 (about 5%) links constituting branching points appearing every 22-70 glucose units (Pérez et al., 2009, Moates et al., 2001). Depending on the source, amylose content of starch can vary from <1% to 83% (Tan et al., 2007).Increasing the proportion of amylose, being a more linear polymer, has will increase the crystallinity of starch. This will further impact on characteristics of starch such as mechanical and rheological properties (Liu et al., 2010, Lourdin et al., 1995) and will be discussed below in section 2.2.4. Starch is a hydrophilic material. Raw starch has an equilibrium moisture percentage of 10%-18% under ambient conditions depending on the species of origin (Zhang et al., 2014). This moisture percentage changes according to the fluctuation of the relative humidity (RH) of the atmosphere where it is stored (Tester et al., 2004). Raw starch granules are insoluble in cold water. However, when starch is heated in water, starch granules will swell and transform into an amorphous polymer (Fang et al., 2004). This phenomenon is known as "gelatinisation", which will be further discussed in 2.2.1.

Native starch granules are biosynthetically assembled as semicrystalline structures which consist of amorphous and crystalline regions. Both amylose chains and the most external branches of amylopectin can form double helices and crystallites within the native starch granules (Hizukuri, 1986, Tester et al., 2004). X-ray diffraction (XRD) indicates that three crystal patterns exist in native starch granules, namely A, B and C-types. In an A-type crystal lattice, the double helices are closely packed in a left-handed, parallel stranded pattern forming a monoclinic unit-cell (figure 2-2). Whereas in B-type crystal pattern, the double helices pack in the same pattern as A-type, but form a hexagonal unit cell with two helices per cell, allowing an open space that is filled with water molecules (Imberty et al., 1991, Imberty et al., 1987, Imberty et al., 1988, Imberty and Perez, 1988). The C-type crystal pattern is an intermediate structure between A and B-types. A further type of crystal polymorph, induced by processing, namely the V-type, has been described to arise from single amylose helices, in contrast to the double helical nature of the A and B-type crystal structures (Lopez-Rubio et al., 2008). Compared to the double helical A and B-type lattices, the V-type lattice has a relatively large cavity, which is able to contain small molecules like iodine or fatty acids (Averous and Halley, 2009). This type of structure is formed by the crystallisation of amylose. The organisation of the crystal lattice and the abundance of the various single helical crystal structures is dependent on processing conditions such as shear, temperature and composition. Due to the high

temperatures and high shear conditions, single helical structures can crystallize rapidly on cooling (van Soest et al., 1996a, van Soest et al., 1996b).

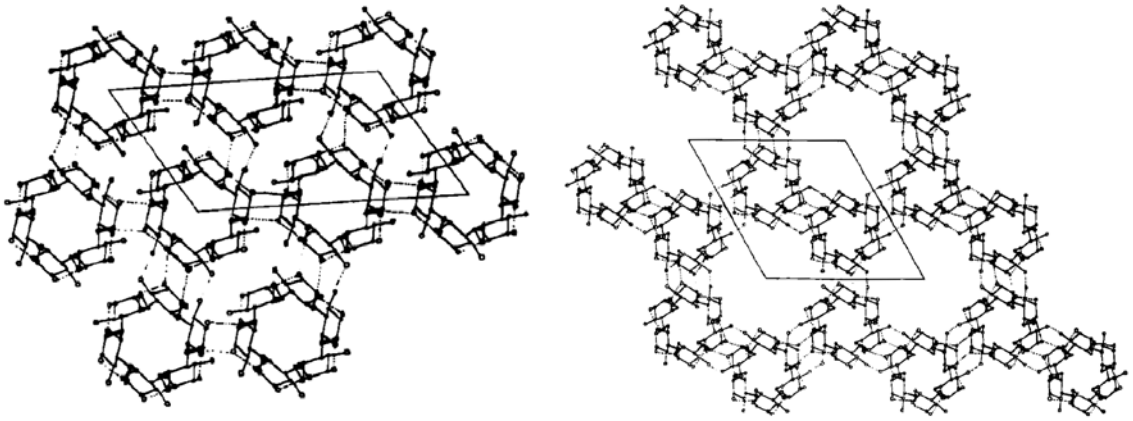

Figure 2-2 Molecular model of double helix packing and unit cells in A (left) and B (right)-type crystalline structures in starches. Unit cells are outlined and hydrogen bonds are shown as dashed lines. Water molecules have been omitted for clarity (Imberty et al., 1991).

Understanding the crystallisation behaviour of starch is crucial to study the degree of crystallinity which influences the physical, mechanical properties (Mizuno et al., 1998, Ramkumar and Bhattacharya, 1997).

2.2 Formation of TPS

2.2.1 Gelatinisation

When starch granules are heated in excess water, one of the most widely used and effective plasticisers, the semicrystalline structures will break down to give a fully amorphous structure with polymer chains of amylose and amylopectin entangling with each other in a similar fashion to conventional polymers. The process that turns the granular structure of native starch into this disordered state is called gelatinisation (Ratnayake and Jackson, 2009, Lelievre, 1974, Atwell et al., 1988). According to an early theory developed in the 1970s (French, 1973), gelatinisation could be described as follows. First, when the starch granules are gradually heated before the gelatinisation temperature, they will absorb water and then swell to a limited extent. At this stage, if the starch granules subsequently dehydrate, they will return to their origin appearance and their semicrystalline structure will not be disrupted. During the second phase when the gelatinisation temperature is reached, the granules will continue to absorb 50% or more of their mass in water (French, 1973) and the semi-crystalline regions will break down (Liu et al., 2009). This can be observed as a loss of birefringence and a sudden rise in the viscosity of the starch-water suspension, as parts of starch are solubilized in the suspension. After that, starch granules will not be able to return to their original state even when cooled or

dehydrated. Ultimately when the suspension cools down, it will form a viscous mixture, where viscosity will depend on the starch concentration.

This theory is based on the situation where starch is gelatinised with a water content of more than 40% (Liu et al., 2006). Studies (Liu et al., 2006, Liu et al., 2005, Donovan, 1979, Lai and Kokini, 1991) point out that in this mechanism, starch crystallites are disrupted by swelling in water, while melting at higher temperature is a minor factor. In the instance where there is a limited water content, the swelling forces produced by water are much lower, and so a higher temperature is required to enable the mobility of starch molecules and disruption of crystalline regions (Donovan, 1979). Researchers have reported that the transition temperature and the enthalpy of this process increased with decreasing water content for potato starch. In their DSC characterisation of potato starch performed at a heating rate of 10°C/min, a single peak was found when the water level was 81% (Donovan, 1979). A second endothermic peak appeared at higher temperatures when the moisture content decreased to 64%. This endotherm then became predominant when the water percentage dropped below 51%, as shown in figure 2-3. For such a temperature change manifested in a water limited condition, it is apparent that the starch crystalline region disruption is more dependent on high temperature, rather than swelling forces. In this case the phenomenon would be more accurately referred to as the "melting" of starch.

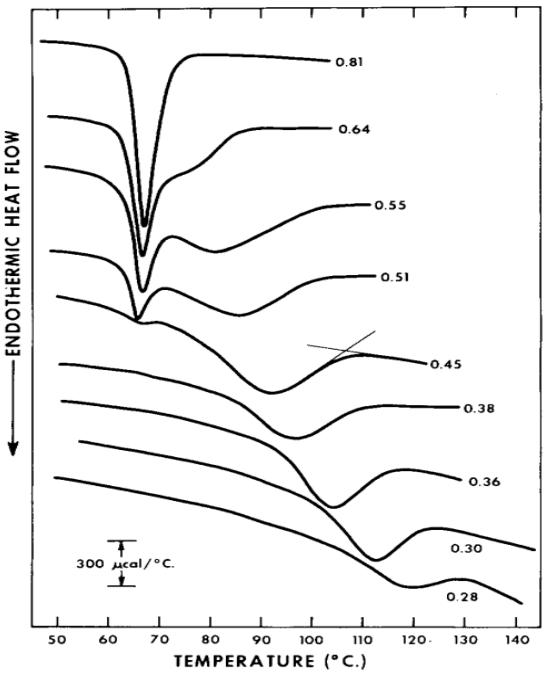

Figure 2-3 DSC thermograms of potato starch obtained at a heating rate of 10°C/min, for various volume fractions of water (as labelled). (Donovan, 1979).

When gelatinising/melting starch is subject to shear, it is observed that shearing can enhance the destruction of starch granules in abundant water (Yu et al., 2006, Chen et al., 2007) and the melting of crystallites with limited water (Xue et al., 2008, Wang et al., 2010, Xie et al., 2008). By destroying the natural crystalline structure, native granular starch is then converted into an amorphous molten state which can be further processed in conventional ways such as screw extruding, compression moulding and so on. The product of this process is widely known as thermoplastic starch (TPS). Since gelatinisation and melting are processes that involve breaking down the biological structure of the starch granule, the process is not reversible after native starch is converted into TPS.

2.2.2 TPS Processing

TPS can be processed by casting, compression moulding, injection moulding and extrusion (Averous, 2004, Averous and Halley, 2009, Liu et al., 2009). Film casting has been widely used for starch-based polymer film processing for food, conventional plastic replacing material and agricultural use (Bourtoom and Chinnan, 2008, Grazuleviciene et al., 2012, Koch et al., 2010, Lu et al., 2012, Wu and Zhang, 2001, Jimenez et al., 2012a). The general process includes the preparation of a suspension mixture followed by gelatinisation, casting and drying. While an easy way to produce TPS products, this method does not satisfy the need of high accuracy products and it is not efficient because it is not a continuous process.

The extrusion of TPS offers a more efficient processing methodology. Extrusion gives more stable processing, both in terms of processing conditions and product quality (Liu et al., 2009). It has been shown that different types of extruded starch differ in their water solubility index which give them a more adhesive property and thermal stability (Sharma et al., 2015). Another study (Gilfillan et al., 2016) has reported that hot pressed film created by extruded TPS containing glycerol and alcohols displayed increased stiffness and crystallinity but decreased moisture uptake. Young's modulus, tensile strength and elongation at break increased by 60%, 15% and 32% respectively, for 5wt% methanol derived film compared to the control. Film moisture was reduced by up to 15wt% for 5wt% ethanol derived film.

Meanwhile, two-stage extrusion processing techniques have been developed by some other researchers. During their processing procedure, preparation of premixed powders is the first step. After the premixing, sheet or films are produced by extrusion (Fishman et al., 2006, Matzinos et al., 2002a, Matzinos et al., 2002b). Although extrusion improves TPS processing by making the product properties more consistent and broadening the application areas, it is

still difficult to process high amylose content starches by extrusion. Die pressure will be much higher due to the higher melt viscosity of TPS (Shogren and Jasberg, 1994). In addition, the instability of melt flow is one of the main factors contributing to processing difficulties (Thuwall et al., 2006, Li et al., 2011). Based on different requirements for the final material, sometimes a high content of low-viscosity polymer such as PE is blended or plasticisers are utilized to lower the melt viscosity of TPS. For example, a corn starch (30% amylose)/LDPE blend with a PE proportion from 60% to 90%, can lower the melt viscosity to 100-300 Pa·s at a shear rate of 100 s^{-1} (Sabetzadeh et al., 2012), compared to 500-3000 Pa·s for waxy maize starch (less than 2% amylose) (Willett et al., 1997), and 2000-20000 Pa·s for high amylose potato starch (86% amylose) at the same shear rate (Thuwall et al., 2006).

Poor flow properties and high melt viscosity of starch-based polymers make injection moulding difficult to conduct. Injection moulding offers an efficient methodology to produce many specialised parts, but requires extensive modelling and processing consistency. The processing parameters of TPS, however, are highly inconsistent, which results in difficulties in not only product design, but flow modelling. For example, due to the water evaporation during thermal processing, the melt flow index (which as a measure of viscosity is key to understanding the flow behaviour in a mould) is nearly impossible to obtain by conventional methods. As such, pure raw starch or TPS has not been applied to this processing technique yet. Instead, TPS is usually blended with synthetic polymers which are easy to process (Averous et al., 2001, Funke et al., 1998, Mani and Bhattacharya, 1998a, Mani and Bhattacharya, 1998b, Mondragon et al., 2009, Ramkumar et al., 1996, Ramkumar et al., 1997).

Compression moulding is generally applied to starch foaming products for containers and packaging, etc. But the properties of the resulting product vary depending on the moisture content. The efficiency and accuracy of the production process are poor (Shogren et al., 1998, Tiefenbacher, 1993). Studies conducted on compression moulding of TPS have been mostly focused on the resulting material properties (Glenn and Orts, 2001, Thunwall et al., 2006, Bootklad and Kaewtatip, 2013). New methods such as microwave heating from extruded pellets (Zhou et al., 2006) are being explored to achieve a better quality of packaging material.

2.2.3 Plasticisation

Plasticisation is a phenomenon which occurs when one or several specific types of ingredients are blended with the polymer mixture to alter the material properties such as processing viscosity and flexibility, and the glass transition temperature. It typically affects the polymer

matrix, making it softer and more flexible. A number of different theories have been proposed to explain the mechanism of plasticisation depending on different situations, however it is widely accepted that molecular interactions between different ingredients is the major factor involved (Voskresenskii et al., 1971).

The glass transition temperature (T_g) is the characteristic temperature at which "frozen polymer chains" have enough energy and free volume to make bigger movements. At this temperature, a polymer converts from a glassy state to a rubbery state, with a sudden decrease of Young's modulus and an increase of flexibility (Young and Lovell, 2011). This renders the material more ductile rather than rigid and brittle. The T_g of native starch is around 52°C to 60°C while TPS has a greater range of T_g depending on plasticiser type and content (Liu et al., 2010, Mitrus, 2005). In addition, less heat is required to soften TPS and less power is needed to force the material to flow in manufacturing. Therefore, a lower T_g of TPS means a wider material use range and lower energy requirement in TPS processing. T_g is mainly affected by the flexibility as well as the microstructure of polymer chains and interactions between polymer molecules. Generally speaking, if the polymer chain is more flexible, the glass transition temperature will be comparatively low (Lu and Jiang, 1991). On the other hand, if strong molecular interactions like hydrogen bonds exist between polymer molecules in the matrix, this will result in inflexibility in the polymer and consequently an increase in the glass transition temperature at a macro scale.

The introduction of a flexible molecular structure which has strong interactions that compete with the existing interactions between ingredients, is an approach to obtain a better plasticisation effect. One good example is the structural plasticisation theory which claims that by weakening the molecular interaction on the boundary of ingredients, a structural plasticisation can increase the mobility of molecular "blocks" and thus achieve a better plasticisation effect (Andriano.Gp et al., 1971).

In terms of starch, the role of plasticisers is to destruct granular starch by breaking the inter/intra molecular hydrogen bonds and lowering the melting temperature of starch (Souza and Andrade, 2002, Stepto, 2003). Regarding the function of starch granule destruction, plasticisers are also considered gelatinisation agents in some studies. Currently, widely used plasticisers for TPS processing include water, glycerol, sucrose, fructose, glucose, glycols, urea, amides, and amino acids (Zhang and Han, 2006a, Zhang and Han, 2006b, Pushpadass et al., 2008).

As previously mentioned, there are several problems involved in starch processing, many of which are related to the choice of plasticisers used during processing. A typical example is using water as a gelatinisation agent/plasticiser. Water is a good starch plasticiser and is conventionally used in starch gelatinisation. It is, however, volatile. The viscosity of starch is very sensitive to water level, which means that the processing conditions will not be stable. Besides, starch requires relatively high temperatures to be melt-processed, and at such a high temperature the volatile plasticiser will evaporate too fast. As a consequence, inconsistent gelatinisation status and high melt viscosities will lead to the material degrading during processing. These disadvantages have limited the application of starch polymers.

In order to lower the melt viscosity and melt temperature, researchers have been trying to find another kind of plasticiser which is better than water. One of the options is glycerol. It is reported that (Liu et al., 2009) glycerol is beneficial to lower the apparent viscosity during melting, leading to improved strength and flexibility of the final product. In earlier research findings (Rodriguez-Gonzalez et al., 2004), it has been shown that TPS plasticized by glycerol can be considered as a homogeneous system composed of a hard elastic network and soft amorphous regions. Amylose complex crystallites, highly entangled starch molecules and poorly plasticized starch-rich sites compose the hard elastic network whereas the soft amorphous regions are composed of well-plasticized glycerol-rich starch. When glycerol content is lower than 30% in TPS, the melt viscoelastic response will be dominated by the hard elastic network. In contrast, the soft amorphous regions will dominate the viscoelastic response when glycerol content is higher than 30%. Regardless of which region dominates the properties of TPS, the plasticisation effect is better than TPS plasticized by pure water. When pure water is used as the plasticiser, water is absorbed by the amorphous regions first leaving the crystallites not well plasticized, which therefore melt at high temperature. This results in the crystalline structure reorganising after cooling down, rather than having interactions with the plasticiser (Donovan, 1979).

Moreover, the low vapour pressure of glycerol also improves the stability of starch processing. However, it is found that glycerol works as a co-agent to gelatinisation (Liu et al., 2011a) which means glycerol does not affect starch in the absence of water. Water needs to be added into the starch/glycerol system to give a greater extent of gelatinisation. Though a higher temperature can enable glycerol to facilitate starch phase transitions, if abundant plasticiser other than glycerol is not present, it will result in the gelatinisation temperature increasing. Furthermore,

the amount of plasticiser required will be even higher if the amylose content of starch is higher. It is, thus, considered an inefficient gelatinisation agent compared to water.

Some small molecules consisting of –CO-NH- groups, such as urea, formamide, ethanolamine and ethylene bisformamide have demonstrated to be effective plasticisers for TPS (Ma and Yu, 2004, Huang et al., 2006, Yang et al., 2006b, Yang et al., 2006a, Wang et al., 2008). These chemicals are believed to suppress retrogradation and enhance TPS mechanical properties (Ma et al., 2005a, Ma et al., 2005b). However, plasticisers such as formamide for example, would potentially leach out (Ma et al., 2005b). Hence, the material properties might not be stable in the long term and, moreover, toxic material could potentially leached out to detrimental effect. Therefore, it is important to seek alternative plasticisers which can solve these problems.

2.2.4 TPS Mechanical Properties

Mechanical properties are fundamental to TPS with tensile strength, Young's modulus and elongation at break the main parameters used to characterise this. The mechanical properties of TPS can be influenced by moisture uptake during conditioning, amylose/amylopectin ratio, types and amount of plasticisers used, and starch type, etc. Previous studies (summarized in table 2-2) have shown that TPS has comparatively low Young's modulus and tensile strength, which limits its potential applications. For instance, it is reported that the Young's modulus of TPS can range from low values of a few 10's of MPa to up to a maximum of about 1500MPa. This is generally lower than the values for common conventional plastics.

Table 2-2 Typical Young's modulus and tensile strength of different starches and conventional plastics

Materials	Amylose Content [%]	Plasticiser Used	Young's modulus [MPa]	Tensile Strength [MPa]	Reference
Waxy Starch	<0.5	25–40%Water	730.7± 120.0	12.7 ± 2.4	(Li et al., 2011)
Maize Starch	26	25–40%Water	866.6 ± 124.9	15.7 ± 2.1	
Gelose 50 Starch	50	25–40%Water	1139.9 ± 382.6	20.2 ± 1.7	
Gelose 80 Starch	80	25–40%Water	1217.2 ± 334.7	23.8 ± 1.9	
Corn Starch	26	20%Glycerol	550 ± 50	17 ± 6	(Jiménez et al., 2011)
Corn Starch	26	30%Glycerol	840 ± 61	11.8 ± 0.6	
Rice Starch		20%Glycerol	532.8 ± 115.6	10.9 ± 1.2	(Dias et al., 2010)
Rice Starch		30%Glycerol	21.3 ± 5.0	1.6 ± 2	
Polypropylene(PP)		-	950~1770	26~41.4	(Ku et al., 2011)
Polystyrene(PS)		-	4000~5000	25~69	
HDPE		-	400~1500	14.5 – 38	
Nylon 6		-	2900	43~79	
Nylon 6,6		-	2500~3900	12.4~94	

2.3 Ionic Liquid

2.3.1 Ionic Liquids

Ionic liquids have been increasingly attracting the attention of academia and industry as a material which has many functional and "green" applications to chemical industries. For example, it can be used for chemical syntheses as solvents (Keskin et al., 2007). Also, the wide potential window (large difference in the oxidation and reduction potentials) of ILs promises applications as new electrochemical materials. New types of catalysts based on ILs have been explored (Hamaguchi and Ozawa, 2005).

Ionic liquid molecules are usually composed of large asymmetric organic cations and anions, either organic or inorganic. The major properties of ionic liquid are strongly dependent on the structure (Marsh et al., 2004, Werner et al., 2010, Coleman and Gathergood, 2010). Similar to the conventional molten salts which exhibit high melting temperatures, ILs consist entirely of ions. But unlike those conventional salts, ILs are non-aqueous room temperature molten salts due to their special structures. The low melting points of ionic liquids are a result of their chemical composition. The combination of larger asymmetric organic cation and smaller

inorganic counterparts lower the lattice energy and hence the melting point of the resulting ionic medium (Keskin et al., 2007). In some cases, the anions are also relatively large and play a role in lowering the melting point (Yang and Dionysiou, 2004). Ionic liquids have extraordinary low vapour pressures below their thermal decomposition temperatures (Werner et al., 2010). These characteristics mean IL can have strong interactions on matrix boundaries, but do not readily evaporate.

The following figure shows parts of the cations and anions frequently used to form ionic liquid.

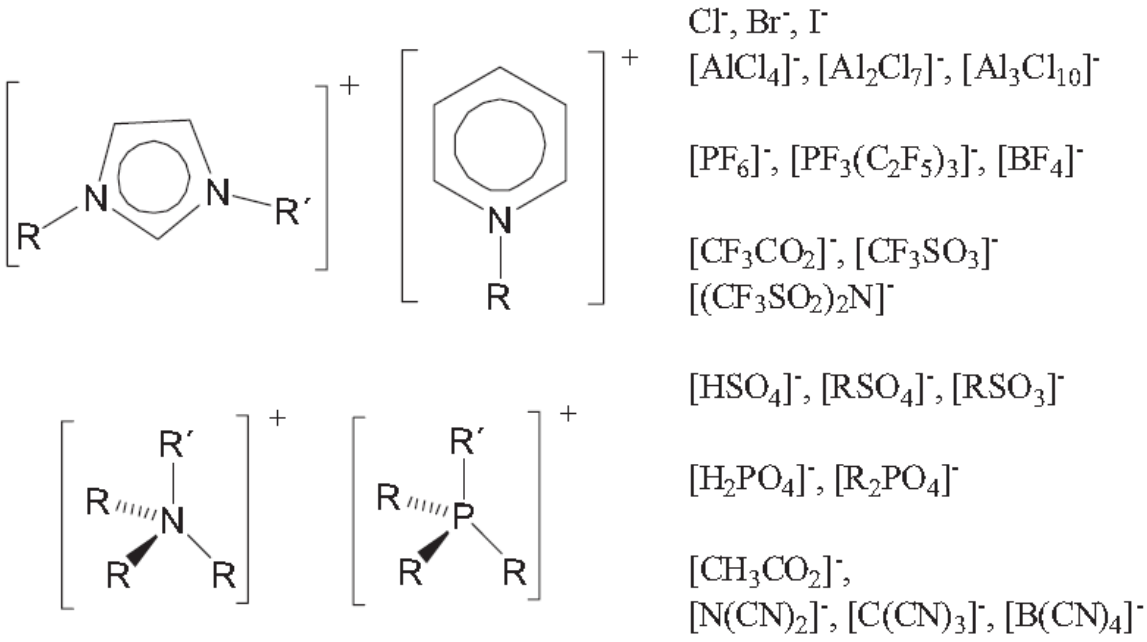

Figure 2-4 Typical cations and anions used to form ionic liquids (Werner et al., 2010)

As figure 2-4 shows, the substituents R and R' can be various including linear or branched alkyl chains, functionalized or aromatic groups. Thus, the number of combinations between different cations and anions is enormous, giving the possibility to tailor the IL chemical structure according to needs. By tailoring the molecular structure of IL, physical properties such as viscosity, density, solubility and melting point can be adapted to the desired requirements (Coleman and Gathergood, 2010).

Because of the interesting polarity and nucleophilicity which ionic liquids exhibit, inter-molecular interactions like coulombic, hydrogen bonding, and van der Waals interaction between ionic liquids and the other substances in the matrix are expected.

2.3.2 Ionic Liquids as Plasticisers

ILs have been widely utilized as plasticisers for conventional polymers such as PVC and PMMA, and these studies may be useful in understanding the use of ILs with TPS plasticisation. Various types of ILs such as ammonium, imidazolium and phosphonium based ILs have been investigated in terms of their plasticiser effects on PVC (Rahman and Brazel, 2006). It is found that ILs are potentially better plasticisers than the conventional plasticisers for PVC as some of them demonstrate good thermodynamic compatibility as well as good plasticizing effects. Wang and Hou have studied specifically the plasticiser effects of [Bmim]PF_6 and [Hmim]PF_6 to PVC paste resin. It is found that these two types of ILs can effectively lower the tensile strength and elastic modulus while increasing the elongation at break, thermal stability as well as UV stability (Wang and Hou, 2011). However, exposing samples in high temperature, strong acidic, alkaline or alcoholic environments can lead to plasticiser leaching. A previous study (Scott et al., 2003) has compared [Bmim]PF_6 and [Hmim]PF_6 with dioctyl phthalate as a plasticiser for PMMA, finding ILs of [Bmim]PF_6 and [Hmim]PF_6 are more efficient to lower glass transition temperature T_g and Young's modulus, which are indicators of an effective plasticiser. Another similar study (Zhao et al., 2012) has reported the multifunctional role of [Bmim]PF_6 in plasticizing PMMA/MWCNTs composite matrix. It is found that [Bmim]PF_6 is not only a good plasticiser which can lower glass transition temperature T_g significantly, but also a compatibilizer which is able to improve the dispersion of MWCNTs in PMMA matrix. It acts as a processing aid by decreasing melt viscosity. It is also worth noting that [Bmim]PF_6 was able to give a dopant effect, which increased the electrical conductivity of the polymer matrix.

ILs have also been widely studied for their use on plasticizing bio-polymers such as chitosan, cellulose and starch. The IL [Bmim][OAc] has been studied as a plasticiser for chitosan based biopolymer, where the IL's charge carrying behaviour was found to be a major contributing factor to material electrical conductivity (Shamsudin et al., 2015). Experiments on DSC and XRD have supported that such a kind of IL can effectively lower the T_g and decrease the crystallinity of chitosan based biopolymer. The highest electrical conductivity of $(2.44 \pm 0.41) \times 10^{-3}$ S/cm has been attained at 90 wt.% IL at ambient temperature, again demonstrating IL can potentially turn the base material conductive. Similarly, [Bmim]Cl has been compared to glycerol on the plasticiser effects to biomimetic composites of chitosan and clay in another study (Boesel, 2015). In this study, it is also reported that IL can efficiently lower the T_g and

increase the elongation of this biomimetic composites, without deleterious effect on their excellent barrier properties.

In another study, [Bmim]Cl as an IL plasticiser has been investigated in cellulose processing (Wu et al., 2015). It was found that the tensile strength and Young's modulus of ionic liquid plasticized cellulose decreased with increasing IL content. Correspondingly the cellulose crystallinity decreased. These ILs such as [Bmim]Cl and [Amim]Cl are more frequently utilized as solvents to extract cellulose and produce regenerated cellulose films (Jin et al., 2012, Suzuki et al., 2014, Wang et al., 2011, Jinhui et al., 2013).

Many authors have studied the interactions of ILs with starch (Wilpiszewska and Spychaj, 2011). For example, casting TPS which is plasticized by [Amim]Cl, have been studied (Ning et al., 2009). [Amim]Cl as the IL plasticiser has been proved to have a strong hydrogen bond-forming ability with starch which means it is effective. It is also reported in this article that the maximum conductance that TPS plasticized by [Amim]Cl can achieve is $10^{-1.6}$ S cm^{-1} at 14.5 wt% water content, which means IL can also broaden the application of TPS film. TPS processed by extruders utilising IL as plasticiser has been reported in another study (Sankri et al., 2010). In this study it was shown that IL (in this case [Bmim]Cl) has a better effect on reducing T_g to a lower level compared to glycerol. In addition, TPS plasticized by [Bmim]Cl is more hydrophobic than those plasticized by glycerol, which means the properties of TPS will be less sensitive to water uptake level. Tensile testing results, including an increase on elongation at break and a decline of Young's modulus, indicate that [Bmim]Cl has an explicit plasticisation on TPS.

Plasticisation effects of [Bmim]Cl, glycerol and their mixtures on cassava starch has been studied (Xie et al., 2014). This showed that the combined plasticisers contribute to a significant reduction in granule remnants compared with glycerol, resulting in highly amorphous structure. Infrared results suggested the starch films plasticized by combined plasticisers exhibit a weaker interaction with water molecules than glycerol plasticized ones, resulting in a decrease in water uptake. These factors make the starch films more flexible in mechanical tests as the tensile strengths decreased while elongation increased. The combined plasticisers also can lower glass transition temperature and increase the thermal stability of starch film. Different types of starches with different amylose content plasticized by [Emim][OAc] has been investigated by the same research group (Xie et al., 2015). It is found that in this case, amylose content has minor effects on the crystalline structure and the mobility of the amorphous chain segments.

Nevertheless, this structural difference does not significantly impact on mechanical properties, glass transition temperature, thermal stability or electrical conductivity of plasticized starch films. In comparison, the relative humidity during conditioning of the samples, and thus the sample water content, had a predominant influence on the material properties. A high amylose content starch plasticized by [Emim][OAc] was also investigated (Zhang et al., 2016). It was shown that, compared to glycerol, [Emim][OAc] can achieve greater homogeneity and flexibility in starch-based materials because it provides stronger starch-IL interactions which weaken the starch-starch interactions. Also, IL in this case can more effectively maintain the plasticised state during ageing than glycerol, which means the material would be more stable.

Some studies investigated starch composites using ILs as plasticisers. 1-methyl-3-propy-limidazolium iodide (MPII) has been utilised to process rice starch with lithium iodide salt (LiI) and titanium dioxide (TiO_2) nanoparticles for solar cell application (Khanmirzaei and Ramesh, 2014). The use of ILs here proved to be beneficial to the ionic conductivity of the starch composites. In another study of starch/zein blends plasticized by [Bmim]Cl (Leroy et al., 2012), IL has also been proved effective as a plasticiser as indicated by the reduced final melt viscosity of material processing and mechanical property tests.

2.3.3 Ionic Liquid/Starch Interaction

There is no doubt that ILs have strong interactions in plasticizing starch. However, the molecular interaction mechanism between ILs and starch is still not fully understood.

A study has been carried out to observe the mechanism of IL (in this case [Emim][OAc]) effects on different starches (Mateyawa et al., 2013). It is reported that IL actually behaves as a solvent rather than a gelatinisation agent as shown by DSC. Usually gelatinisation is characterized as an endothermic peak in DSC results while dissolution is exothermic. The dominating process depends on the ratio between IL and water. Because water can interact with IL strongly, when the water content is comparatively high, the starch granule disruption will be dominated by gelatinisation. Otherwise, the starch granule disruption will be mainly affected by dissolution. Though water and IL competitively interact in starches, it is similarly reported in this work that water is fundamental in starch granule disruption since pure IL diffuses slowly in starch. Similar conclusions have been reported in another two studies which used [Emim][OAc] on unmodified waxy starch (Liu and Budtova, 2013, Zhang et al., 2015). Meanwhile, the dissolving effect of [Emim][OAc] reported above has also been demonstrated to exist in [Amim]Cl (Zhao et al., 2015). The morphology of waxy and normal corn starches plasticized

by [Amim]Cl has been studied by scanning electron microscopy (SEM) and confocal laser scanning microscopy (CLSM). It was proposed that starch gelatinisation remained the dominant mechanism up to an IL concentration of 50%.

The molecular interactions between starch and [Emim][OAc] proposed above are considered mild compared to [Bmim]Cl. This is because it does not contain [Cl^-] anion which can lead to starch depolymerisation due to protonation (Kärkkäinen et al., 2011). The formation of HCl (as a result of the protonation of [Cl^-] anions in the presence of moisture) can catalyse the depolymerisation of starch. If so, a similar assumption could be made in the case of [Amim]Cl, however thus has not been reported yet.

Researchers have started to investigate the effect of ionic liquids on starch gelatinisation since it was shown that ionic liquids are effective to the dissolution of polysaccharides (Swatloski et al., 2002, Zhang et al., 2005). Such effects on disrupting the polysaccharides molecule are beneficial for processing. However, in another work, it is shown that pure ionic liquid is not always effective on starch disruption. Research (Stevenson et al., 2007) has shown that starch containing phosphomonoesters such as potato starch will have less effects with [Bmim]Cl, because phosphomonoesters can covalently link to the imidazolium rings which are the cations of that type of ionic liquid. In addition, the larger potato starch granules will prevent the ionic liquid from penetration.

Interactions between starch and ILs are various because this is affected by many factors such as processing techniques, temperature and types of ILs and starches. The molecular interaction mechanism of IL plasticized starch still needs to be investigated more deeply as it is still not clear which part of IL molecules interacts with starch molecules and vice versa. Furthermore, the relationship between these interactions and material properties such as crystallinity, crystal structure, thermal stability and mechanical properties is still unclear.

2.4 Carbon Nanotubes

2.4.1 Carbon Nanotubes

Carbon nanotubes (CNTs) have attracted a great deal of attention since they were initially discovered by Iijima in 1991 (Sumio, 1991) because of their special microstructure with strong C-C bonds combining to a cylindrical geometry, which can give a very stiff structure strengthening to the material matrix. Also, the sp^2-bonded hexagonal network of CNT gives

rise to an extended π-electron system of highly mobile delocalized electrons contributing to electronic conductivities. There are basically two types of CNTs. Single-wall carbon nanotube (SWCNT) (see figure 2-5), consisting of only one single tube of graphite and multi-wall carbon nanotube (MWCNT) (shown in figure 2-6), where several concentric graphitic tubes lie inside each other like a shallot. The length of these two types of CNTs can reach hundreds of microns, and sometimes even centimetres (Dai, 2002).

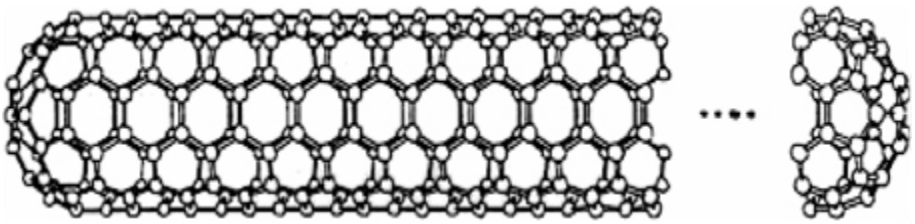

Figure 2-5 Simulation image of Single-wall Carbon Nanotube (Baxendale, 2003)

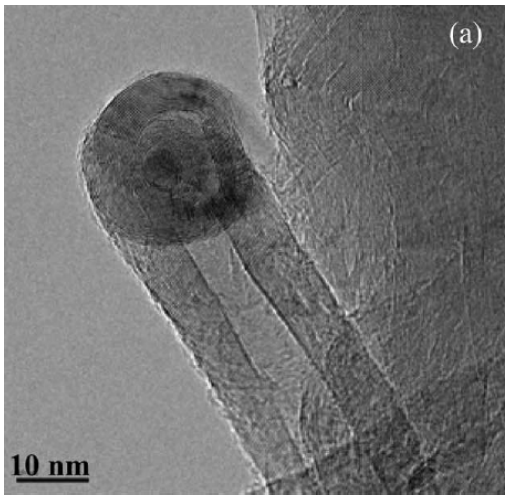

Figure 2-6 Multi-walled Carbon Nanotube (Dervishi et al., 2009)

These two types of CNTs have similar properties. For example, both of them have a high aspect ratio, high tensile strength, low mass density, high heat conductivity and large surface area (Sinnott and Andrews, 2001, Terrones, 2003). Small differences in mechanical properties (e.g. Young's modulus) are apparent because of differences in their structure. Additionally, CNTs are strong mechanically with excellent electronic conductivity (Dervishi et al., 2009). The electrical resistivity of CNTs is found to be as low as 10^{-6} Ω·m. SWCNTs with the diameter between 1 and 2 nm are found to have an extremely high Young's modulus around 1TPa while MWCNTs can be approximately 1.2TPa (Dresselhaus, 2001). The Young's modulus of MWCNTs is generally higher than the SWCNTs because of the concentric structure in

MWCNTs and the van der Walls forces between the concentric tubes. It is because the CNTs have few defects that they could hardly break to fragments, even when bent severely.

2.4.2 Polymer Carbon-Nanotube Composites

Both types of CNTs show excellent performance in reinforcing polymer materials. For example, a study has been carried out to investigate polypropylene (PP) fibres reinforced with CNTs (Kearns and Shambaugh, 2002). Decahydronapthalene (decalin) has been used to mix with SWCNTs before sonicating treatment for a good dispersion. The results show that PP fibres extruded with 1wt% SWCNTs has achieved an increased value of tensile strength and Young's modulus.

Polyethylene (PE) has also been investigated with CNTs. Researchers (Yang et al., 2007) have applied polyethylene-grafted MWCNTs to thermal processing of PE and have successfully achieved a good dispersion of MWCNTs. Hence, the storage modulus, Young's modulus, tensile strength, yield stress, ultimate strain and toughness have all been proved to be increased by adding PE grafted MWCNTs.

In another case, Nylon-6/SWCNTs composites have been studied (Zhang et al., 2003). PA-6 has been twin-screw mixed with nitric acid treated MWCNTs then compression moulded. It is reported that the tensile strength and Young's modulus are increased 120% and 115% respectively by adding 1wt% of MWCNTs. SEM results have showed that the MWCNTs are well dispersed.

A study of polyurethane/SWCNTs composites has also been carried out by using functionalized SWCNTs (Buffa et al., 2007). The results of this study show that the modulus, tensile strength and Elongation at break were all increased by introducing CNTs into polyurethane. In this case, though functionalisation of the CNTs leads to a minor improvement of CNTs dispersion, it also destroys the inherent electrical conductivity of the CNTs as well.

The studies mentioned above are just a fraction of the whole research field. There are many other studies which have applied CNTs to reinforce polymer matrices and demonstrated the effectiveness, as reviewed by Coleman et al. as well as Rahmat and Hubert (Coleman et al., 2006, Rahmat and Hubert, 2011). The efficiency of adding CNTs to polymers is significantly dependent on their dispersion and distribution in the matrix. It has been reported (Mitchell et al., 2002) that the better dispersion achieved by using modified CNTs in polystyrene can obtain similar viscoelastic properties to that attained by using double the quantity of unmodified CNTs.

Further, another study (Ferreira et al., 2013) shows a better dispersion of CNTs in PA-6 can yield better mechanical properties. Hence achieving a good dispersion and distribution of CNTs in polymer processing is a key factor to achieving good material properties.

2.4.3 Starch/Carbon-Nanotubes Composites

Many authors have investigated the possibility of using CNTs to enhance the mechanical properties of TPS (Ma et al., 2008, Cao et al., 2007, Liu et al., 2011b, Famá et al., 2011, Cheng et al., 2013). Most of these studies employ MWCNTs, probably due to the lower price and more abundance of MWCNTs than SWCNTs. Besides, MWCNTs exhibit high aspect ratio and excellent mechanical, thermal, electrical properties (Xie et al., 2013).

A study conducted by Cao et al. (Cao et al., 2007) has investigated the material properties of plasticised MWCNTs/pea starch composites. MWCNTs treated with a mixture of sulphuric acid and nitric acid have been found to increase the tensile strength and Young's modulus of glycerol plasticized pea starch. A good dispersion was observed in the SEM, and the elongation at break of nano-composites was higher than that of pea TPS samples without CNTs. It is also shown that the presence of MWCNTs decreased the water uptake at moisture equilibrium of the nano-composites. The strong hydrogen bonding between MWCNTs fillers and pea starch matrix is assumed to be the reason of these material property changes.

As an attempt to develop an electroactive polymer, a study has been conducted on MWCNTs/glycerol plasticized corn starch (Ma et al., 2008). In this case, nitric acid treated MWCNTs have been shown to improve the tensile strength, Young's modulus and the electrical conductivity of the material. By introducing a greater level of MWCNTs into the matrix, the dependence of electrical conductivity on water content can be eliminated above the electrical percolation threshold of 3.8 wt% MWCNTs loading. A typical electrical conductivity of 10^0 S/cm has been achieved by adding 4.75 wt% MWCNTs into the composites. Another similar research has been reported later in 2011 (Liu et al., 2011b). Similarly, MWCNTs treated with oxidative acid have been cast with corn starch. In this study, the presence of MWCNTs has been established to increase the pasting viscosity of corn starch and thermal stability of the resulting TPS matrix. However electrical percolation thresholds of 1.5 wt% MWCNTs are exhibited in this case. Exceeding this threshold resulted in a deterioration in the plasticisation of TPS and the mechanical properties of the composites.

Meanwhile, Fama et al. has reported their work using MWCNTs to strengthen tapioca starch in 2011 (Famá et al., 2011). MWCNTs were treated with an aqueous solution of starch-iodine complex and then mixed with glycerol and starch. The results showed that MWCNTs were well dispersed and significantly increased the stiffness by almost 70% and ultimate tensile strength by about 35% with only 0.055 wt% of MWCNTs.

Recently Cheng et al. reported a comparative study of potato starch strengthened by different types of oxidized MWCNTs (Cheng et al., 2013). MWCNTs have been differently treated to obtain two different oxygen containing groups. Based on the fact that oxidized MWCNTs are effective in improving tensile strength, moisture resistance and electrical properties, it was shown that the reduced oxidized MWCNTs are even more effective in reinforcing mechanical properties while the extent of CNTs oxidation did not affect electrical conductivity. Both types of oxidized MWCNTs are showed to be effective in dispersion.

Ultrasonic treatment has been utilized in all the mentioned works above to achieve homogeneous dispersion of MWCNTs. Also, pre-treatments of the MWCNTs seem to be essential to increase the interfacial adhesion between different ingredients. Overall, the reviewed results suggest that blending CNTs into the starch matrix is an effective method to improve mechanical properties. However, as reviewed by Xie et al. (Xie et al., 2013), most of the research reported employed solution casting techniques which would further limit the production efficiency in industry.

2.5 Review Summary

To conclude, starch is a promising raw material because it is biodegradable and renewable, though its mechanical properties limit its application. Processing starch using conventional polymer processing techniques such as extrusion and compression moulding is potentially feasible, however, due to the high viscosity and water sensitivity of TPS melt, continuous thermal processing is hard to perform in many cases. The product quality is heavily influenced by these factors and this further limits the application of TPS.

The most common plasticiser used is water, but this gives rise to problems because of volatility. The effects of other plasticisers such as glycerol have been studied, but the processing benefits and final product properties are not as good as expected. Therefore, ILs appear to be a promising substitute due to their strong interaction potential and stability. Attempts to use ILs to plasticize starch have been reported by several authors and they have shown that ILs are

effective in TPS processing. However, the interaction mechanisms between ILs and starch, as well as its effects on material properties such as crystallinity, crystal structure, thermal and mechanical properties are still unclear.

In terms of the mechanical properties, pure TPS is not as good as conventional polymers. On the other hand, CNTs have been proven to be effective in reinforcing polymers and in further enabling the material's electrical conductivity. Hence, CNTs have been studied and have been found to effectively strengthen TPS as well as give additional function to TPS composites recently. As reviewed, the key factors of effective TPS/CNTs composites processing are to establish strong interfacial adhesion between CNTs and TPS while achieving good CNTs dispersion and distribution in composites. Current processing techniques are mostly limited to solution casting with sonicating treatment, which is complicated and of low efficiency compared to continuous processing methods. Hence it would be useful to explore continuous processing methodologies for TPS/CNTs composites with a view to achieving industrial scales of production in the future. Finding highly effective plasticiser for TPS processing is therefore important. Another challenge in achieving a material with useful final properties is finding a new method to disperse CNTs without sonicating treatment. Recently four types of ILs, including [Bmim]Cl, have been reported to be effective in terms of dispersing SWCNTs (Hameed et al., 2013). Presumably, other types of ILs might have the same effect on MWCNTs while also being a plasticiser of TPS.

Therefore, this thesis sets out to investigate the interaction between TPS, IL and CNTs and understand the interaction mechanism. It then aims to explore the material properties and potential functions of Starch/ILs/CNTs composites for any further optimisation of material properties in the future.

3 METHODOLOGY AND MATERIALS

3.1 Introduction

This chapter establishes an understanding of the raw materials which were used in different stages of the study including starch (two different types), MWCNT, 1-ethyl-3-methylimidazolium acetate ([Emim][OAc]), glycerol, 1-Allyl-3-methylimidazolium chloride ([Amim]Cl), 1-Butyl- 3-methylimidazolium chloride ([Bmim]Cl). Preliminary experiments on regular maize starch (RMS) and Gelose 50, which guided the selection of RMS as the starch to be used in the remainder of this thesis are described in appendix A. Methodologies applied to sample preparation and characterisation are described in detail.

3.2 Materials

Two types of commercially available maize starches were used in this work: regular maize starch (RMS) and Gelose 50 (G50). RMS was supplied by New Zealand Starch Ltd. (Onehunga, Auckland, New Zealand) and G50 was supplied by National Starch Pty Ltd. (Lane Cove NSW 2066, Australia). Both starches were chemically unmodified and the amylose contents for these starches were 24.4% and 56.3% respectively, as measured by Tan et al. (Tan et al., 2007) using the iodine colorimetric method. All of the starch samples used were from the same batch. Deionised water was used in all instances. Glycerol (AR) was supplied by Chem-Supply Pty Ltd (Gillman, SA, Australia) and used as received. [Emim][OAc] of purity ≥ 95%, [Amim]Cl of purity ≥ 98% and [Bmim]Cl of purity ≥ 99%, produced by IoLiTec Ionic Liquids Technologies GmbH (Salzstraβe 184, D-74076 Heilbronn, German), were also supplied by Chem-Supply Pty Ltd. These ILs were used as received without further purification. MWCNTs used in this project were the NANOCYL^{TM} NC7000 series thin multi-wall carbon nanotubes produced via the Catalytic Chemical Vapour Deposition (CCVD) process as supplied by Nanocyl S.A. Belgium. They were produced via the catalytic carbon vapour deposition (CCVD) process and used as received. Average diameter and length of the MWCNTs were 9.5 nm and 1.5 μm respectively.

3.3 Methodology

3.3.1 TPS Production

3.3.1.1 Starch Premix Preparation

Starch was firstly manually mixed in a mortar by a pestle. The amount of plasticiser required (see the detailed compositions in the individual experimental chapters, tables 4-1, 5-1, 6-1 and

7-1) was added drop by drop and the compound was ground until homogeneous. In the case when CNTs were added, CNTs were firstly mixed with the plasticiser. Then the mixture was added to the starch powder drop by drop using a pipette. The procedure after this step was the same as those samples without CNTs.

3.3.1.2 Premixed Sample Processing

The purpose of this methodology is to plasticise the premixed starch into TPS samples. A Brabender Plasti-corder PL-2000 at the Plastic and Rubber Technical Education Centre (PARTEC), Brisbane, Australia was used to process TPS for 15 mins, at a temperature of 90°C and a rotor speed of 30 rpm.

In order to log detailed data on the process, the experiment was repeated using the same parameters on a Haake PolyLab OS RheoDrive 7 series at the University of Warwick, UK.

3.3.1.3 Tensile Testing Sample Preparation by Compression Moulding

TPS samples were cut into fragments by scissors and distributed evenly between Teflon sheets in a 1 mm thickness mould. This was then placed in a compression moulding machine constructed in our labs and the sample compressed under a pressure of 6.5-7 bar and a temperature of 130°C for 15 mins. The resulting TPS sheets were sealed in plastic bags immediately after they were removed from the compression mould and frozen until they were used.

Dumbbell samples (gauge length 10 mm, width 2 mm) for tensile testing were cut from the thin hot-pressed sheets using a cutting die which was available in the laboratory. All samples were cut with the same cutting die so they would be comparable. Before cutting, the frozen sheets were defrosted whilst remained sealed in plastic bags. After cutting all the dumbbell samples were dried in a SalvisLab Vacucenter vacuum drying oven VC50 at a temperature of 50°C for 3 days.

3.3.2 Sample Conditioning

Dried samples were conditioned in sealed plastic containers at relative humidities of 33%, 52% or 75%, controlled by saturated salts (Xie et al., 2015). Saturated magnesium chloride ($MgCl_2 \cdot 6H_2O$) solution was used to obtain the relative humidity of 33%, magnesium nitrate hexahydrate [$Mg(NO_3)_2 \cdot 6H_2O$] for 52% and sodium chloride (NaCl) for 75%. These sealed plastic containers were stored in a temperature and humidity controlled laboratory.

It was found that the actual RH in the containers did not remain at the desired level as the RH would decrease when retrieving samples for testing and take up to 2 weeks to rebalance to the target RH. Since the experimental timetable required frequent removal of samples for testing the container with magnesium chloride ($MgCl_2 \cdot 6H_2O$) saturated solution, which was targeted to be 33%, had an averaged RH of 30%~33%; the container with magnesium nitrate hexahydrate [Mg(NO3)2·6H2O], which was targeted to 52%, had an averaged RH of 41%~42%; and the container with sodium chloride (NaCl), which was targeted to 75%, had an averaged RH of 59%~61%. Though the actual RH variation was different from what was expected, it was found to be consistent. Hence, this is still considered a valid methodology since the three conditioning conditions had a good difference in RH.

3.3.2.1 Water Uptake Measurement

For each humidity level, five dumbbell samples were individually labelled and weighed as soon as they were removed from the vacuum oven on a Mettler Toledo AB204-S Analytical Balance which has an accuracy of 0.1 mg. Their mass was remeasured according to the experimental schedule at room temperature. The variation of mass over time was calculated and plotted.

3.3.3 Sample Characterisation

3.3.3.1 Tensile Testing

Additional dumbbell samples, conditioned at the same time, were used for tensile testing on an Instron Video Extensometer AVE 5584 according to the experimental schedule. At each time point, at least 10 dumbbells were tested for each TPS formula and humidity combination. The laboratory, where the tests were conducted, was air-conditioned at 25°C. TPS samples were not exposed to the open air until testing.

During the test, samples which were broken as soon as they were mounted on the machine were considered too brittle and their data were not included in discussion. Similarly, tests which stopped as soon as they started due to sample brittleness would not be included either. Only reasonably repeatable results will be discussed in later chapters. Results for samples where three of fewer reliable results were obtained from ten attempts were ignored, and for other samples which were reasonably repeatable, an averaged result of at least 7 replicates were calculated with relative error.

3.3.3.2 TGA (Thermal Gravimetric Analysis)

TGA samples were freshly prepared for the test in ME-26763 40 µl Al-Crucibles provided by Mettler Toledo. Using a balance (Mettler Toledo MX5) to measure the mass to an accuracy of 1 µg, samples of 3-5 mg were cut from the conditioned sample sheets. The prepared samples were then tested on a Mettler Toledo TGA/DSC1 STAR from 25°C to 550°C with a heating rate of 3°C/min.

3.3.3.3 FTIR (Fourier Transform Infrared) Spectroscopy

The infrared absorption spectra of the starch sample were obtained at 4 cm^{-1} resolution by using a Nicolet 5700 FT-IR Spectrometer equipped with a DTGS-TEC detector. The spectra were acquired at wavelength between 525 and 4000 cm^{-1} with 4 cm^{-1} resolution using OMNIC software. Each spectrum was collected by performing 64 scans without baseline correction nor normalisation.

3.3.3.4 Raman Spectroscopy

Conditioned sample square sheets with 1mm thickness and 2mm edge length were setup in a sample holder. The spectra of these starch sheets were collected with a low resolution (18.7-34.5 cm^{-1}, estimated automatically by the equipment) in the range of 83-3472 cm^{-1} using a Nicolet Almega^{TM} Visible Raman Spectrometer. The number of scans was 32 for each of the tests. The raw data were not normalised.

Note that Raman and FTIR spectroscopy respond to different aspects of the system so they give complementary information. In particular it is of note that Raman Spectroscopy is not sensitive to dipoles, hence the signal would be relatively weak compared to FTIR Spectroscopy for polar systems such as ILs.

3.3.3.5 XRD (X-Ray Diffraction)

The conditioned RMS samples were cut into a 2 mm × 2 mm square sheet and placed in the sample holder of an X-ray diffractometer (D8 Advance, Bruker AXS Inc., Madison, WI, USA) equipped with a copper tube and a LynxEye detector. The diffractograms were recorded over an angular range of 3-40°, with a step size of 0.02° and a rate of 0.5 s per step. The radiation generator was set to be at 40 kV and 30 mA, with a slit of 2 mm. Traces were processed using the Diffrac^{plus} Evaluation Package Release V4.2 to determine the X-ray diffractograms of the samples. The degree of crystallinity was calculated using the method of Lopez-Rubio et al.

(Lopez-Rubio et al., 2008), with the PeakFit software (Version 4.12, Systat Software, Inc., San Jose, CA, USA), using equation (1):

$$x_c = \frac{\sum_{i=1}^{n} A_{ci}}{A_t} \cdots (1)$$

Where A_{ci} is the area under individual crystalline peak with index i, and A_t is the total area including amorphous background and crystalline peaks.

The V-type crystallinity was calculated based on the total crystalline peak areas at 7, 13, 20 and 22˚ (van Soest et al., 1996b).

3.3.3.6 TEM (Transmission Electron Microscopy)

The unconditioned RMS samples were sectioned at -140°C in a Leica UC6 cryo-ultramicrotome with a thickness of 100nm. Sections were placed on formvar-coated copper grids and viewed in a Jeol 1011 TEM at 100kV. Images were collected with an Olympus Morada digital camera under a magnification of 4k to 200k.

3.3.3.7 Electrical Conductivity Measurement

A two-point probe method was used to measure the resistance of samples using a Keighley electrometer (Model 6517B, Keithley Instruments, Inc., Cleveland, OH, USA). A length of 15mm was set between the two probes for measurement. The resistance measurement was repeated 10 times on each sample. The resistivity was obtained by equation (2):

$$\rho = \frac{RL}{A} \quad \cdots (2)$$

Where ρ is resistivity (Ω/cm), R is measured resistance (Ω), L is length (cm) and A is cross sectional area (cm^2). Conductivity (S/cm) is the reciprocal of the resistivity (Ω/cm) (Petty, 2007).

4 EFFECTS OF GLYCEROL/[EMIM][OAC] ON RMS PROCESSING

4.1 Introduction

In this chapter, the plasticizing effects of [Emim][OAc] and glycerol on RMS processing and material properties will be studied. Spectroscopic studies of the resulting TPS will be used to investigate the molecular interactions between [Emim][OAc] or glycerol and RMS. This will help to understand how the other material characteristics and properties are affected and hence help to develop guidelines for material properties optimisation.

1-ethyl-3-methylimidazolium acetate ([Emim][OAc]) was chosen for this study as it does not contain any aggressive anions which have been shown to lead to starch depolymerisation due to protonation (Kärkkäinen et al., 2011). This IL also has the advantages of low vapour pressure, high thermal stability, and relatively low viscosity at room temperature, which enables it to be stable over wide processing conditions (Liu and Budtova, 2013) which should result in a consistent processing.

RMS processed with three different levels of [Emim][OAc] will be investigated and compared to those plasticized by corresponding amounts of glycerol. Mechanical properties and water absorption will be studied during conditioning. Other sample characters such as crystallinity, thermal stability and will be studied after conditioning.

4.2 Experimental

4.2.1 Materials

The starch used in this experiment was RMS. Glycerol and [Emim][OAc] were used as plasticisers. Details are outlined in Chapter 3.2.

4.2.2 Experimental Methods

Six types of samples of TPS were produced and compression moulded according to the compositions shown in table 4-1, following the methodology outlined in chapter 3.3.1. For example, for every 100 g of starch in RMS-G9, 21 g of water and 9 g of glycerol would be added to plasticize the mixture. The sample size made in each batch was approximately 100 g in the Brabender Plasti-corder PL-2000 and 50 g in the Haake PolyLab OS RheoDrive 7 series.

Table 4-1 Experimental RMS sample compositions used in chapter 4. Amounts are proportions by mass. Each batch made was about 50g in total.

Code	Starch Type	Starch Amount	Water	Glycerol	[Emim][OAc]
RMS-G9	RMS	100	21	9	-
RMS-G18	RMS	100	12	18	-
RMS-G27	RMS	100	3	27	-
RMS-E9	RMS	100	21	-	9
RMS-E18	RMS	100	12	-	18
RMS-E27	RMS	100	3	-	27

The sample sheets were then conditioned at three different humidity levels and characterised over time using the following techniques:

Mechanical properties — Tensile testing (section 3.3.3.1)

Water absorption — Water uptake measurement (section 3.3.2.1)

After conditioning was completed, (as indicated by no further mass change in the water uptake measurement) the samples were characterised by the following methods:

Molecular Structure — FTIR spectroscopy (section3.3.3.3)

Raman spectroscopy (section 3.3.3.4)

Crystal structure — XRD (section3.3.3.5)

Thermal stability — TGA (section3.3.3.2)

These tests were performed according to the schedule given in table 4-2. Note that the samples are very sensitive to RH environment at the beginning of conditioning, therefore, the tensile tests were not performed until 7 days conditioning as it would take several hours to finish testing all samples. In addition, some of the samples were too brittle at time zero. Also by definition, water uptake at time zero is zero. Therefore, there is no time zero measurement for either of the tests.

Table 4-2 Conditioning schedule

Time (days)	0.25	1	3	7	14	28	42
Water uptake measurement	×	×	×	×	×	×	×
Tensile testing				×	×	×	×

4.3 Results and Discussion

4.3.1 Mixing Torque

Material compounding and processing by a mixer is the first step of the sample preparation for this study. It is also of great importance to the starch gelatinisation while thermal processing. The resulting homogeneity of the material, as well as the dispersion and distribution of different ingredients are heavily impacted by this step.

Figure 4-1 (a) and 4-1 (b) summarizes typical torque values recorded by a Haake PolyLab OS RheoDrive 7 series over the mixing time of each sample. All samples have a typical loading peak at the beginning and a rise in the torque to a maximum value except for RMS-E27. Peak torque is generally at about 3 to 4 minutes, except for RMS-G27 (5.3 min) and E27 (0.4 min). All of the torque values then drop off to an asymptote. This is very similar to what has been reported for starch “gelatinisation” when the temperature at peak torque value is approximately the gelatinisation temperature (Liu et al., 2009). For RMS-E27, it appears that the sample was melting rather than gelatinizing, as it does not show a gelatinisation peak. This behaviour could be explained by an observation in a study by Mateyawa et al. (Mateyawa et al., 2013) who showed that as the proportion of [Emim][OAc] increased, the blend dissolved prior to gelatinisation at low temperatures. Therefore, in the RMS-E27 sample here it is suggested that the starch had dissolved prior to processing, hence a high viscosity and high torque were observed initially

(a)

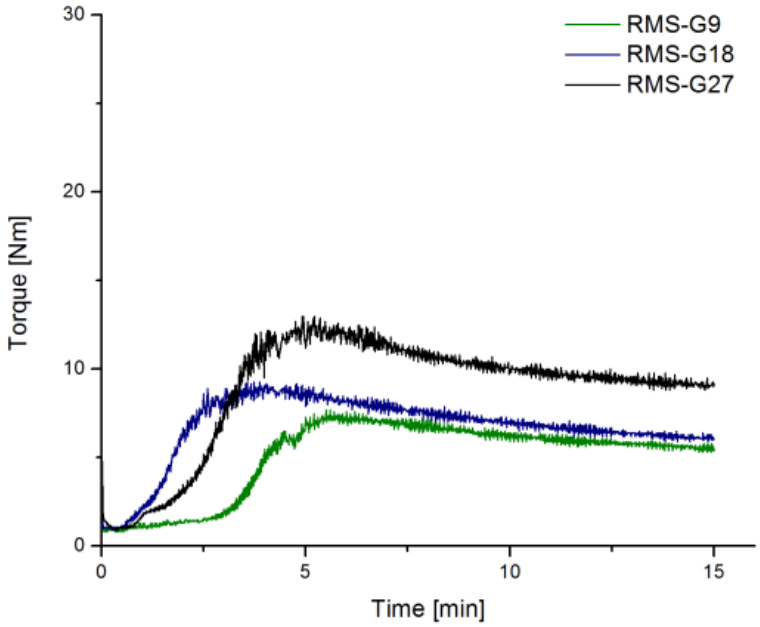

(b)

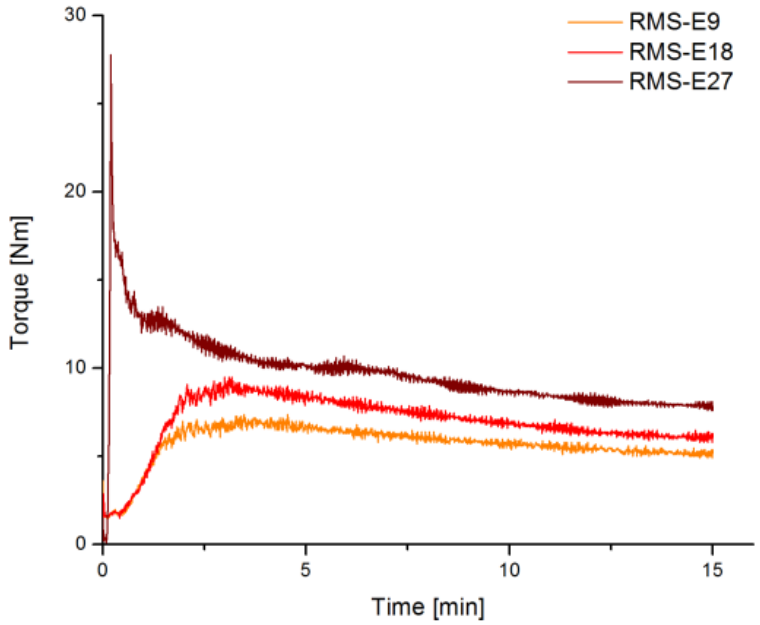

Figure 4-1(a) Mixing torque over processing time of RMS-G series; (b) Mixing torque over processing time of RMS-E series

As the results are reasonably reproducible and only 3 trials have been performed on each formula, data summary of mixing process is shown as mean values without standard deviations in table 4-3. Any significant differences between the samples, calculated by the Fisher post hoc

method, are indicated by superscript letters where, in any column, samples that do not share a letter are significantly different at $p<0.05$.

Table 4-3 Mean value of thermal mixing data of RMS-G and RMS-E series samples (in each column entries that do not share a letter are significantly different, Fisher comparisons $p<0.05$)

Code	Time of peak torque [min]	Peak Torque [Nm]	Final Torque [Nm]	Temp at Peak [°C]	Final Temp [°C]
RMS-G9	3.3^{cd}	9.1^{b}	5.9^{cd}	93.2^{c}	97.9^{d}
RMS-G18	4.0^{b}	9.0^{b}	6.1^{cd}	95.5^{b}	98.5^{c}
RMS-G27	5.3^{a}	12.2^{b}	9.3^{a}	99.1^{a}	100.4^{a}
RMS-E9	3.7^{bc}	7.4^{b}	5.5^{d}	94.7^{b}	97.9^{d}
RMS-E18	3.1^{d}	9.3^{b}	6.2^{c}	93.4^{c}	98.4^{c}
RMS-E27	0.4^{e}	21.4^{a}	7.5^{b}	81.2^{d}	99.0^{b}

The samples had subtle differences in their nature after mixing. The RMS-G9 and E9 were generally a little crumbly when cleaning the mixer. There was noticeable water on the metal tray where the material was being scraped into the tray at the end of the run. Hence this may be related to water loss after the run. The mixing chamber was sealed so there should not be much water loss during the test. RMS-G18 and E18 were pliable, while G27 and especially E27 were quite elastic in nature.

As seen in table 4-3, nearly all of the mean values of final torque and final temperature increased with an increase in plasticiser amount. The peak torque also increased, but only in the case of RMS-E27 in the E-series was this significant. Such results suggested that higher plasticiser levels potentially enhanced molecular interactions between ingredients of the materials. Stronger molecular interaction between ingredients could have given the material a more ductile structure, which required more energy to be pulled and kneaded when mixing. Therefore, a higher peak torque and final torque value were observed, likely due to higher friction in the mixing chamber, which coincides with a high final temperature.

4.3.2 Water Uptake

As mentioned in introduction (Chapter 2), starch is a hydrophilic material. Thus, water uptake may happen after processing and lead to further effects on many material properties. Therefore, water uptake measurement has been performed and mean percentages have been calculated out of 5 results from each type of samples and displayed in table 4-4.

Table 4-4 Water uptake mean percentages (increased from original mass) at equilibrium

Code	RMS-G9	RMS-G18	RMS-G27	RMS-E9	RMS-E18	RMS-E27
RH33	0.32%	-2.06%	-1.44%	-0.18%	-0.52%	-1.71%
RH52	2.41%	1.01%	3.00%	1.79%	3.38%	4.54%
RH75	8.63%	11.06%	13.16%	8.66%	13.33%	17.54%

All of the samples in 33% humidity (excepting RMS-G9) show a negative absorbance at equilibrium suggesting that samples were not completely dried in the vacuum oven. In fact, water condensation was found at a small corner inside the screen glass of the oven door. Presumably, the samples were not completely dried for this reason.

From table 4-4, only samples conditioned in RH75% show that a higher plasticiser level leads to a high water absorption percentage. For samples conditioned in RH 33%, the results are not conclusive because the water uptake progress of some samples was not started from absolute "zero" humidity. However, if comparing the equilibrium results of RH33% and RH52%, it can be found that samples with a higher level of plasticiser have a greater water uptake interval between different conditioning RH. For samples conditioned in RH75%, samples plasticized by a same level of [Emim][OAc] compared to glycerol can absorb a greater amount of water. Most obviously, a higher humidity circumstance is the key factor to high water absorption.

Water uptake results over time of RMS-G9 are shown in figure 4-2 as an example. Similar patterns can be found in other samples (see appendix B 10.2). It was found that once water uptake experiments had finished according to the schedule (table 4-2), the samples in RH75% had potentially not equilibrated yet. Hence, the samples were left in RH75% containers and tested again at up to 98 days. In fact, compared to the data collected at the check point of 42 days, the final equilibrium results are not much different. It suggests that at 42 days after the commencement of conditioning, the samples conditioned at RH75% had already reached equilibrium. The trend in water uptake reaches a peak before reaching to equilibrium. These most obvious peaks can be observed from samples conditioned at RH75%. The same trend can be observed at any other samples which is less obvious compared to those conditioned in RH75%. Superficially, the water uptake curves show that moisture was trapped by TPS and released afterwards. It is believed that these water uptake trends are related to complex microstructure change caused by different molecular interactions. This will be further discussed in FTIR/Raman spectroscopy analysis (4.3.4.1) and XRD analysis (4.3.4.2).

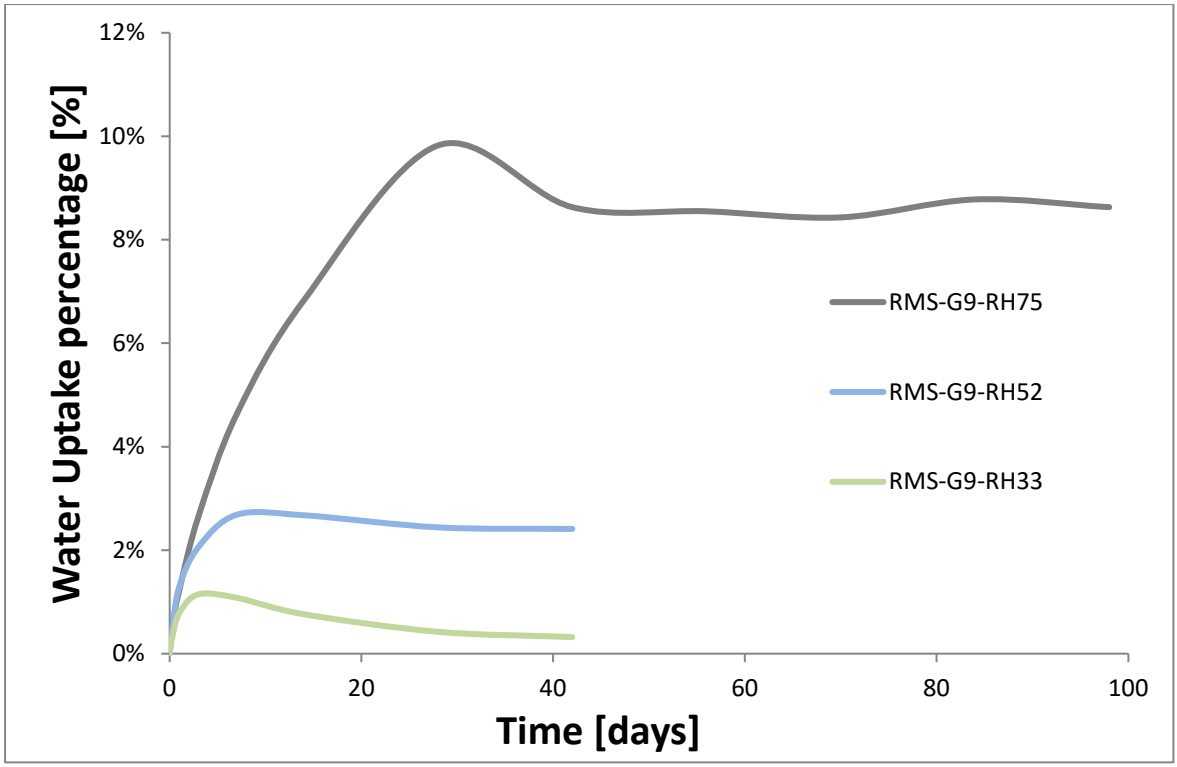

Figure 4-2 Water uptake ratio of RMS-G9 in different relative humidity levels over time

4.3.3 Tensile Tests during Conditioning

The resulting water uptake heavily influences the material's mechanical properties such as tensile strength and Young's modulus. In order to investigate this, tensile testing was conducted according to the plan in table 4-2. Note however that there were insufficient specimens to be able to test beyond the planned 42 days for those conditioned for an extended time. Figure 4-3 showed tensile stress over strain curves of RMS-G18 and E18 as representative examples. Most of the other samples have similar shapes of these curves.

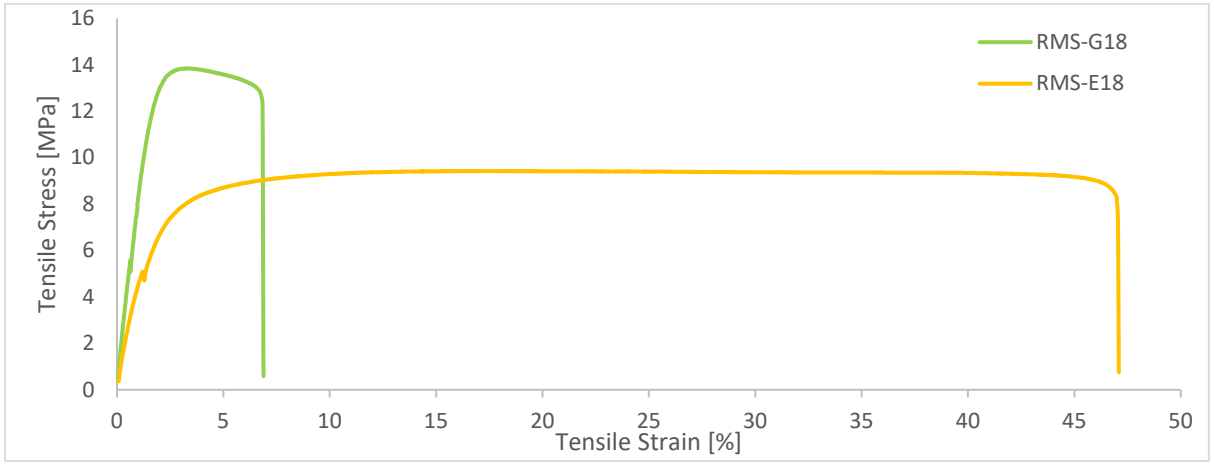

Figure 4-3 Representative tensile testing curves for RMS-G18 and E18 conditioned at RH 52%.

As displayed in figure 4-4, figure 4-5 and table 4-5, the amount of plasticiser plays a key role in Young's modulus and tensile strength of the samples conditioned at RH75%. With a constant plasticiser amount, the Young's modulus decreases with the increase of conditioning humidity level. Similarly, at a given humidity condition, the Young's modulus decreases when the plasticiser content increases. For each of the humidity conditions of the same plasticiser levels, samples plasticized by glycerol always have a higher Young's modulus than [Emim][OAc]. That shows [Emim][OAc] has a stronger effect on making the samples more flexible than glycerol. In contrast, it indicates that glycerol can give RMS a stronger mechanical strength than [Emim][OAc]. Higher conditioning humidity level and plasticiser level are relevant to the decrease of material Young's modulus in this case. This result is supported by two similar studies (Xie et al., 2015, Xie et al., 2014). In these studies, it was suggested that the reduced sample strength and stiffness was due to the hydrogen bonding disruption with the -OH sites of starch by plasticiser.

The elongation at break data show a more complex pattern than tensile strength and Young's modulus as they are not changing progressively. The error bars for these results are large, so the results may not be significant, however observing the mean values suggests that an increase in plasticiser level initially increases the elongation at break and then decreases this value. It was proposed (Xie et al., 2015) that the IL could disrupt starch H-bonding and prevent macromolecular entanglement, making the polymer less connected. This leads to the initial increase of elongation at break. However, much less entanglement of macromolecules (mainly amylose), due to further plasticisation by plasticiser, could result in a reduction of elongation at break. As the [Emim][OAc] gives higher elongation at break compared to glycerol respectively, it suggests that [Emim][OAc] has a stronger plasticisation effect than glycerol.

Table 4-5 Tensile testing data of samples after conditioned at RH75%

Code	Tensile strength [MPa]		Young's modulus [MPa]		Elongation at Break [%]	
	Mean	RE*	Mean	RE	Mean	RE
RMS-G9	11	0.14	960	0.17	9	1.07
RMS-G18	5	0.06	95	0.23	35	0.39
RMS-G27	2	0.10	28	0.04	13	0.18
RMS-E9	9	0.11	663	0.17	25	0.60
RMS-E18	5	0.06	62	0.19	43	0.23
RMS-E27	3	0.03	24	0.11	27	0.09

*Relative error

As summarized in table 4-5, the relative error can provide some more information variability of the TPS produced. In general samples with a low level of plasticiser (both G and E) have a higher relative error. This suggests that these samples have a higher variability which could be an issue in practical applications.

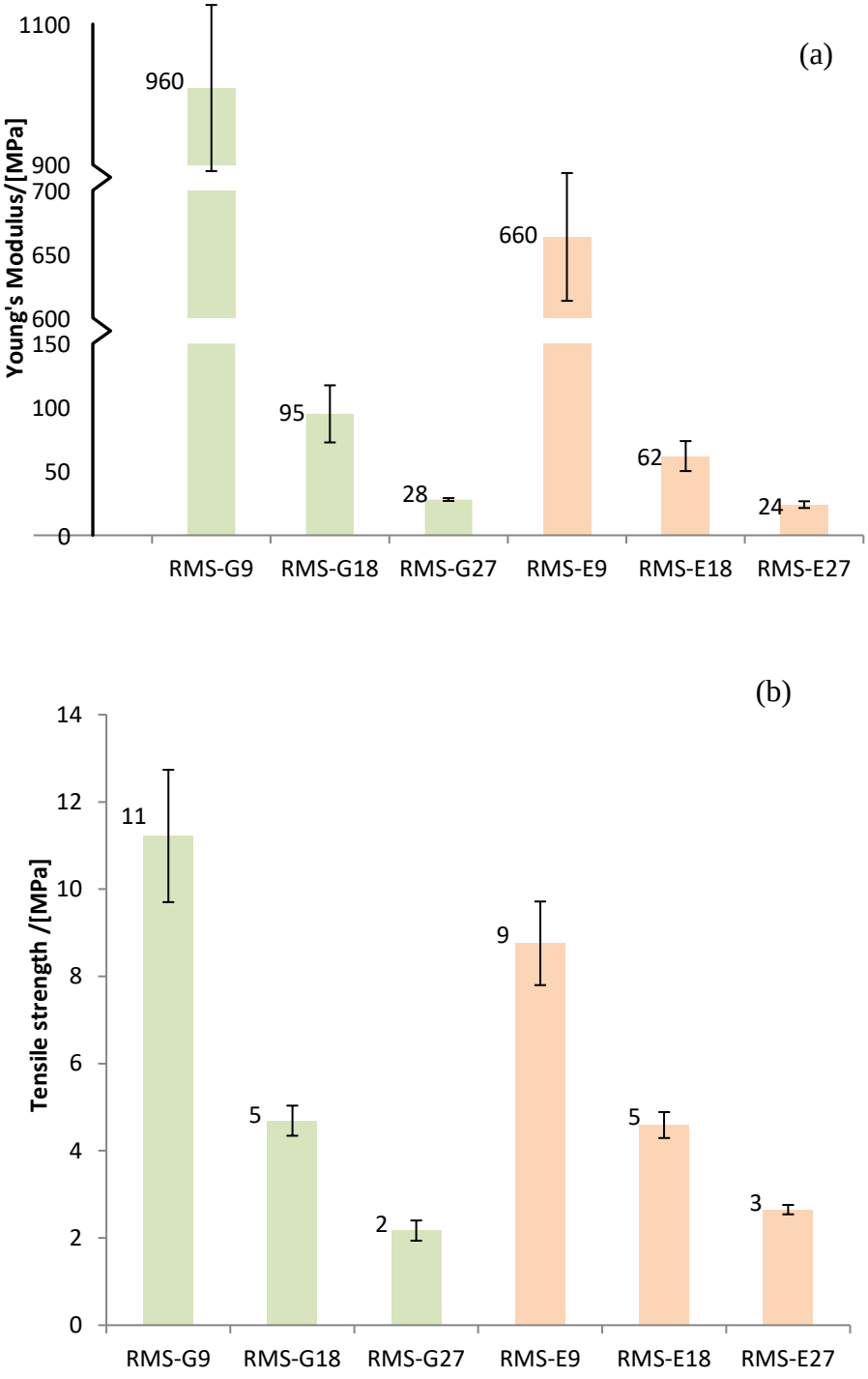

Figure 4-4 (a) Young's modulus of samples conditioned at RH75% [MPa]; (b) Tensile strength of samples after conditioned in RH75% [MPa]

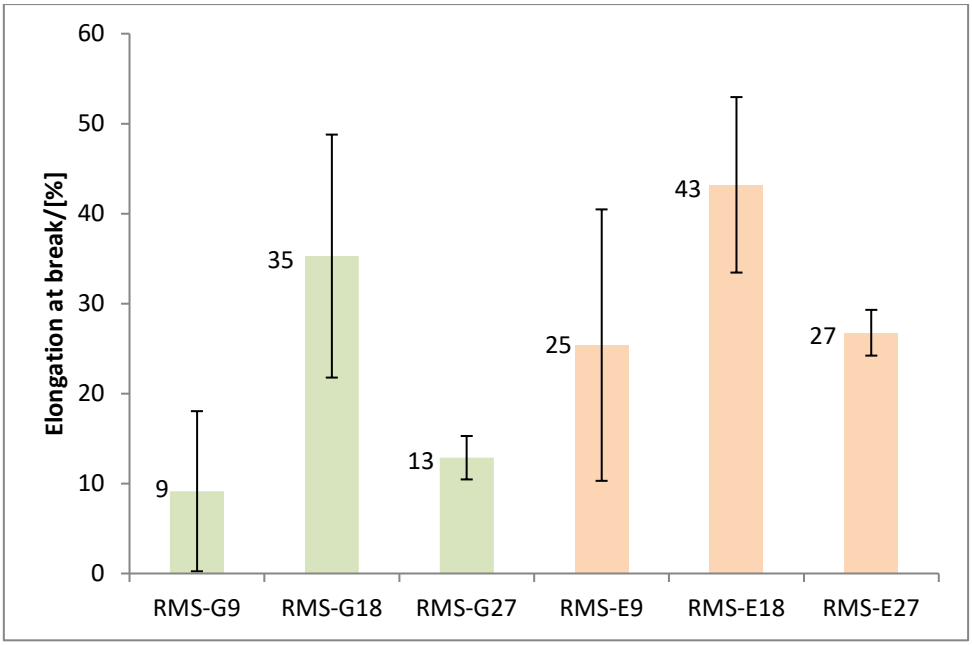

Figure 4-5 Elongation at break of samples after conditioned in RH75% [%]

Table 4-6 Tensile results of RMS-G27 and RMS-E27. RH0 are data for the dried samples from the vacuum oven, RH33, RH52 and RH75 are data from samples conditioned for 42 days at these design humidities

Code	Humidity	Tensile strength [MPa]		Young's modulus [MPa]		Elongation at break [%]	
		Mean	RE	Mean	RE	Mean	RE
RMS-G27	RH0	9.0	0.04	56	2.32	31	0.28
	RH33	13	0.03	890	0.09	23	0.23
	RH52	5.9	0.03	160	0.09	34	0.22
	RH75	2.2	0.10	28	0.04	13	0.18
RMS-E27	RH0	7.0	0.04	120	0.06	87	0.15
	RH33	9.7	0.04	310	0.02	67	0.15
	RH52	4.6	0.05	60	0.09	49	0.20
	RH75	2.7	0.04	24	0.11	27	0.09

To observe how the water uptake resulting from the conditioning RH affects the tensile properties, examples are given by table 4-6 and 4-7. At modest increases in water uptake the Young's modulus increases, but then at higher levels the Young's modulus falls sharply. Similar results were obtained in another study (Xie et al., 2015). A possible explanation of this is that water is considered an effective plasticiser of RMS (Mateyawa et al., 2013, Lourdin et al., 1997). Thus, to dry and rigid samples, increasing plasticiser amount can help in reducing the brittleness of the samples. However, over-absorption of water, as a plasticiser, will over-plasticize the RMS resulting in decreased tensile properties. The variation of tensile properties during the conditioning is uncertain due to this reason and in many cases the sample brittleness again made analysis of this problematic. Hence, it makes studying the molecular interaction

and crystallisation behaviour very significant to understanding the mechanical property changing mechanism and optimising the mechanical properties.

Table 4-7 Tensile testing results of RMS-G27 and E27 conditioned at RH75% over time

Code	Time (days)	Water Uptake Percentage	Tensile strength [MPa]		Young's modulus [MPa]		Elongation at break [%]	
		Mean	Mean	RE	Mean	RE	Mean	RE
RMS-G27	0	0.00%	9.0	0.04	560	0.23	31	0.28
	7	7.92%	3.1	0.06	24	0.17	28	0.21
	14	10.43%	3.1	0.08	46	0.16	27	0.23
	28	14.45%	2.5	0.17	27	0.10	19	0.41
	42	12.94%	2.2	0.10	28	0.04	13	0.18
RMS-E27	0	0.00%	7.0	0.04	120	0.06	87	0.16
	7	11.18%	3.6	0.04	25	0.07	48	0.11
	14	14.29%	2.7	0.08	24	0.08	29	0.18
	28	19.37%	2.6	0.06	22	0.08	25	0.12
	42	17.05%	2.7	0.04	24	0.11	27	0.09

4.3.4 Characterisation after Sample Conditioning

4.3.4.1 FTIR and Raman Spectroscopy

FTIR spectra were analysed using the band assignment information in table 4-8 which were derived from literature.

Table 4-8 FTIR and Raman spectra assignment

Material	Band assignment	Infrared	Raman	References
[Emim][OAc]	CN bond oscillation	634	608,642	(Dhumal et al., 2009)
	CCH wag from imidazole ring		710	
	OCO bend from acetic anion		908	
	CNC stretch from imidazole ring		966	
	CCH scissor		1028	
	CH_2 wag (C6 H16 H17)		1099	
	NCH twist	1174		
	CH_2 bending			
	- from anion	1325	1342,1392,1	
	- from linking part of ethyl at the cation side	1377	460	
	CH_2 scissor		1427	
	NCH bend	1560	1576	
	CH stretching	2800-3000		
Regular maize Starch	Skeletal modes of pyranose ring		488	(Cael et al., 1974, Cael et al., 1973, Dhital et al., 2011, Kizil et al., 2002)
	CH_2 deformation		872,1470	
	COC α-1,4 glycosidic linkage	930	947	
	COH bending mode		1092	
	CO and CC stretching with COH bend combination		1134	
	CH_2OH side chain related mode		1263	
	COH deformation	993		
	CH bending	1078		
	COC stretching from pyranose ring	1151		
	CH_2OH (side chain) related mode	1248		
	Water adsorbed in the amorphous regions of starch	1641		
	CH stretching	2800-3000	2800-3000	
	OH stretching	3000-3600		
Glycerol	Primary CO stretching	1032		(Mendelovici et al., 2000, Pouchert, 1981, Simons, 1978)
	Secondary CO stretching	1109		
	Aliphatic CH stretching	2800-3000		
	OH stretching	3000-3600		

Figure 4-6 shows the fingerprint region for the RMS-E samples compared to those of the raw ingredients. The behaviour of the bands assigned at 1335 cm^{-1}, 1404 cm^{-1} and 1566 cm^{-1} are related to the interactions between the starch and IL as none of these could be seen in the raw

starch spectra. It can be observed that bands at 1335 cm^{-1}, 1404 cm^{-1} and 1566 cm^{-1} of processed TPS samples seem to be the up-shifted bands from 1325 cm^{-1}, 1377 cm^{-1} and 1560 cm^{-1} of IL spectra respectively. Since all of these bands are assigned to a bending mode, an up-shift of wavenumber suggests that a stronger molecular interaction is occurring (usually hydrogen bonding). In this case, it is assumed that CH_2 groups from the acetic anion, the CH_2 group of ethyl adjacent to the imidazole ring from the cation and the NH group on the imidazole ring which correspond to the 1325 cm^{-1}, 1377 cm^{-1} and 1560 cm^{-1} peaks respectively are interacting with starch molecules (figure 4-7).

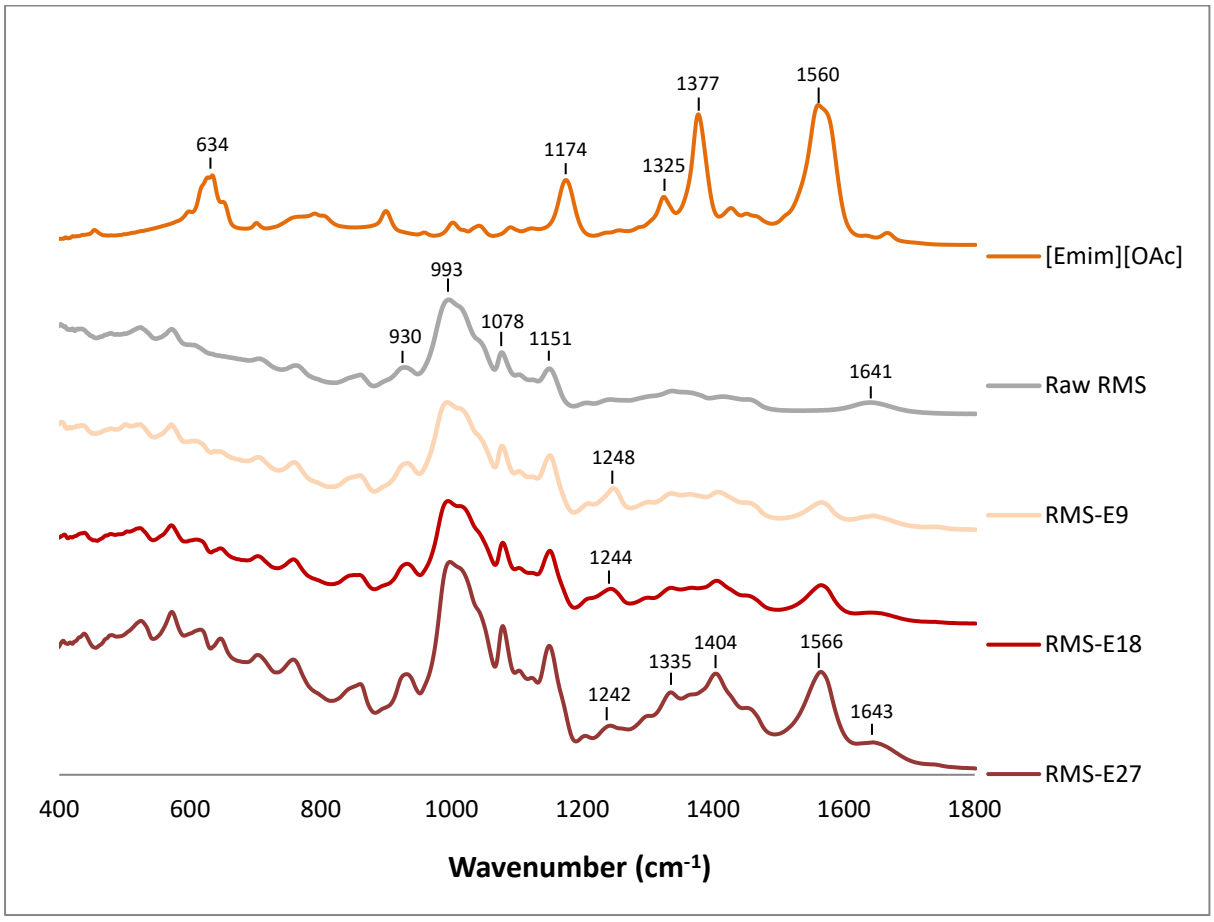

Figure 4-6 FTIR fingerprint region spectra of raw RMS, pure [Emim][OAc] and RMS-E series

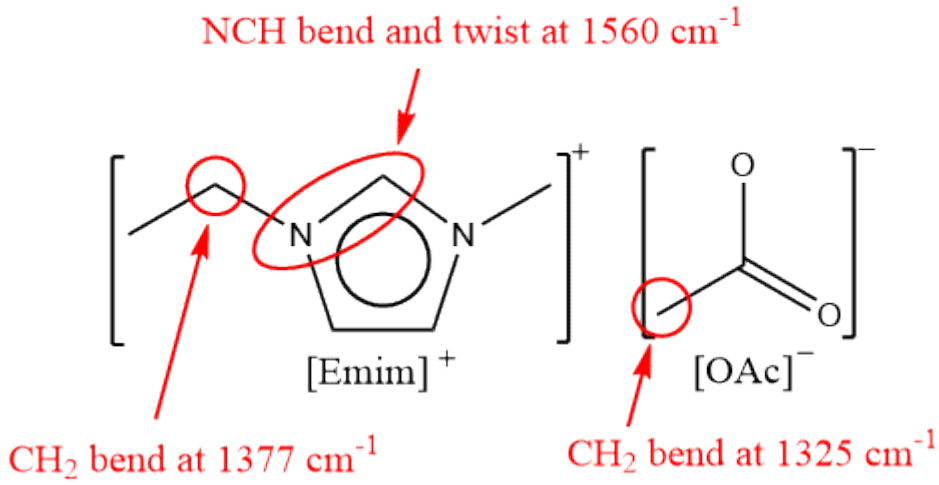

Figure 4-7 Corresponding molecular interactions on [Emim][OAc] structure indicated by FTIR spectroscopy at 1325 cm-1, 1377 cm-1 and 1560 cm-1.

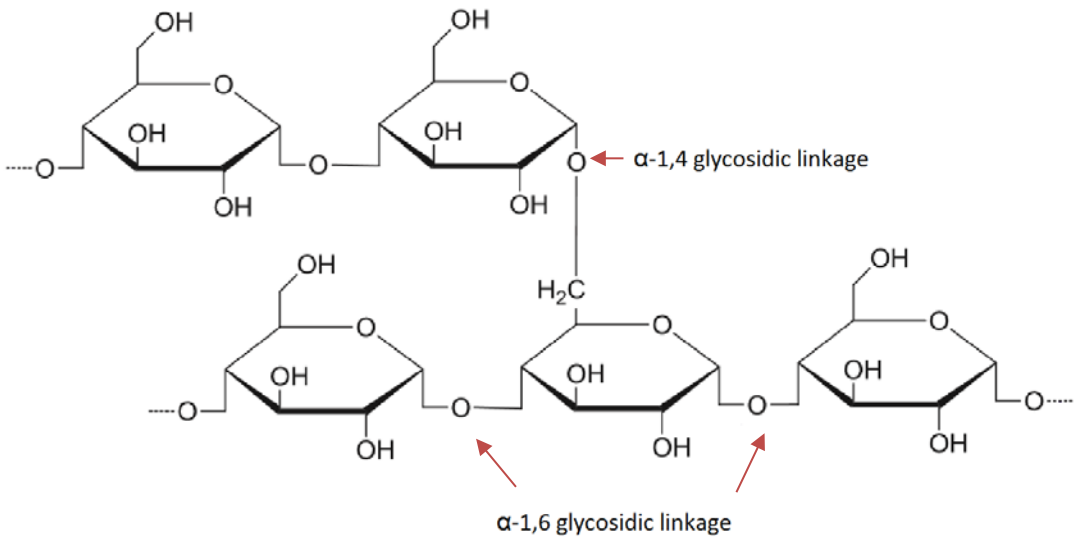

Figure 4-8 Amylopectin structure (adapted from Xie et al., 2013)

The band positions from raw starch and TPS spectra at 930 cm^{-1}, 993cm^{-1}, 1151cm^{-1} suggests that a-1,4 glycosidic linkage of starch molecules, COH and COC structure from pyranose are less likely to interact with IL (figure 4-8). However, a small band at 1248cm^{-1} from TPS sample spectra indicates that CH_2OH group from the side chain is more likely to interact with the IL.

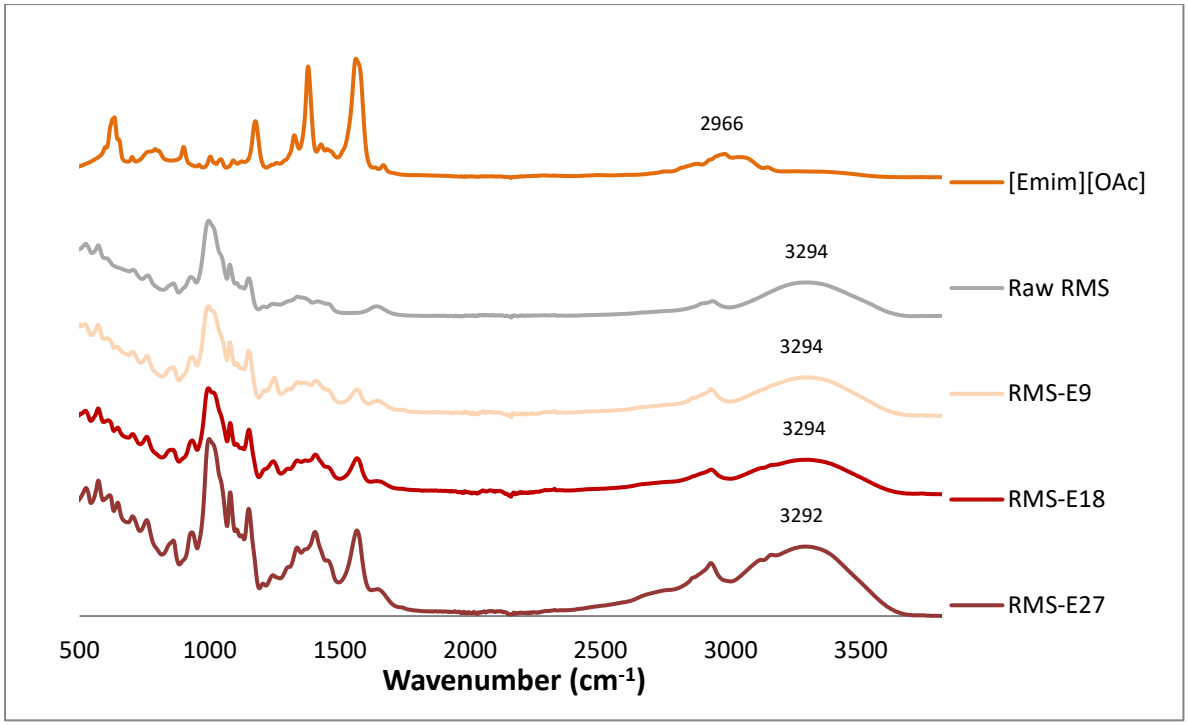

Figure 4-9 Full FTIR spectra of raw RMS, pure [Emim][OAc] and RMS-E series

Figure 4-9 shows the full spectra for the RMS/IL samples. The strong and broad band with a peak location at 3294 cm^{-1} in raw RMS sample indicates the existence of a strong OH polymeric interaction (in contrast the peak in an isolated hydroxyl group is at 3450-3570 cm^{-1}) (Pouchert, 1981, Simons, 1978). This band is absent in [Emim][OAc]. The TPS samples plasticized by [Emim][OAc] have the same bands at about the same position, which suggests that the IL does not have a stronger effect on OH groups of starch.

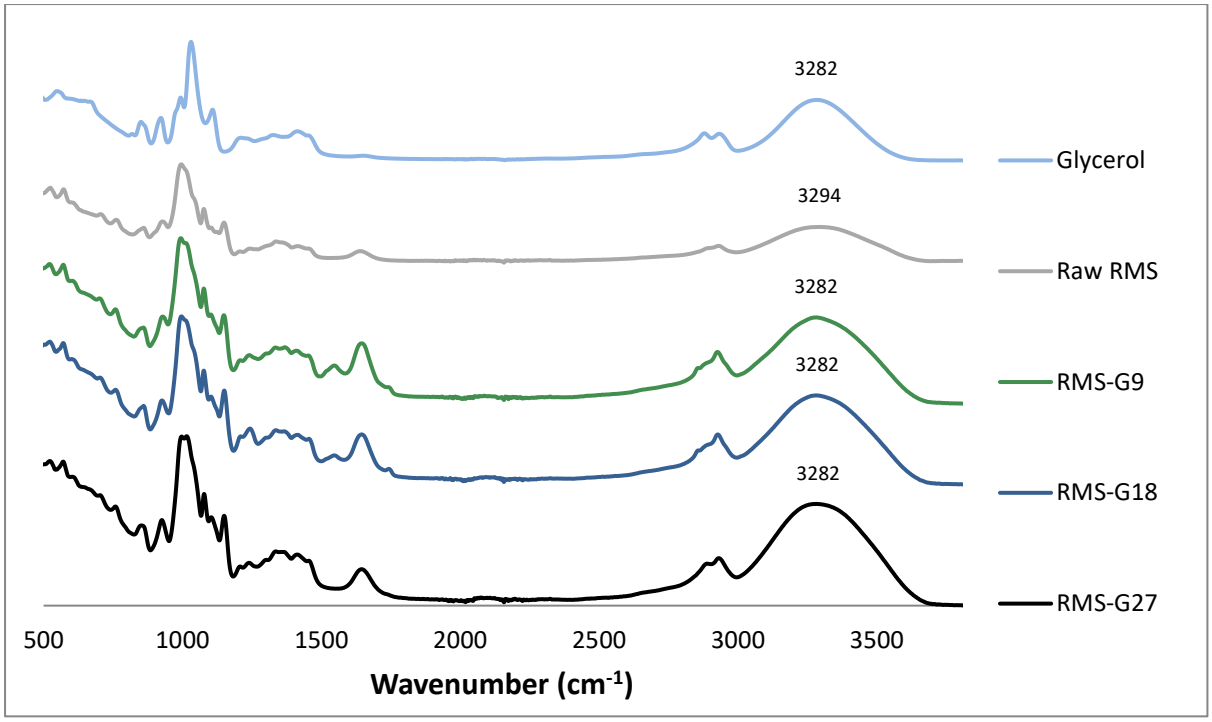

Figure 4-10 Full FTIR spectra of raw RMS, pure glycerol and RMS-G series

Figure 4-10 displays the FTIR spectra of TPS plasticized by glycerol. Since glycerol and RMS have peaks in similar positions, it is difficult to identify changes which occur during plasticisation. However, at higher wavenumber it is observed that the OH stretching vibration of these samples shifts down to 3282 cm^{-1}, the same as pure glycerol. This suggests that the dominant interaction between glycerol and starch occurs at the hydroxyl. Compared to [Emim][OAc], OH groups mostly contributed by starch molecules would have a stronger hydrogen bonding in glycerol plasticized TPS. The results of FTIR spectra reveal that the effect on starch of IL and glycerol is different. It can be concluded that glycerol interacts with TPS by mainly affecting the hydrogen bonds between hydroxyl group of starch and glycerol. In contrast, [Emim][OAc] interacts with starch on its conjugated system.

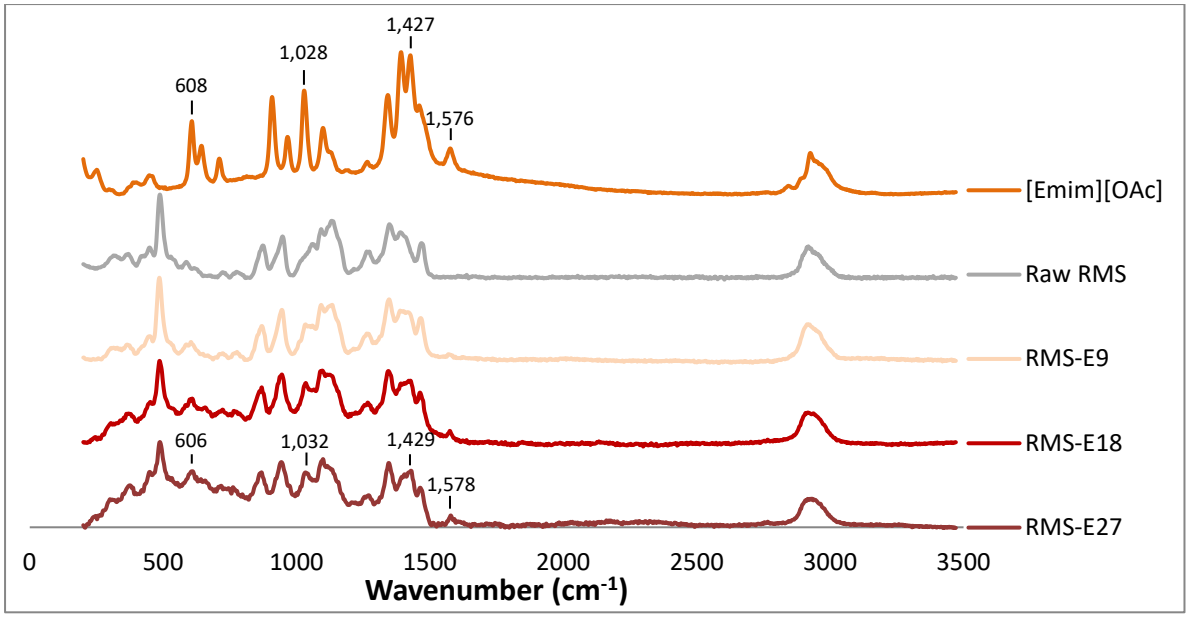

Figure 4-11 Full FT-Raman spectra of raw RMS, pure [Emim][OAc] and RMS-E series

The suggested molecular interaction of starch and [Emim][OAc] is also supported by Raman spectra of these (see figure 4-11). Details of band characterisation are given in table 4-8. The majority of assigned bands are very similar between raw RMS samples and IL plasticized TPS samples. However, significant changes can be seen at 1032 and 1429 cm^{-1} which are related to the CCH and CH_2 scissoring vibration of [Emim][OAc] as analysed from FTIR spectra. CN oscillation has a slight change at 606 cm^{-1} suggesting potential interaction position but this signal is not very obvious.

In contrast, Raman spectra of glycerol plasticized TPS (figure 4-12) does not have any apparent differences in the results. This is due to the dipole OH stretching signal being very weak in Raman spectra. Hence interaction between hydroxyl groups cannot be characterized either.

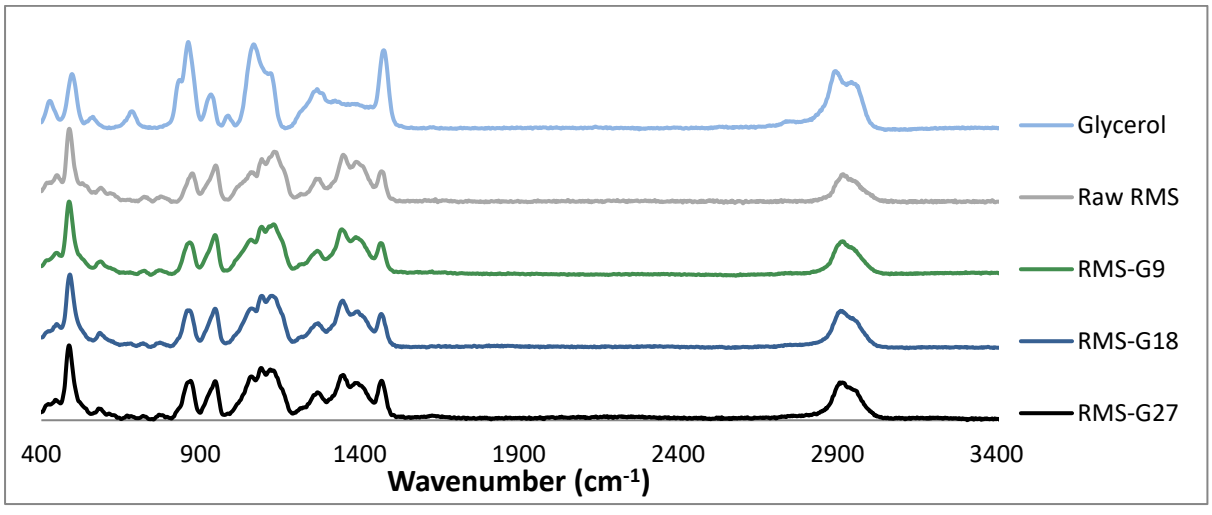

Figure 4-12 Full FT-Raman spectra of raw RMS, pure glycerol and RMS-G series

4.3.4.2 XRD

The X-ray diffractograms of TPS samples plasticized by [Emim][OAc] and glycerol are presented in figure 4-13 and figure 4-14 respectively. Samples which were dried before conditioning and samples which were conditioned at RH75% are coded with RH0 and RH75, respectively.

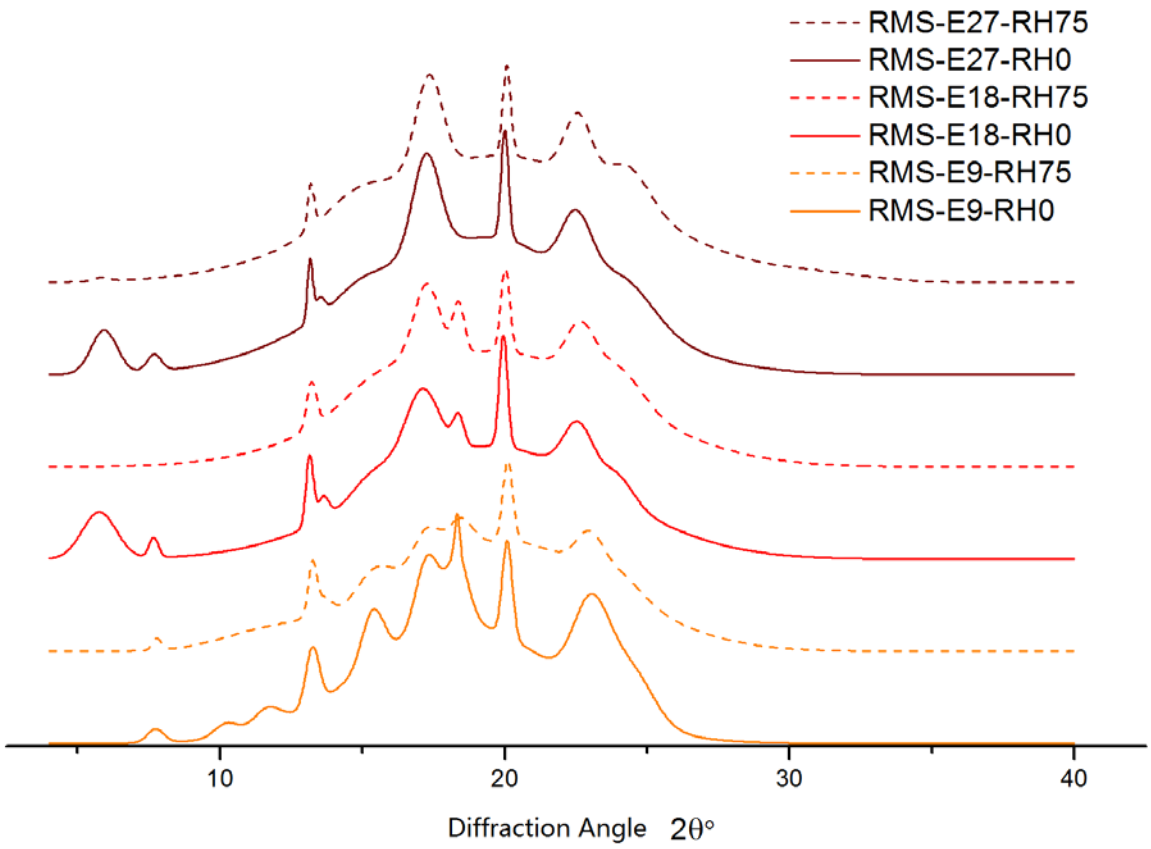

Figure 4-13 XRD diffractogram of RMS-E series samples. The baseline of individual pattern is shifted.

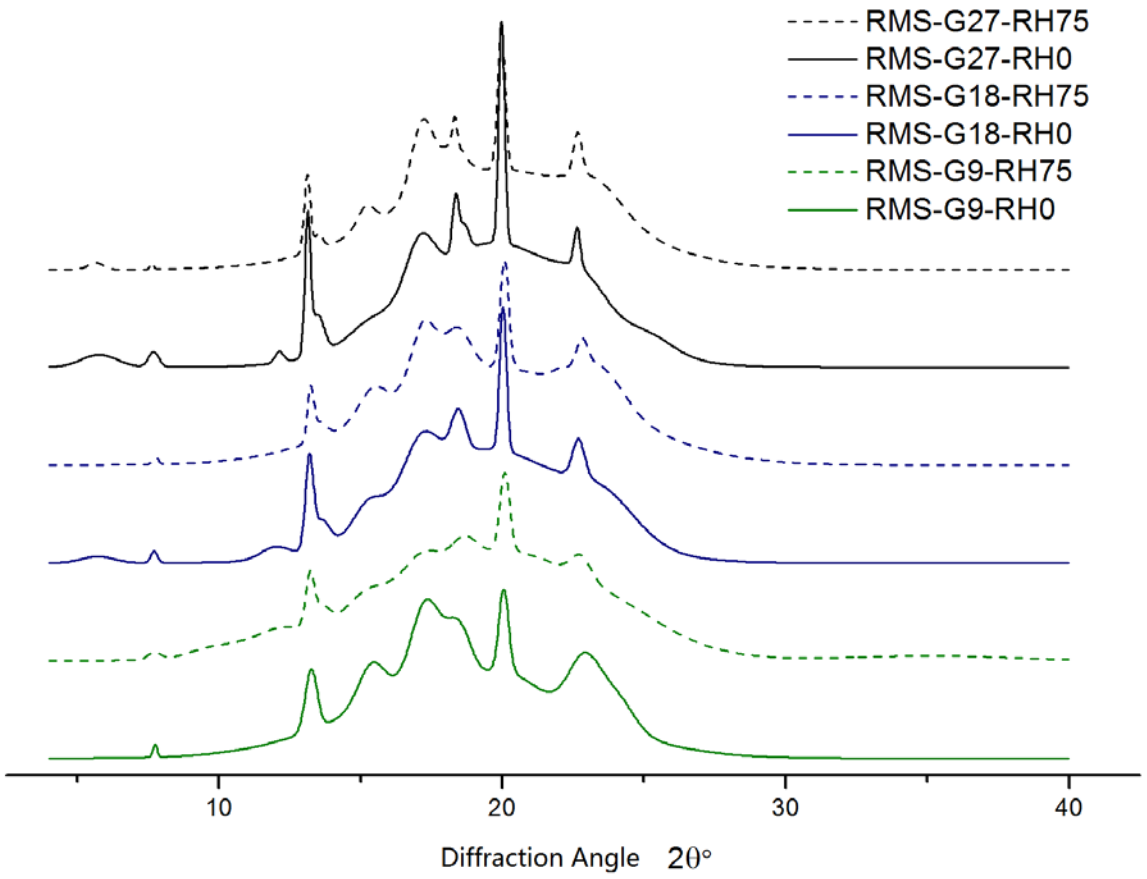

Figure 4-14 RMS-G Series XRD diffractogram

The XRD results show that crystalline structures exist in all of the samples. Possibly part of the crystalline structure corresponds to undestroyed crystals from the natural starch granules and part from recrystallisation. As summarised in table 4-9, thermal processing significantly decreased the degree of crystallinity of native starch from 39.5% (Xie et al., 2015).

RMS-E9-RH0 shows obvious peaks at 2θ of 15°, 23° and a doublet at 17° and 18°, which are evidence of the A-type crystalline structure (Cheetham and Tao, 1998, Lopez-Rubio et al., 2008, Xie et al., 2014, Xie et al., 2015). Other strong peaks at 2θ of 7°, 13°, 20° and 22°, which overlaps with 23°, are indicative of a V-type crystalline structure (Xie et al., 2014). The diffractogram of RMS-E9-RH75 shows a similar pattern, however with lower intensity. The main characteristics of A-type crystalline and V-type crystalline remains suggesting that the crystal structures have not changed. However, broader peaks suggest either a reduction in the size or increasing defects of the crystallites, leading the total crystallinity of RMS-E9-RH75 being lower compared to RMS-E9-RH0 (see table 4-9).

It has been found that V-type crystal structure exists in all of the samples. RMS-E18-RH0 displays strong reflections at 2θ of 17°, 23°, a characteristic peak at 5° 2θ and a small peak at 14° 2θ. These peaks significantly suggest a characteristic B-type crystallinity. With a small peak at 18° 2θ suggesting that A-type crystals still exist, subtle shoulders are also observed at 15° and 23° 2θ. Together, these facts indicate that the crystalline structure of this sample includes both A- and B-type features. Thus RMS-E18-RH0 is classified as C-type. However, when it comes to RMS-E18-RH75, the fact that specific reflections at 2θ of 5° and 14° have disappeared and the doublet becomes obvious means B-type crystal structure disappeared and A-type crystal come to be predominant after conditioning.

RMS-E27-RH0 shows a typical B-type crystal pattern which includes a diagnostic peak at 2θ of 5°, isolated strong peak at 17° 2θ without doublet and a shoulder affected by V-type crystal at 23° 2θ and a small shoulder at about 14° 2θ. However, the reduced peaks at 5° 2θ and 14° 2θ implies the reduction of B-type crystal after conditioning.

Glycerol samples have the same V-type crystal characteristics in all different samples. Similarly, peaks at 2θ of 15° and 23°, and a doublet at 17° and 18° identify the typical A-type structure in all of the glycerol samples. However, a very small but broad peak appears at 5° 2θ suggesting the existence of B-type structure in RMS-G18-RH0, RMS-G27-RH0 and RMS-G27-RH75. Therefore, the crystalline structure of these samples is classified as C-type while the others are A-type.

Potentially due to the strong interaction between plasticisers and starch, the increase of plasticiser level is converting A-type crystalline to B-type crystalline in samples (as C-type is a combination of A and B-type, hence , it could be an intermediate state in this case) (Imberty et al., 1991, Lopez-Rubio et al., 2008), allowing more cavities in crystals to trap water from the environment. This also leads to a reduction in degree of crystallinity prior to conditioning from 34.81% to 23.52% for [Emim][OAc] and 35.87% to 25.74% for glycerol.

To the contrary, water absorption tends to decrease the B-type crystalline structure by potentially mobilizing the molecules of starch and relaxing the material. Similarly, the degree of crystallinity decreases after conditioning. As a result of B-type crystalline being destroyed, the cavities which can hold water were also destroyed and released water out from the TPS. Thus, this potentially explains the peak in water uptake trend mentioned in 4.3.2.

Compared to the same level, generally [Emim][OAc] plasticized RMS has a lower crystallinity than glycerol. The reason is believed to be that [Emim][OAc] has a different type of interactions with starch, and starch molecular connections of RMS-E series sample are weaker than RMS-G series, as indicted by FTIR/Raman spectroscopy results. The [Emim][OAc] plasticized RMS therefore forms either more amorphous regions in TPS or looser packed crystals, which will fall apart when water is absorbed, when compared to glycerol. Thermal mixing and compression moulding would induce the newly formed single helix V-type crystalline structures (van Soest et al., 1996b, Xie et al., 2014). V-type crystallinity decreases when a higher level [Emim][OAc] was used. The water uptake can be another cause of V-type crystallinity reduction. However, the presence of glycerol in TPS results in either larger or more perfect V-type crystallites as the diagnostic peaks of V-type crystal are sharper in figure 4-14. Referring to the tensile testing results, it can be found that usually highly crystallized samples have a higher tensile strength and Young's modulus.

Overall, the choice of plasticiser type and quantity is the predominant factor in controlling mechanical properties, as the molecular interaction has a direct effect on the resulting intermolecular forces. Mechanical properties are also related to the degree of crystallinity, though this effect is less prominent. The types of crystallites are influenced by plasticiser, processing and conditioning RH and this in turn is correlated with the moisture uptake.

Table 4-9 Crystalline pattern and crystallinity of RMS samples

Code	RH 0				RH 75%			
	Degree of crystallinity [%]			Pattern	Degree of crystallinity [%]			Pattern
	Double Helices	V-type	Total		Double Helices	V-type	Total	
Native RMS*	39.5	-	-		39.5	-	-	
RMS-E9	29.45	5.36	34.81	A	21.27	4.00	25.27	A
RMS-E18	22.09	4.62	26.71	C	19.33	3.29	22.62	A
RMS-E27	20.28	3.24	23.52	B	18.25	2.35	20.60	B
RMS-G9	30.03	5.84	35.87	A	22.29	4.30	26.59	A
RMS-G18	23.25	6.47	29.72	C	20.96	4.53	25.49	A
RMS-G27	17.82	7.92	25.74	C	18.54	5.75	24.29	C

*Note that the native RMS was not conditioned. Also the V-type crystallinity pattern was not achievable due to weak and overlapping signals (Xie et al., 2015).

4.3.5 TGA

Figure 4-15 and 4-16 show first derivative curves showing the temperatures at which mass loss occurs were calculated from the heat flow raw data. Different RH conditions do not affect TGA results. Hence only the effects of different formulations are displayed.

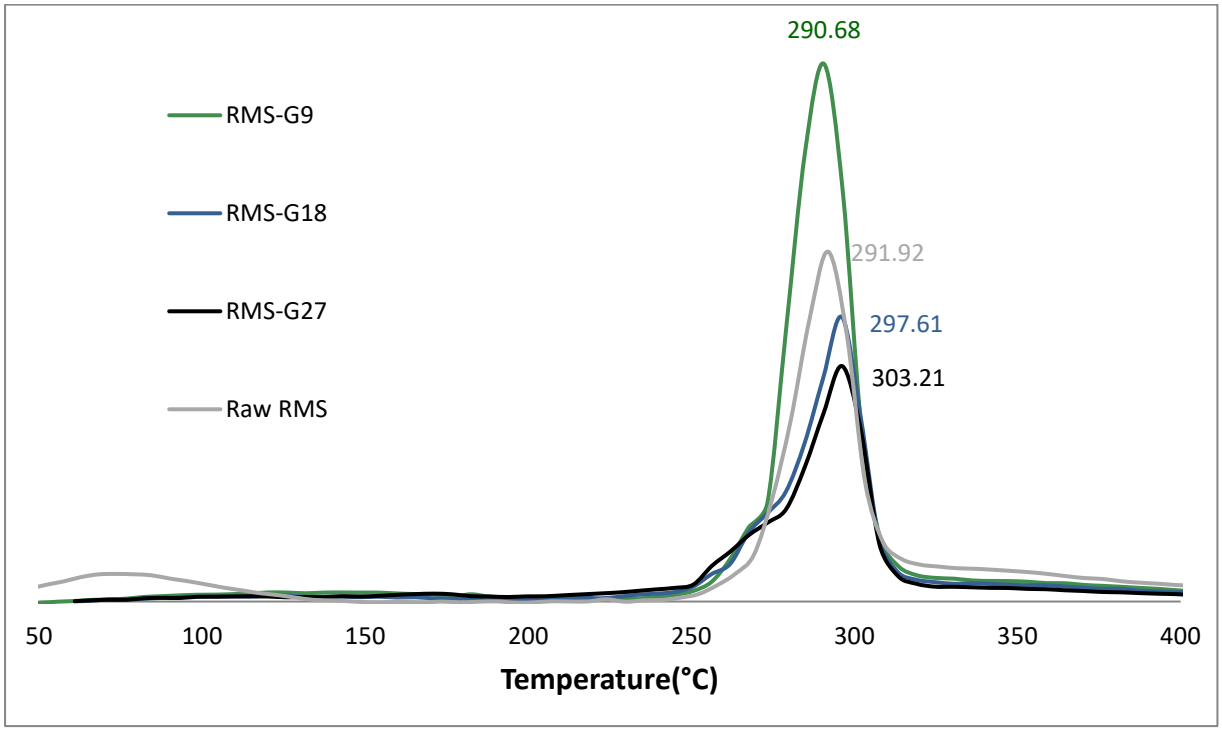

Figure 4-15 First derivative TGA results of RMS-G series compared with raw RMS

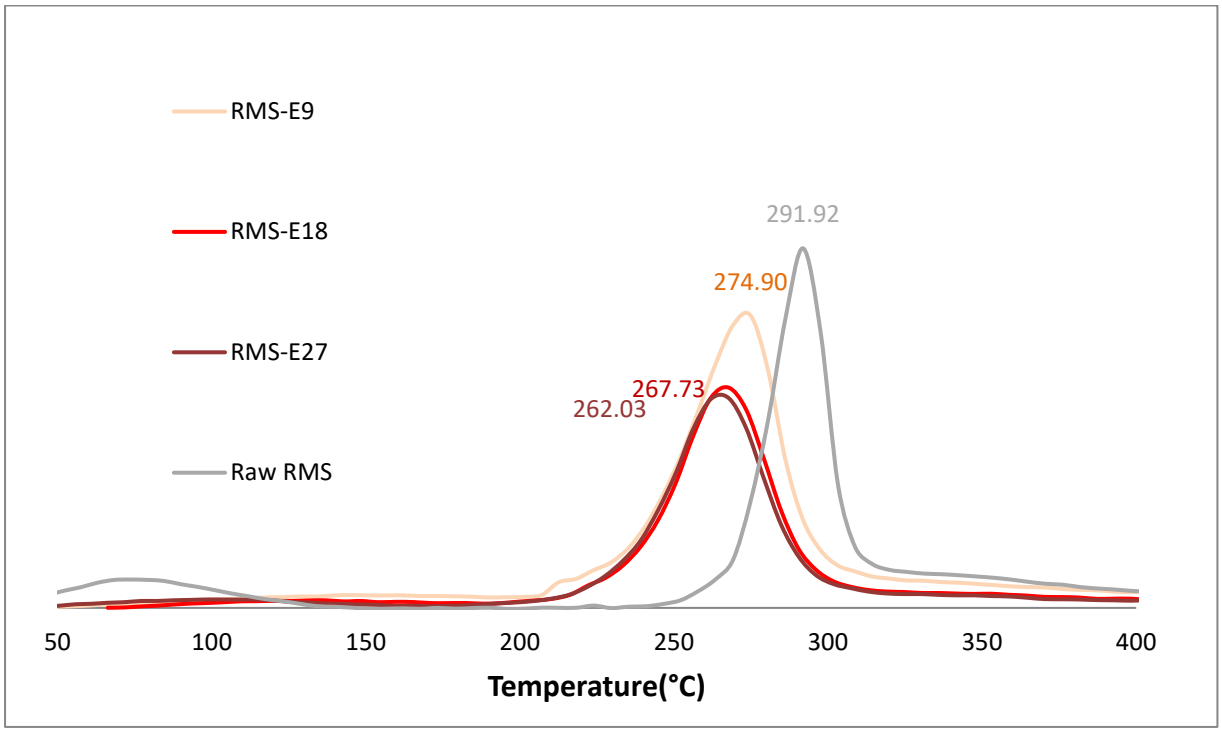

Figure 4-16 First derivative TGA results of RMS-E series compared with raw RMS

Raw RMS has a broad peak at about 80°C which starts approximately from 40°C and ends at around 120°C. Water evaporation is most likely responsible for this peak. A study suggests that water evaporation beyond 100°C is related to molecular interaction between water and starch which restrains the water loss (Esmaeili et al., 2017). Centred at about 292°C, a sharp peak appears corresponding to the highest degradation rate of the raw starch starting at approximately 240°C.

RMS-G9, RMS-G18, RMS-G27 do not show any water evaporation which suggests that glycerol has a good ability to bind starch and water. In terms of the temperature at the peak thermal degradation rate, RMS-G9 is at about 291°C, RMS-G18 is at about 298°C, RMS-G27 is at about 296°C which are close to the glycerol boiling point 290°C (Esmaeili et al., 2017). All of them start at between 240°C-250°C. Therefore, it is seen that adding glycerol does not have much effect on the temperature of the peak degradation rate, with a range observed of less than 10°C. Similarly, the onset temperature of heat degradation is not largely affected.

At lower temperatures [Emim][OAc] plasticised samples behave similarly. The lack of water evaporation peak at low temperature in processed samples indicates that [Emim][OAc] has a parallel ability of water capturing compared to glycerol. However, the peak degradation rate temperature of RMS-E9, RMS-E18 and RMS-E27 lower to 275°C, 268°C and 262°C respectively. The range of degradation temperature change is up to about 30°C. Degradation onset temperature drops from near 240°C to 200°C.

Such results are supported by similar studies which suggest that the decrease of thermal degradation temperature of the starch is caused by molecular weight decrease during solution processing with heat (Xie et al., 2014, Zhang et al., 2016).

In this case, combining the results from FTIR and Raman spectroscopy, it is believed that the nature of interactions with [Emim][OAc] creates this difference. Strong hydrogen bonding between starch OH groups and glycerol in RMS-G series makes the degradation onset and peak temperature higher, as supported by a similar study which showed that a higher starch thermal stability can be obtained by using sorbitol compared to glycerol (Esmaeili et al., 2017). In contrast, the molecular interactions between the conjugated system of [Emim][OAc] and starch leads to a lower degradation onset and peak temperature in these samples.

4.4 Conclusions

The results from FTIR spectroscopy and Raman spectroscopy, revealed that higher levels of plasticisers give stronger molecular interactions in the TPS system. Consequently, mixing results during processing are obviously influenced by this factor. Stronger interactions result in lower mixing torques and hence lower energy for processing. Meanwhile, the molecular interactions with [Emim][OAc] are different from glycerol. XRD analysis shows that the crystallisation behaviour, crystal morphology and crystallinity are all influenced by the plasticisers. An interaction between starch hydroxyls and conjugated systems of [Emim][OAc] tends to form more amorphous regions or looser packed crystals than glycerol plasticized samples. As a result, the RMS-E series samples generally showed a greater water uptake, resulting in lower mechanical strength and higher flexibility than the RMS-G series.

In this study, [Emim][OAc] as an IL has demonstrated its ability to lower processing torques and actual melt temperatures which is good for processing. At the same time, it makes RMS a more ductile material. Also, it was found that the mechanical properties are related to the crystallite structure and crystallinity changes during conditioning. However, the mechanical strength and thermal stability are reduced which are potentially undesirable. Hence, it would be significant to balance these different material characteristics to achieve material properties optimisation.

Even though the properties of RMS plasticised with [Emim][OAc]were poorer than for glycerol, there was a clear processing advantage. Therefore, studying alternative ILs would be beneficial, which is the focus of the following chapter. Further investigation on how starch interacts with different chemical parts and how these interactions affect the microstructure and material properties of TPS would also be of great significance in further studies in order to optimize material properties.

5 EFFECTS OF [AMIM]CL/[BMIM]CL ON RMS PROCESSING

5.1 Introduction

In Chapter 4, the effects of [Emim][OAc] were investigated and compared to glycerol. It was found that using [Emim][OAc] yielded a more ductile material with a reduction of thermal degradation temperature and lower tensile strength and Young's modulus. It was found that the interactions with ionic liquid were very different to glycerol, and hence this greatly influenced the final properties. However, whether these kinds of interactions are unique to [Emim][OAc] and how they can be controlled and optimized are still unclear. Therefore, in order to expand knowledge of starch plasticisation by ionic liquids, this chapter will investigate the effects of RMS processed by two other ILs, 1-Allyl-3-methylimidazolium chloride [Amim]Cl and 1-Butyl- 3-methylimidazolium chloride [Bmim]Cl. These ILs have been widely investigated and reported to be effective in plasticizing starch and other bio-polymers (Ren et al., 2017, Zhao et al., 2015).

[Amim]Cl and [Bmim]Cl also have an imidazole ring which can potentially interact with starch in a similar way to [Emim][OAc]. The great electronegativity of the Cl anion means it is very likely to form hydrogen bonding with any OH group it encounters.

In this chapter, mechanical properties and water uptake will again be studied during conditioning. Crystallinity, thermal stability and molecular interaction will be studied after conditioning. Results of RMS plasticized by [Amim]Cl and [Bmim]Cl will be compared to each other and also along with the outcomes in Chapter 4.

5.2 Experimental

5.2.1 Materials

The starch used in this experiment was still RMS. [Amim]Cl and [Bmim]Cl were used as plasticisers. Details are as outlined in chapter 3.2. Experimental Methods.

Since the results obtained with a low plasticiser level and low (RH 33%) proved unreliable this chapter only focusses on the higher plasticiser and humidity levels. Samples were prepared similarly by compression moulding and mixing as described in chapter 3.3.1, with the compositions as detailed in table 5-1.

Table 5-1 Sample formulation design

Code	Starch Type	Starch Amount	Water	[Amim]Cl	[Bmim]Cl
RMS-A9	RMS	100	21	9	
RMS-A18	RMS	100	12	18	-
RMS-A27	RMS	100	3	27	-
RMS-B9	RMS	100	21	-	9
RMS-B18	RMS	100	12	-	18
RMS-B27	RMS	100	3	-	27

The sample sheets produced by compression moulding were then conditioned at two different humidity levels and characterised over time using the following techniques:

Mechanical properties — Tensile testing (section 3.3.3.1)

Water absorption — Water uptake measurement (section 3.3.2.1)

After conditioning was completed, (as indicated by no further weight change in the water uptake measurement) the samples were characterised by the following methods:

Molecular Structure — FTIR spectroscopy (section3.3.3.3)

Raman spectroscopy (section 3.3.3.4)

Crystal structure — XRD (section3.3.3.5)

Thermal stability — TGA (section3.3.3.2)

These tests were performed according to the schedule given in table 5-2. Note that the samples are very sensitive to RH environment at the beginning of conditioning. The tensile tests, therefore, were not performed until 7 days conditioning as it would take several hours to finish testing all samples. In addition, some of the samples were too brittle at time zero. Also by definition, water uptake at time zero is zero. Therefore, there is no time zero measurement for either of the tests.

Table 5-2 Conditioning schedule

Time (days)	0.25	1	3	7	14	28	42
Water uptake measurement	×	×	×	×	×	×	×
Tensile testing				×	×	×	×

5.3 Results and Discussion

5.3.1 Mixing Torque

Similarly to the work described in chapter 4, material compounding and processing are fundamental to this study since achieving homogeneous material is still the basic goal.

Figure 5-1 (a) and 5-1 (b) summarizes typical torque values recorded over the mixing time of each sample. Every sample displayed a typical loading peak at the start and a rise in the torque to a maximum value. In both the RMS-A and RMS-B series the latest peak time was found in the samples with the middle level of plasticiser. All the mixing curves approached an asymptote, indicating a homogeneous outcome. The results obtained were reasonably reproducible over the 3 replicates of each formulation, therefore the data summary of mixing process is shown in table 5-3 as mean values together with Fisher post hoc comparisons of significant differences ($p<0.05$), where, in a column, values that do not share a letter are significantly different.

Table 5-3 Mean value of thermal mixing data of RMS-A and RMS-B series samples (in each column entries that do not share a letter are significantly different, Fisher comparisons $p<0.05$)

Code	Peak Time [min]	Peak Torque [Nm]	Final Torque [Nm]	Temp at Peak [°C]	Final Temp [°C]
RMS-A9	4.0^{b}	6.6^{c}	4.9^{b}	94.9^{b}	97.8^{d}
RMS-A18	5.2^{a}	7.9^{b}	6.0^{a}	96.8^{a}	98.5^{b}
RMS-A27	3.7^{bc}	10.4^{a}	6.8^{ab}	95.7^{ab}	98.8^{a}
RMS-B9	3.2^{c}	6.5^{c}	4.8^{c}	92.6^{c}	97.4^{e}
RMS-B18	4.4^{b}	7.9^{b}	5.3^{ab}	95.3^{ab}	97.8^{d}
RMS-B27	3.0^{c}	10.4^{a}	6.1^{bc}	94.0^{bc}	98.2^{c}

There was no noticeable smell of chlorine after the processing of RMS-A and B series samples. Samples remained soft even after cooling.

As summarized in table 5-3, increasing levels of plasticiser gave higher values of peak torque, final torque and final temperature. Potentially, larger amounts of plasticisers mean stronger plasticiser-water interaction and less water to interact with starch. Hence, the friction between mixing chamber and material might increase resulting in a higher final torque and final temperature. Comparing samples plasticized by the same level of [Amim]Cl with [Bmim]Cl, it appears that the RMS-B series displays slightly lower processing torques and temperatures, although this is not statistically significant in these data. However, when compared to RMS-G and E series (Table 4-3), it is seen that RMS-A and B can lower the processing torque by about 1-3 Nm and the temperature by 1-2 °C. Bigger differences occur at higher plasticiser levels.

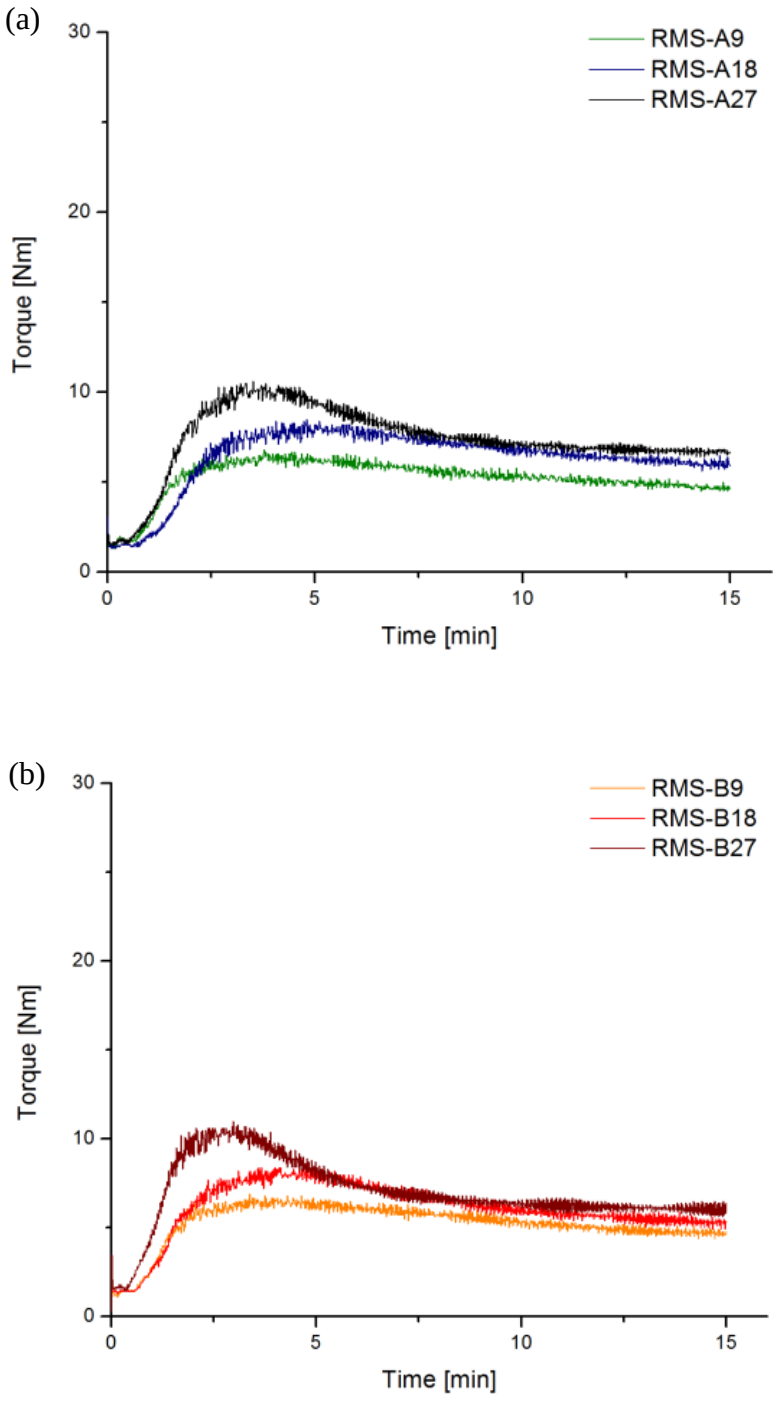

Figure 5-1 (a) Mixing torque over processing time of RMS-A series; (b) Mixing torque over processing time of RMS-B series

5.3.2 Water Uptake

It has been demonstrated that water sensitivity is a vital character of TPS after processing and thus significantly influences most of the material properties in chapter 4. Hence, water uptake measurement has been performed again and mean percentages have been calculated out of 5

results from each type of samples. The water uptake results are displayed in table 5-4, with standard deviation values not presented. Details can be found in figure 5-2 and figure 5-3.

Table 5-4 Water uptake mean percentages (increased from original weight) at equilibrium

Code	RMS-A9	RMS-A18	RMS-A27	RMS-B9	RMS-B18	RMS-B27
RH52	5.44%	7.08%	8.28%	5.50%	6.17%	7.89%
RH75	10.86%	13.70%	17.65%	10.15%	12.24%	15.65%

According to table 5-4, there is almost no doubt that higher plasticiser level and higher conditioning RH can lead to a higher water uptake percentage. Comparing the same levels of plasticiser for [Amim]Cl and [Bmim]Cl, it can be observed that samples plasticized by [Bmim]Cl are more hydrophilic. However, these results show that the water uptake percentages of RMS-A and RMS-B series are generally higher than RMS-G series. The RMS-E series only give similar results at a conditioning RH of 75% and a plasticiser level of 18 or 27. However the major influence on water uptake percentage remains the RH level during conditioning with the roles of plasticisers influencing the upper uptake limits.

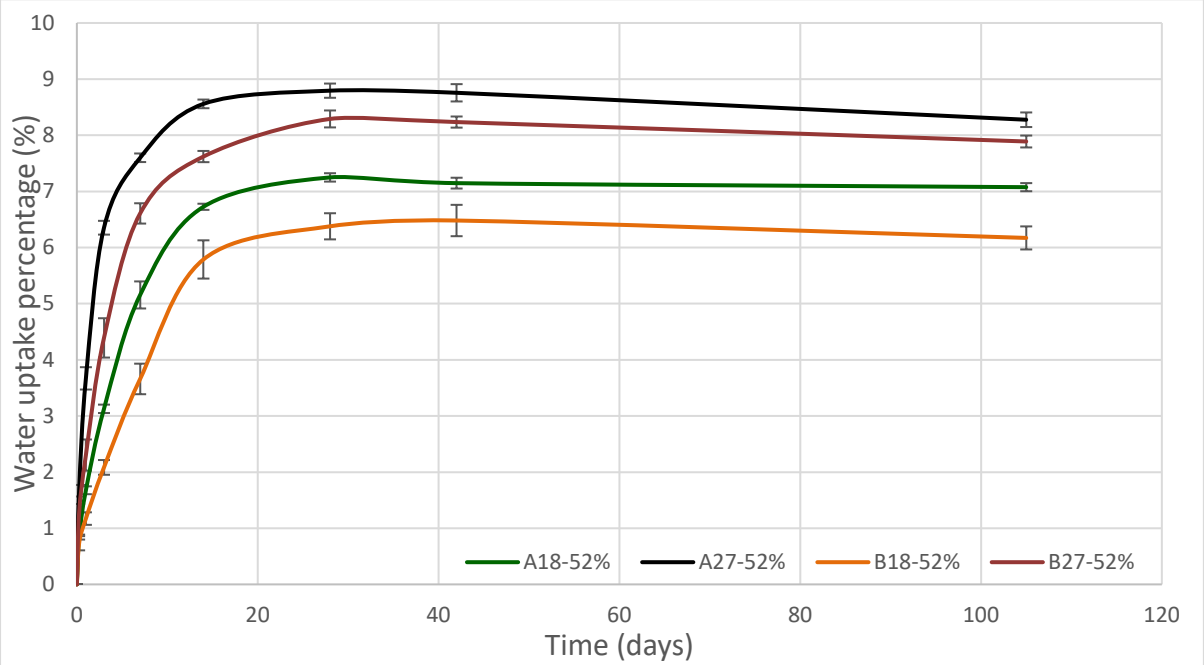

Figure 5-2 Water uptake percentage of RMS-A and RMS-B series in RH52% over time

Similar to what has been observed in RMS-G and RMS-E series (table 4-4 and figure 4-2), the water uptake trends (figure 5-2 and 5-3) in different RH levels all reach a peak value before approaching an equilibrium. This phenomenon is more obvious among the samples conditioned at RH75%. Since in chapter 4 it was proposed that the crystal structure is influenced by interactions with the plasticisers, and consequently this micro-morphology change affects the

water uptake behaviour, it is also assumed that potential interactions between RMS and the two types of ILs ([Amim]Cl and [Bmim]Cl) might lead to some variations of the crystal structures which would affect the water uptake. This will be discussed further with more details in FTIR spectroscopy and Raman spectroscopy analysis (5.3.4.1) and XRD analysis (5.3.4.2) later this chapter.

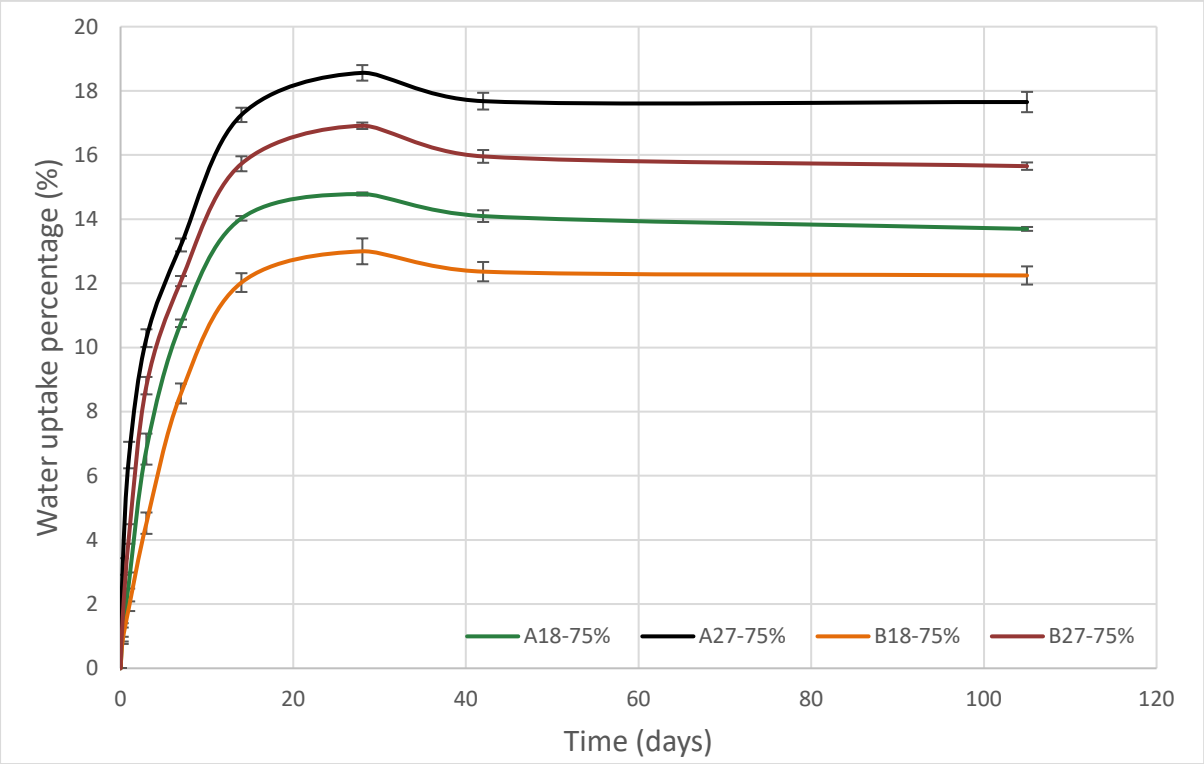

Figure 5-3 Water uptake percentage of RMS-A and RMS-B series in RH75% over time

5.3.3 Tensile Tests during Conditioning

Tensile testing has been performed to investigate the mechanical properties of RMS-A and RMS-B series samples since they can be heavily influenced by water uptake results.

Note however that there were insufficient specimens to be able to test beyond the planned 42 days for those conditioned for an extended time. As the study of RMS-G and E series has found that it was difficult to test samples in dry conditions, none of the dried samples of the RMS-A and B series have been tested. In addition, reliable results for RMS-A9 and RMS-B9 could not be obtained in all conditions. Therefore, the analysis of the tensile testing results will focus on the other samples.

The tensile properties of RMS-A and B series conditioned at RH75% are summarized in table 5-5 and visualized in figure 5-4 (a), (b) and (c). Overall, it can be seen that increasing the amount of ILs can significantly lower the tensile strength and the Young's modulus of the

samples. For example, the average tensile strength of RMS-A27 is 5.6MPa which is less than half of the RMS-A18 average result. The average result of RMS-B27 is only about 20% of the value of RMS-B18. However, the elongation at break, on the other hand has increased substantially. These results indicate that [Amim]Cl and [Bmim]Cl have a significant effect on RMS plasticisation which can effectively turn rigid polymers to a very rubbery state. The tensile properties of RMS-A18 and B18 are quite similar. However, RMS-B27 exhibits a much lower tensile strength and Young's modulus than RMS-A27, along with an elongation at break value almost 10 times that of RMS-A27.

Compared to the results of RMS-G and E series (table 4-5, 4-6 and 4-7), it can be observed that RMS-E series samples exhibit the lowest tensile strength and Young's modulus, and the highest elongation at break, at the plasticiser level of 18. RMS-G18 demonstrates the most rigid character while RMS-A18 and B18 display similar values in between the G and E series.

Table 5-5 Tensile testing data of samples after conditioning at RH52%

Code	Tensile stress [MPa]		Young's modulus [MPa]		Elongation at break [%]	
	Mean	RE	Mean	RE	Mean	RE
RMS-A18	13	0.06	760	0.14	24	0.58
RMS-A27	5.6	0.01	58	0.24	65	0.08
RMS-B18	12	0.10	700	0.13	20	0.75
RMS-B27	2.4	0.06	10	0.16	201	0.08

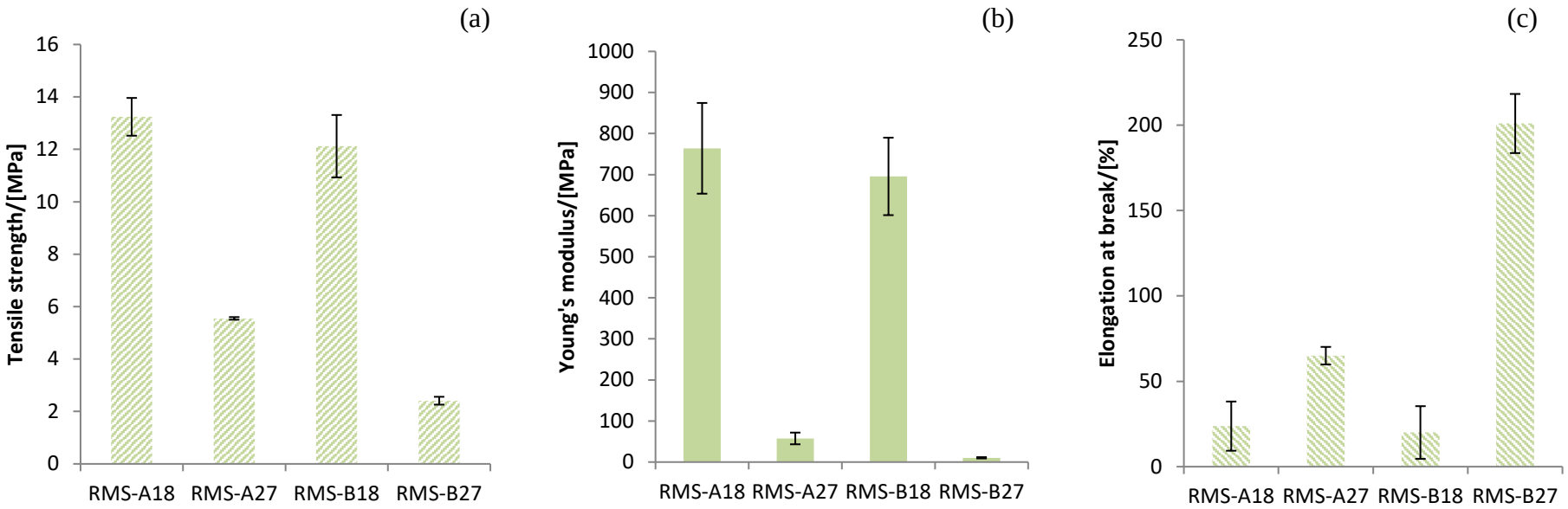

Figure 5-4 (a) Tensile strength of samples conditioned at RH52%; (b) Young's modulus of samples conditioned at RH52%; (c) Elongation at break of samples conditioned at RH52%

Table 5-6 Tensile testing data of samples after conditioning at RH75% for 42 days

Code	Tensile stress [MPa]		Young's modulus [MPa]		Elongation at break [%]	
	Mean	RE	Mean	RE	Mean	RE
RMS-A18	5.0	0.07	93	0.16	33	0.21
RMS-A27	3.0	0.04	16	0.05	38	0.15
RMS-B18	1.6	0.26	15	0.19	52	0.27
RMS-B27	0.89	0.05	1.7	0.08	130	0.10

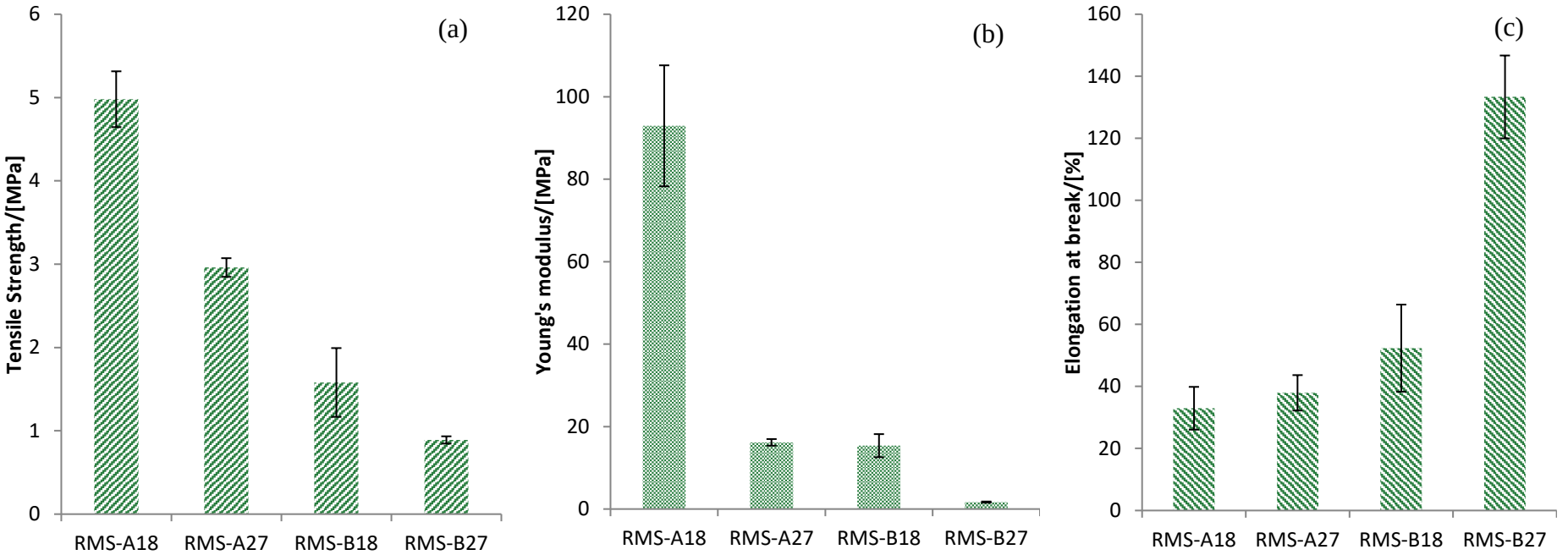

Figure 5-5 (a) Tensile strength of samples conditioned at RH75%; (b) Young's modulus of samples conditioned at RH75%; (c) Elongation at break of samples conditioned at RH75%

With the RH75% samples, the overall trend is similar to the RH52% samples (table 5-6 and figure 5-5). High levels of ILs can lead to lower tensile strength and Young's modulus, but higher elongation at break. For example, the tensile strength, Young's modulus and elongation at break of RMS-A27 are about 60%, 17% and 120% of RMS-A18 respectively. For RMS-B27, they are 56%, 11% and 250% of RMS-B18. When compared to the data of RH52%, the tensile strength and Young's modulus values of each formula decrease to an even lower level. The tensile strength of RMS-A18, A27, B18 and B27 conditioned in RH75% are 38%, 54%, 13% and 37% of those conditioned in RH52% respectively. For the Young's modulus, RMS-A18, A27, B18 and B27 conditioned in RH75% are 12%, 28%, 2.1% and 17% of those conditioned in RH52% respectively. In terms of the elongation at break, RMS-A27 and RMS-B27 seem to be over-plasticized because the measurements for these samples have decreased compared to those in RH52%. These results are similar to that observed in two other studies using [Emim][OAc] as plasticiser (Xie et al., 2015, Zhang et al., 2016). Such a low mechanical strength may limit the material application and, hence, it is necessary to investigate methods to strengthen this material.

A comparison of the RMS-G and E (table 4-5) series samples in RH75%, RMS-A18 shows equivalent tensile strength and Young's modulus to the RMS-G18 samples. The data for RMS-E18 are similar, except for the lower Young's modulus of 62 MPa. RMS-B18 shows the lowest tensile strength and Young's modulus, and the highest elongation at break, at the plasticiser level of 18.

When the plasticiser level increases to 27, the Young's modulus of RMS-A and B series become lower than G and E series. Meanwhile, the values of elongation at break become higher than G and E series.

Table 5-7 Tensile data of RMS-A27 and RMS-B27 conditioned at RH75% over time

Code	Time (Days)	Water Uptake Percentage	Tensile strength [MPa]		Young's modulus [MPa]		Elongation at Break [%]	
		Mean	Mean	RE	Mean	RE	Mean	RE
RMS-A27	7	13.20%	3.61	0.02	26.65	0.05	66	0.05
	14	17.25%	3.18	0.03	20.93	0.05	53.8	0.09
	28	18.56%	2.71	0.04	19.2	0.03	40.00	0.12
	42	17.68%	2.96	0.04	16.17	0.05	37.94	0.15
RMS-B27	7	12.07%	1.13	0.04	1.66	0.17	208	0.07
	14	15.73%	0.82	0.07	1.51	0.11	161.93	0.08
	28	16.91%	0.68	0.04	1.42	0.09	138.27	0.08
	42	15.96%	0.89	0.05	1.68	0.08	133.34	0.10

Table 5-7 illustrate how the tensile properties of the samples change when conditioned in RH75%. No clear correlation can be seen between water uptake percentage and tensile properties. It is assumed therefore that water uptake is not the direct reason for the tensile property changes, and as discussed in chapter 4 it is the crystalline structure, which is affected by water uptake, that is assumed to be the direct factor. Hence, it is important to study the crystallisation behaviour of RMS-A and RMS-B samples to understand the underlying mechanism.

5.3.4 Characterisation after Sample Conditioning

5.3.4.1 FTIR and Raman Spectroscopy

FTIR spectra were analysed using the band assignment information in table 5-8 which were derived from literature as indicated.

Table 5-8 FTIR and Raman spectra assignment

Material	Band assignment	Infrared	Raman	References
[Amim]Cl	CH wag and Ring symmetric deformation	997		(Xuan et al., 2011, Pouchert, 1981, Simons, 1978)
	CH wag	1020		
	CCH bending		1030	
	Ring asymmetric deformation and CH bending	1165		
	C-C stretching and CH bending	1284	1302	
	CH bending, CN stretching and CCN bending		1333, 1423	
	CN stretching and CNC bending	1562	1572	
	C=C stretching	1645	1655	
	CH stretching	2800-3150	2800-3150	
RMS	Skeletal modes of pyranose ring		488	(Cael et al., 1974, Cael et al., 1973, Dhital et al., 2011, Kizil et al., 2002)
	CH2 deformation		872,1470	
	COC α-1,4 glycosidic linkage	930	947	
	COH bending mode		1092	
	CO and CC stretching with COH bend combination		1132	
	CH2OH side chain related mode		1263	
	COH deformation	993, 1014		
	CH bending	1078		
	COC stretching from pyranose ring	1151		
	CH2OH (side chain) related mode	1248		
	CH deformation of all ring hydrogens		1306	
	Water adsorbed in the amorphous regions of starch	1641		
	CH stretching	2800-3000	2800-3000	
	OH stretching	3000-3600		
[Bmim]Cl	CCH bending		1028	(Hamaguchi and Ozawa, 2005, Kathirgamanathan et al., 2015, Kotov et al., 2016, Sankri et al., 2010)
	CH bend	1165		
	CH bending and CN stretching		1421	
	CN stretching and CNC bending	1560	1568	
	CH stretching	2800-3200	2800-3000	

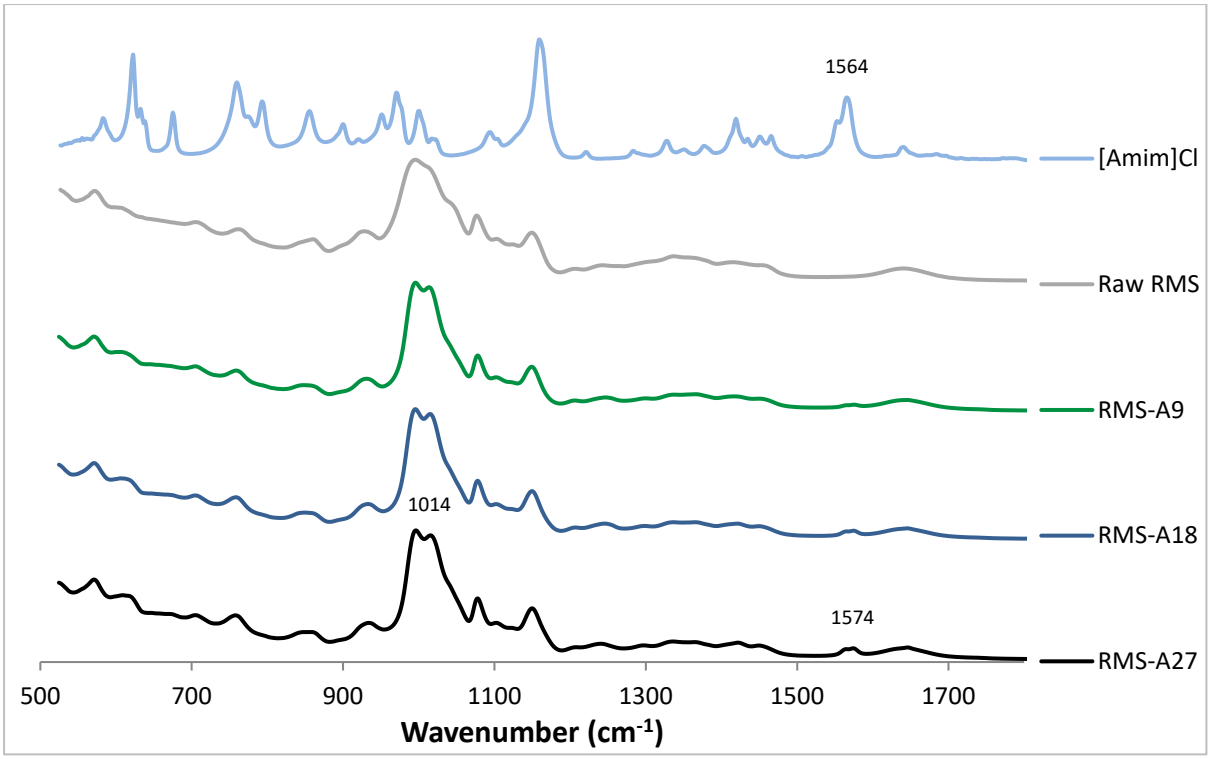

Figure 5-6 FTIR fingerprint region spectra of raw RMS, pure [Amim]Cl and RMS-A series

Figure 5-6 shows the fingerprint region for the RMS-A series samples compared to those of the raw ingredients. Band assignment is as displayed in table 5-8. The differences between the spectra of raw RMS and [Amim]Cl plasticized starch samples are not very obvious. New peaks at 1014 cm^{-1} and 1574 cm^{-1} are observed in RMS-A series samples. The band at 1014 cm^{-1} is assumed to be related to molecular interactions of the OH groups linked to pyranose rings of starch (Cael et al., 1975, Kizil et al., 2002). It is also indicative of the amorphous phase dominating over the crystalline phase in the material (Cozar et al., 2013). The minor peak at 1574 cm^{-1} is likely that shifted from 1566 cm^{-1} of [Amim]Cl which relates to CN stretching and CNC bending from the imidazole ring. Similar patterns can be observed in the RMS-B series samples displayed in figure 5-9. A peak assigned to the same vibration mode of CN stretching and CNC bending is at 1572 cm^{-1}. Compared to the same peak of RMS-E samples (chapter 4.3.4.1) at 1566 cm^{-1}, a down shift of ~12 cm^{-1} is displayed from RMS-B series which is slightly bigger than ~10 cm^{-1} from RMS-A series while RMS-E series display a down shift of ~6 cm^{-1}. This suggests that the interaction between starch and imidazole rings may be stronger in the case of [Amim]Cl and [Bmim]Cl which is significant for their material properties. Also the COH deformation peak up-shifts from 1014 cm^{-1} to 1018 cm^{-1}, suggesting starch interacts slightly stronger with [Bmim]Cl than [Amim]Cl.

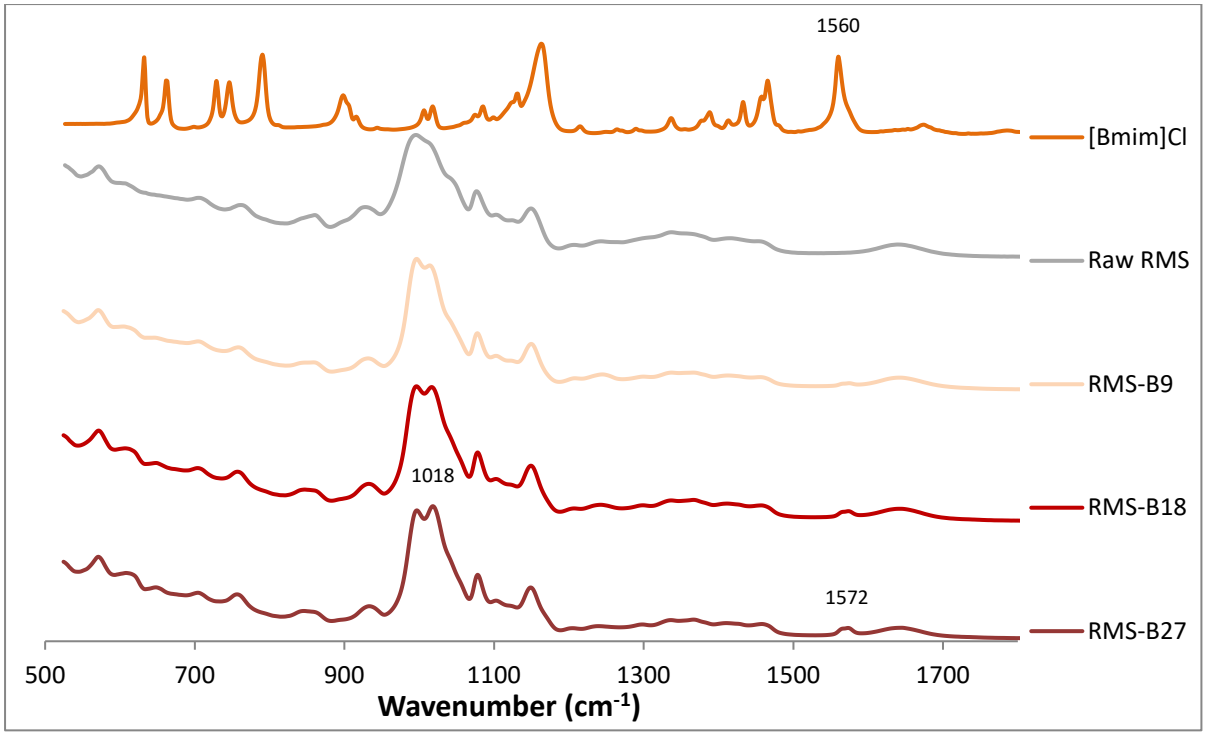

Figure 5-7 FTIR fingerprint region spectra of raw RMS, pure [Bmim]Cl and RMS-B series

Looking at the full spectra of RMS-A and B series (Figure 5-7 and 5-8), it can be seen that the bands corresponding to starch OH stretching do not change much. It is difficult to make definitive conclusions on the variation of the hydrogen bonding between hydroxyl groups as a 2 cm^{-1} shift is not very significant in such a broad OH peak, which is very similar to the behaviour of RMS-E series samples.

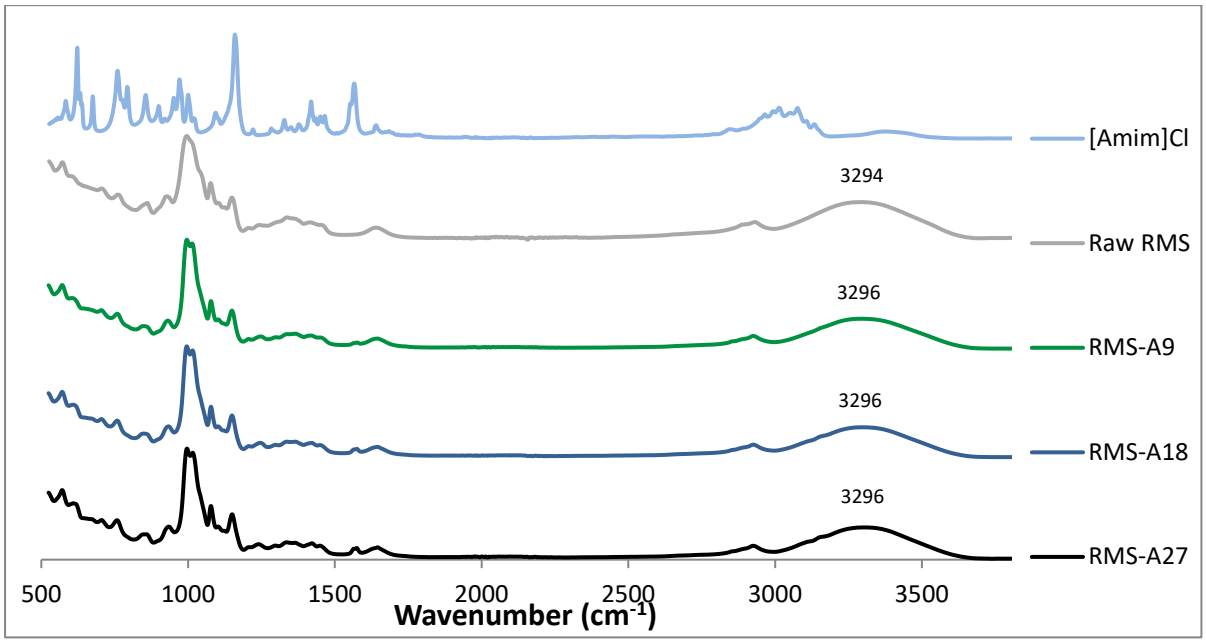

Figure 5-8 Full FTIR spectra of raw RMS, pure [Amim]Cl and RMS-A series

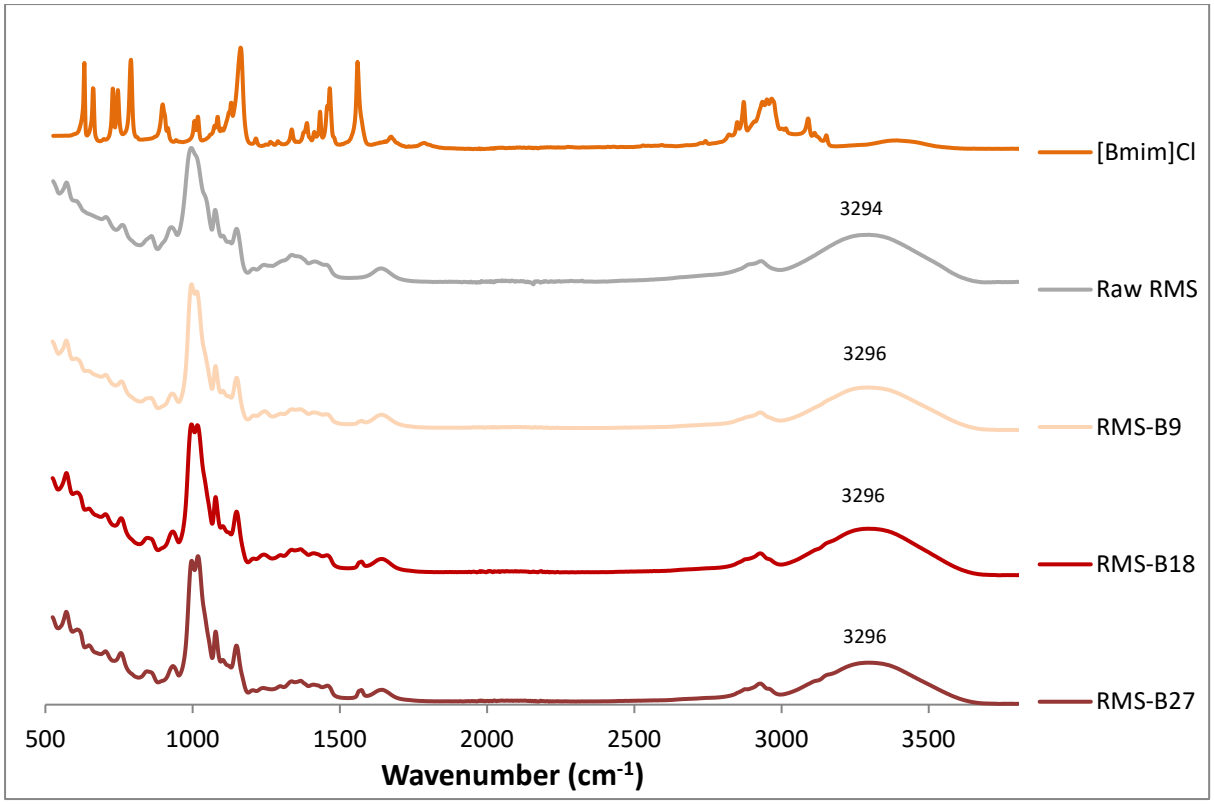

Figure 5-9 Full FTIR spectra of raw RMS, pure [Bmim]Cl and RMS-B series

Raman spectroscopy provides additional information which supports the trends observed in FTIR spectroscopy. Several bands become increasingly obvious in [Amim]Cl plasticized RMS samples at 1032 cm^{-1}, 1306 cm^{-1}, 1425 cm^{-1}, 1574 cm^{-1}, 1624 cm^{-1} and 1655 cm^{-1} (as shown in figure 5-10). These bands are believed to be introduced by [Amim]Cl originally assigned at 1030 cm^{-1}, 1302 cm^{-1}, 1423 cm^{-1}, 1572 cm^{-1}, 1624 cm^{-1} and 1655 cm^{-1}. As suggested by previous studies (Xuan et al., 2011), the peak at 1030 cm^{-1} is assigned for CCH bending and 1302 cm^{-1} is for C-C stretching and CH bending. These factors are potentially strong evidence of interactions existing at C7 as indicated in figure 5-11. A strong peak at 1423 cm^{-1} is assigned for CH bending, CN stretching and CCN bending. A weak peak at 1572 cm^{-1} is related to CN stretching and CNC bending. These two bands suggest the imidazole ring of [Amim]Cl takes a significant role in interacting with starch. A strong absorption at 1655 cm^{-1} is diagnostic for C=C stretching while the small shoulder at 1624 cm^{-1} is not reported yet. Hence, it is indicated that the allyl group is involved in interacting with starch. In terms of the starch structure, it is found that the shape of the band at 486 cm^{-1} changes when [Amim]Cl is added, indicating that the pyranose ring of starch takes part in the interaction which is also suggested by FTIR assignment. In addition, the peaks at 1132 cm^{-1} and 1263 cm^{-1} are diminishing with the increase of plasticiser content, indicating that the hydrogen bonds between starch molecules are being destroyed.

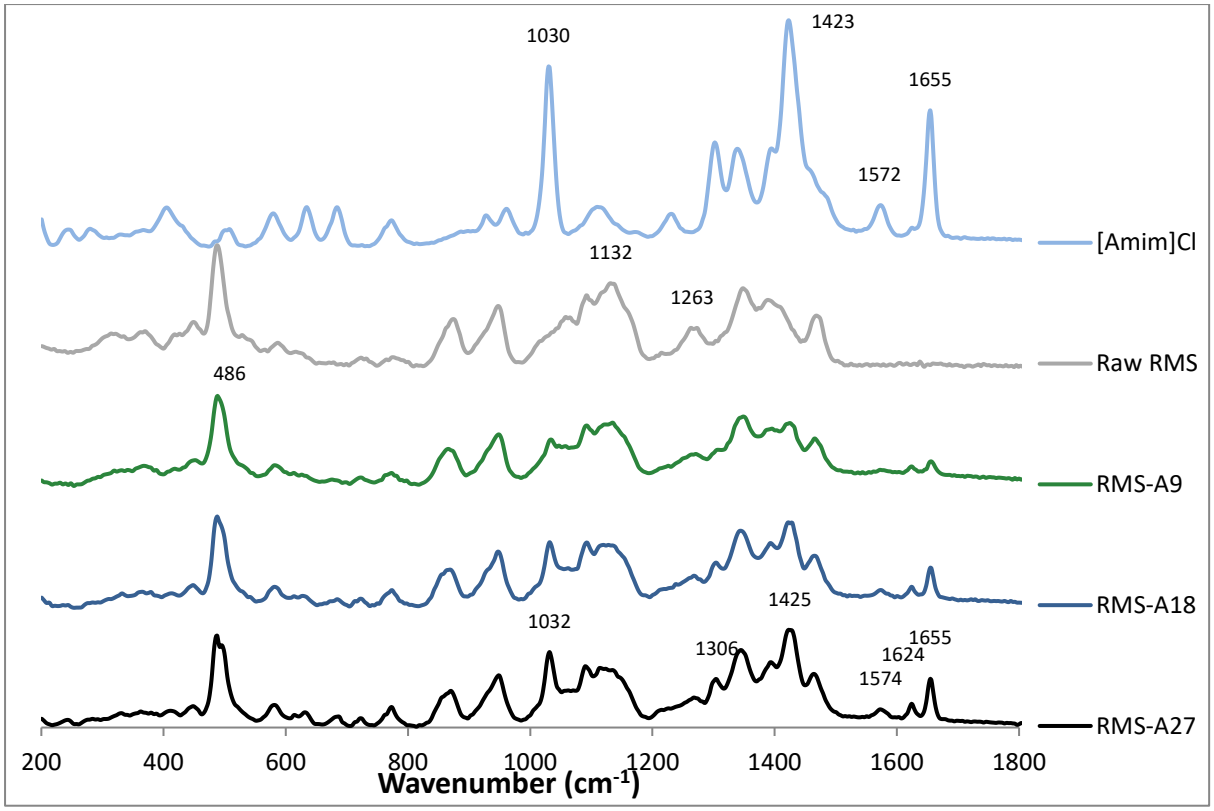

Figure 5-10 FT-Raman fingerprint region spectra of raw RMS, pure [Amim]Cl and RMS-A series

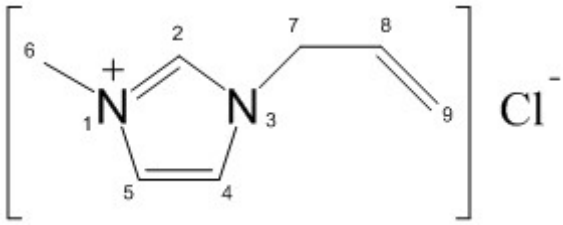

Figure 5-11 Chemical structure of [Amim]Cl

In the case of RMS-B series samples (figure 5-12), bands at 1028 cm^{-1}, 1421 cm^{-1} and 1568 cm^{-1} from pure [Bmim]Cl are introduced to processed starch samples and all display an up-shift to 1032 cm^{-1}, 1427 cm^{-1} and 1574 cm^{-1}. Similarly, this indicates the potential chemical regions which are involved in interaction with RMS. The band at 1028 cm^{-1} is assigned to CCH bending, while the other two at 1421 cm^{-1} and 1568 cm^{-1} suggest chemical parts from the imidazole ring. Compared to the same interactions of [Amim]Cl which all display up-shifts of approximately 2 cm^{-1}, the up-shifts displayed by CCH bending mode, CH bending and CN stretching combination mode, CN stretching and CNC bending combination mode from [Bmim]Cl are 4 cm^{-1}, 6 cm^{-1} and 6 cm^{-1} respectively. This greater shift suggests that the molecular interaction of RMS-B series samples may be stronger than that of the RMS-A series samples (Kuptsov and Zhizhin). However, the potential locations of hydrogen bonds are not very clear since the shape variation of bands at 488 cm^{-1} and 1132 cm^{-1} is minor. Similarly to

the RMS-A series samples, a new minor unknown peak at 1624 cm^{-1} is observed in the RMS-B series samples. This small peak is observed at 1624 cm^{-1} in both [Amim]Cl and [Bmim]Cl in both figure 5-10 (where it appears as a shoulder to the 1655 peak) and 5-12. No assignment of this peak was found in the literature, but given its wavenumber it is likely to be related to C=C and C=N vibration modes in the imidazole ring. This peak is relatively much larger in the plasticised RMS samples' Raman spectra, which suggests a strong interaction with the starch. This peak was not observed in the [Emim][OAc] plasticised RMS samples, so this is further evidence which indicates [Amim]Cl and [Bmim]Cl have stronger interactions.

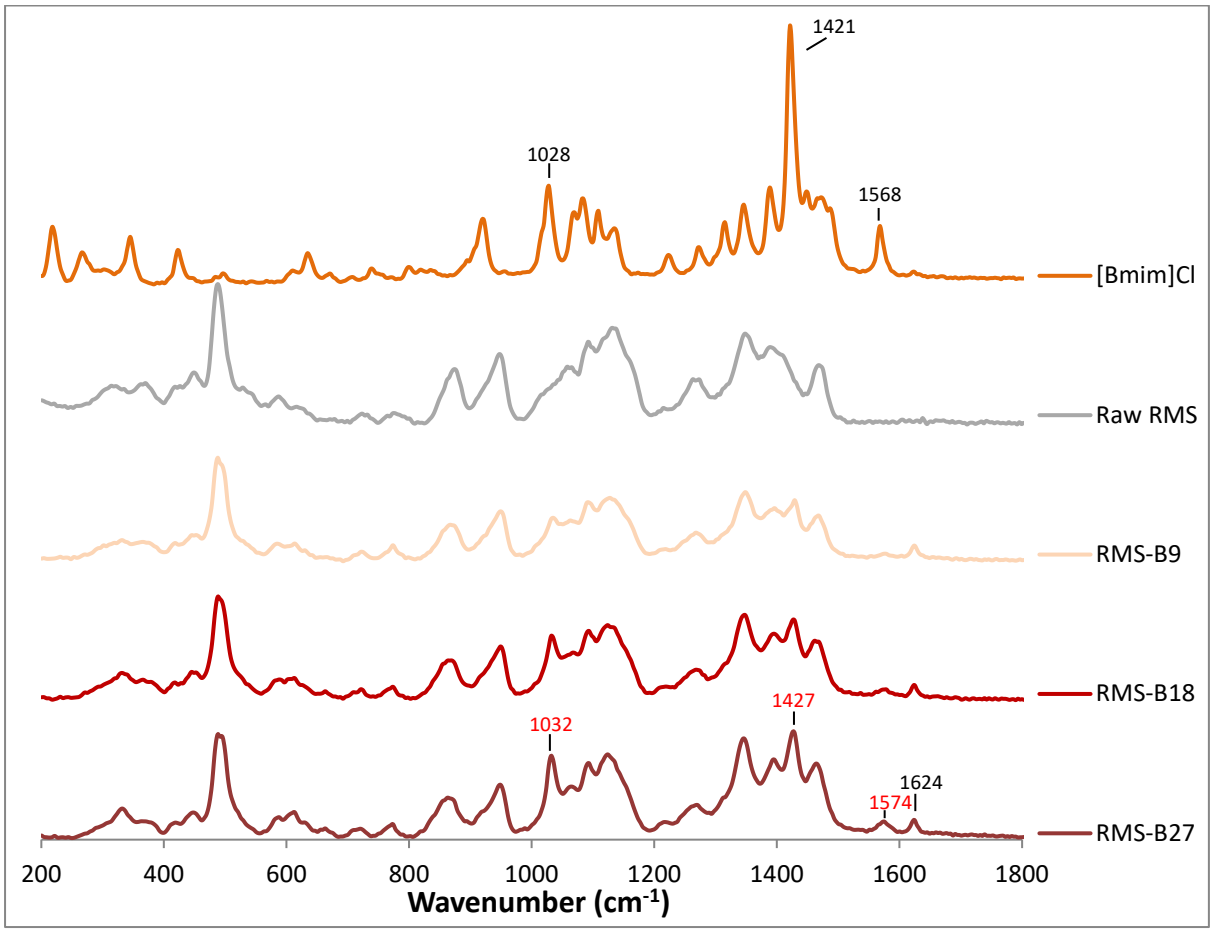

Figure 5-12 FT-Raman fingerprint region spectra of raw RMS, pure [Bmim]Cl and RMS-B series

The full FT-Raman spectra of RMS-A and B series (figure 5-13 and 5-14) show another potential interaction at 2960 cm^{-1}. All of the details mentioned above demonstrate that the interactions introduced by [Amim]Cl and [Bmim]Cl to starch are very similar. The imidazole ring is the major factor of interaction while the substitute groups can affect the strength of interaction. By simply comparing the band shifts of same chemical parts between [Amim]Cl, [Bmim]Cl and [Emim][OAc], it can be found that the strongest interaction is from the RMS-B

series samples, the RMS-A series is slighter weaker than B and the RMS-E series is the weakest among all of the ILs.

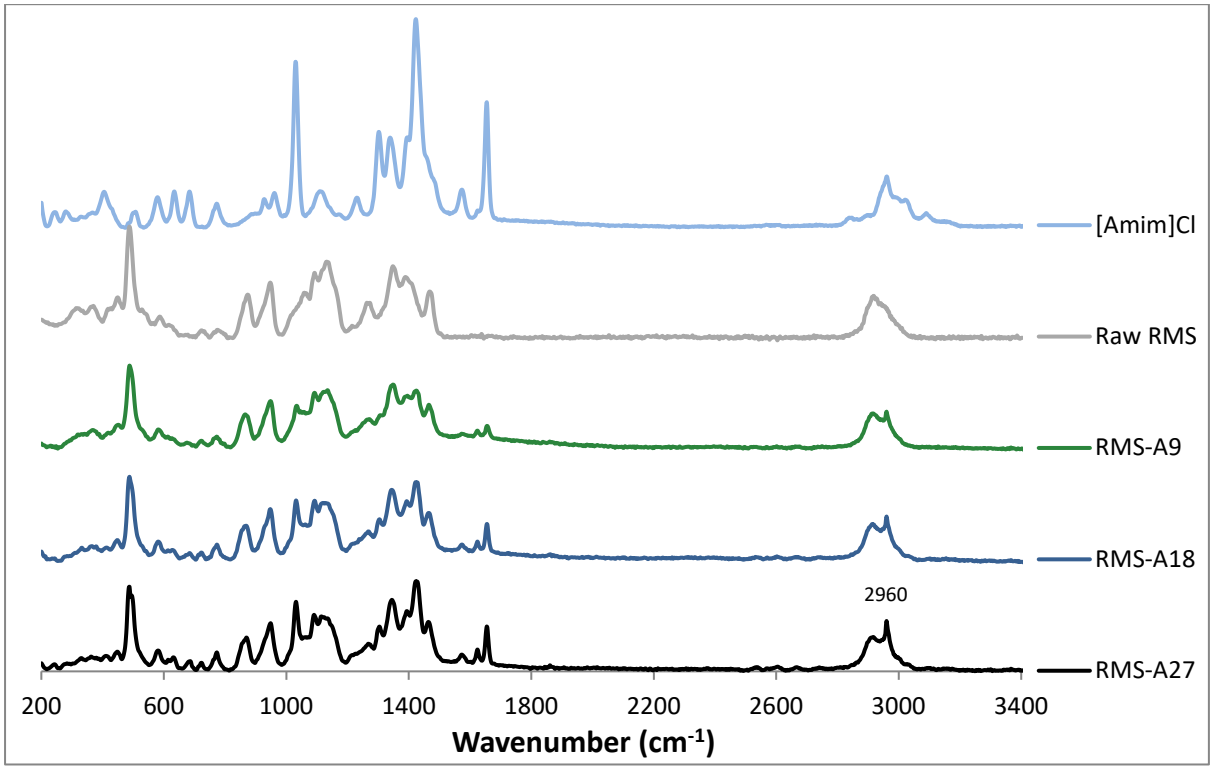

Figure 5-13 Full FT-Raman spectra of raw RMS, pure [Amim]Cl and RMS-A series

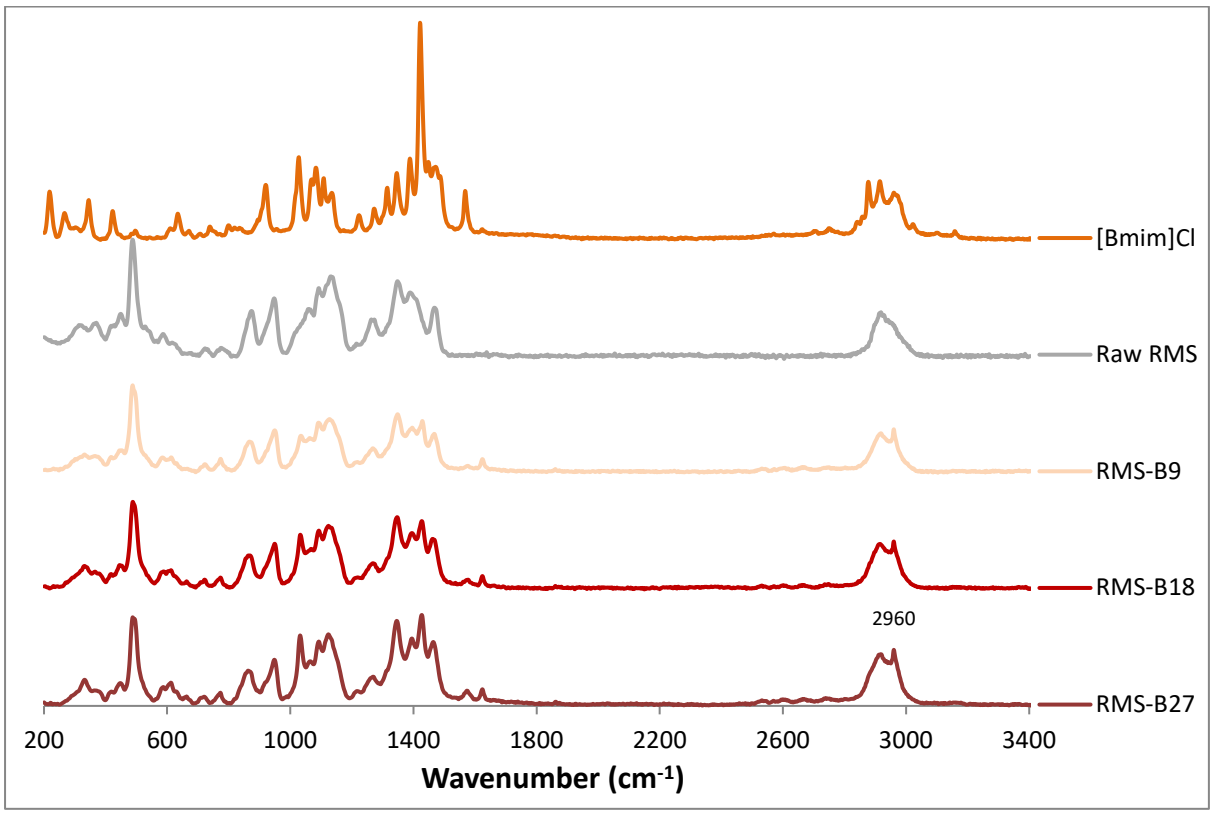

Figure 5-14 Full FT-Raman spectra of raw RMS, pure [Bmim]Cl and RMS-B series

5.3.4.2 XRD

The XRD results of TPS samples plasticized by [Amim]Cl and [Bmim]Cl are displayed in figure 5-15 and figure 5-16 respectively. Dried samples before conditioning are labelled with RH0. Similarly, samples after conditioning at RH52% and RH75% are indicated with RH52 and RH75 respectively. From figure 5-15, it can be easily observed that all RMS-A18 samples display strong peaks at 2θ of 15°, 23° and a doublet at 17° and 18°, which are diagnostic evidences of the A-type crystalline structure (Imberty et al., 1988, Xie et al., 2014). Other strong absorptions at 2θ of 7°, 13°, 20° and 22° which overlaps with 23° indicate a V-type crystalline structure. A small but obvious peak at 2θ of 5° suggests the existence of B-type crystalline structure in RMS-A18-RH75. Hence, it is very likely that the other diagnostic peaks at 2θ of 17 and 23° from B-type crystalline structure are overlapped with the A-type characteristics. Therefore, the crystalline structure of RMS-A18-RH75 is identified as C-type while the other two are A-type. As presented in table 5-9, the total degree of crystallinity of RMS-A18 decreases from 21.59% to 18.02% against the increasing RH trend from 0% to 75%. V-type crystalline structure grows as the conditioning RH increases from 0% to 52%, but then vanishes as the RH further increases from 52% to 75%.

Similarly, weak signals of A-type crystal at 2θ of 15°, 23° and a doublet at 17° and 18° can be observed in RMS-A27-RH0. In a high RH of 52%, these bands become more obvious with the appearance of B-type character which is at 2θ of 5°, suggesting the crystalline structure of the sample turning from A-type to C-type. In RH75%, A-type structure is gone completely, leaving a single strong peak at 2θ of 17°, indicating the crystalline structure has completely turned into B-type. However, the main characters of B-type crystallinity become vague at the same time. For example, the broad band at 2θ of 5° has shrunk into a small peak indicating either the reduced size or increased defects of the crystallites. V-type crystals exists in all RMS-A27 samples. However, it shows the weakest signals in RH0% which have no peak at 2θ of 7° while the peak at 2θ of 13° is broad compared to other RMS-A27 samples. The characteristic peaks of V-type crystalline become sharp and obvious in RH52%. However, they become weak again in RH75%. The total crystallinity and the V-type crystallinity of RMS-A18 samples increase when RH increase from 0% to 52% and then decrease when RH further increases from 52% to 75%.

The crystalline type variation trend of RMS-A series samples develops from A towards B through C as conditioning RH increases, unlike the RMS-G and RMS-E series which follow

the reverse trend. During conditioning, it is suggested by the XRD results that A-type structure will vanish gradually with the growing of B-type crystals. However, B-type crystals are destroyed with further water absorption.

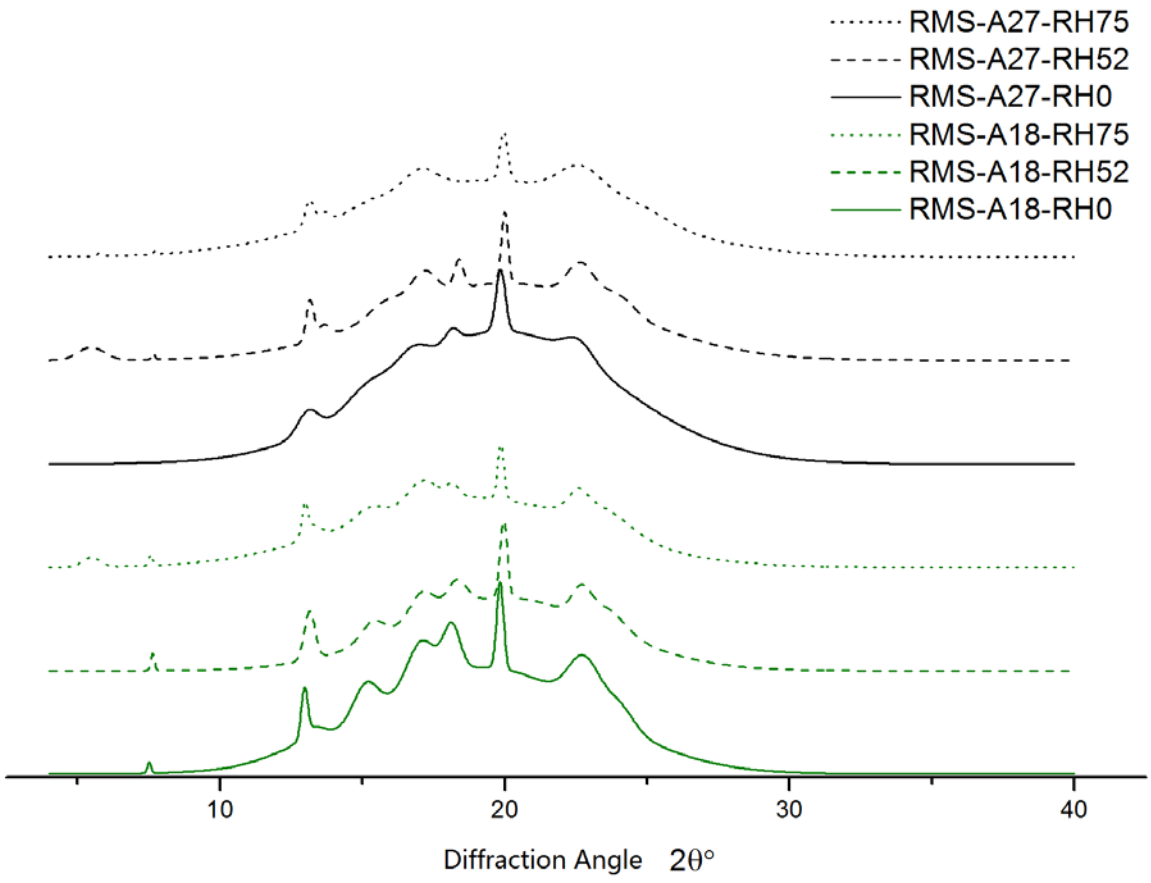

Figure 5-15 RMS-A Series XRD diffractogram

Similar patterns can be found in RMS-B series samples (Figure 5-16). It can be observed that peaks in each diffractogram may be shifted, where RMS-B18-RH0 is the most obvious. A possible explanation of this phenomenon is that the sample is under strain, hence changing the spacing d_0 in Bragg's law and leading to a shifted peak (Cullity and Stock, 2001). However, the cause in this instance is believed to be a slight misalignment of the goniometer or lag in ratemeter-recorder response in the equipment, as this displacement varies progressively from start to end of the spectrum (Bertin, 2012).

V-type crystalline structures exist in all RMS-B series samples which are basically indicated by absorption peaks at 2θ of 7°, 13° and 20°. Typical doublets at 2θ of 17° and 18° and absorption at 2θ of 15° suggest the A-type crystalline structure.

In RMS-B18-RH0, the shoulder at 2θ of 15°, which is believed to be a superimposed peak, and the small doublet at 2θ of 17° and 18° suggest the A-type crystallites are either small or imperfect. However, these details become quite obvious at RH52% and then much weaker at RH75%. In terms of V-type crystallites in RMS-B18 samples, the situation is simular. The small peak at 2θ of 7° actually disappears in RH0%, it shows the most obvious characteristics in RH52% and becomes weaker in RH75%. Again, the degree of crystallinity for all crystal types increases when RH increases from 0% to 52% and then decreases when RH further increases up to 75% as summarized in table 5-9. However, throughout all these variations, the crystalline structure of RMS-B18 remains to be A-type.

Considering the RMS-B27 results, the sample of RH0% is the closest to amorphous state. Except for the obvious characters of V-type crystalline structures, the diagnostic peaks of A-type crystallites at 2θ of 15°, 17°and 18° are too small to identify. A total crystallinity of 9.42% is displayed in this sample of which only 4.13% belongs to A-type crystallites. Vague B-type characteristics appear in the RMS-B27-RH52 sample such as a small hump at 2θ of 5° and a small shoulder at 2θ of 14°, indicating the growth of B-type crystals. Also, peaks of V-type crystallites become sharper and taller representing the growth or refinement of such kind of crystallites. For instance, the small peak at 2θ of 7° rises from nothing between RH0% and RH52%. In RH75%, the B-type crystal signals become even clearer while minor A-type structure still exists in the material since the doublet at 2θ of 17° and 18° remains. In the case of RMS-B27, it is seen that the crystalline structure has changed from A to C when RH is raised from 0% to 75%.

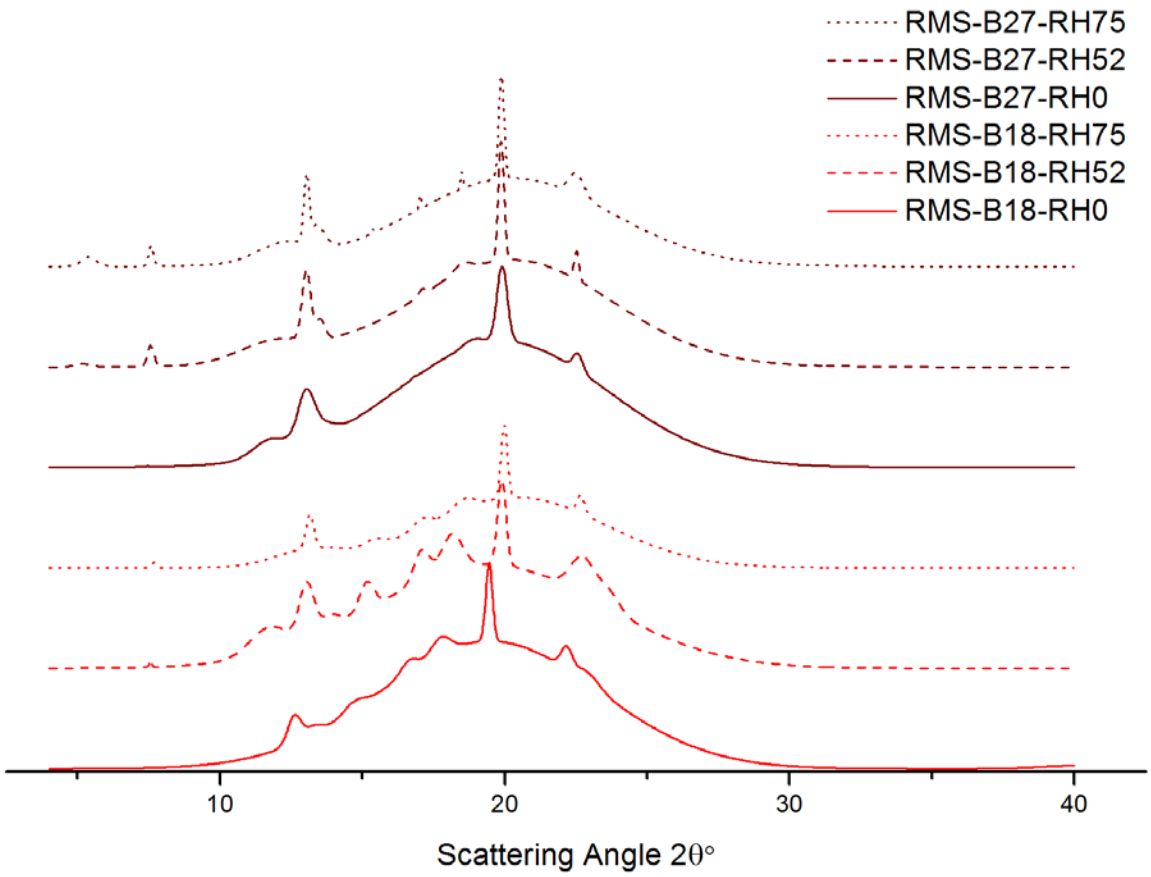

Figure 5-16 RMS-B Series XRD diffactogram

Note that [Bmim]Cl plasticised samples demonstrate lower mechanical properties at similar plasticiser levels to [Amim]Cl plasticised samples, even though their water uptake is generally lower. Thus, it can be concluded that the plasticiser choice is the predominant factor controlling mechanical properties, as the molecular interaction has a direct effect on the resulting intermolecular forces. This was also seen in the RMS-G and E series samples. Mechanical properties are also related to the degree of crystallinity, which is in turn is related to water uptake, although this is a less prominent factor.

The crystallisation behaviour is influenced by the plasticisers. Similar to RMS-G and E series samples, higher plasticiser level tends to destroy more double helix structures in the samples (table 5-9). However, the double helix structures will grow during conditioning and turn from A-type towards B-type with an increase in RH, which is different from the result seen in the RMS-G and E series samples. The crystallinity of RMS-A and B samples increase initially and then decrease as conditioning RH is increased. This may be the key factor to the water uptake trend, where samples with more B-type crystal structures exhibit a more obvious peak before equilibrium.

Table 5-9 Crystalline pattern and crystallinity of RMS samples

Code	RH0			Pattern	RH52			Pattern	RH75			Pattern
	Degree of crystallinity [%]				Degree of crystallinity [%]				Degree of crystallinity [%]			
	Double Helices	V-type	Total		Double Helices	V-type	Total		Double Helices	V-type	Total	
RMS-A18	18.46	3.13	21.59	A	14.6	6.10	20.70	A	15.34	2.68	18.02	C
RMS-A27	5.73	3.10	8.83	A	15.08	3.54	18.62	C	12.96	2.65	15.61	B
RMS-B18	5.22	2.91	8.13	A	13.99	5.21	19.20	A	11.00	4.93	15.93	A
RMS-B27	4.13	5.29	9.42	A	8.52	5.49	14.01	C	9.04	4.74	13.78	C

5.3.4.3 TGA

Figure 5-17 and 5-18 display the first derivative of mass loss data over heating temperature.

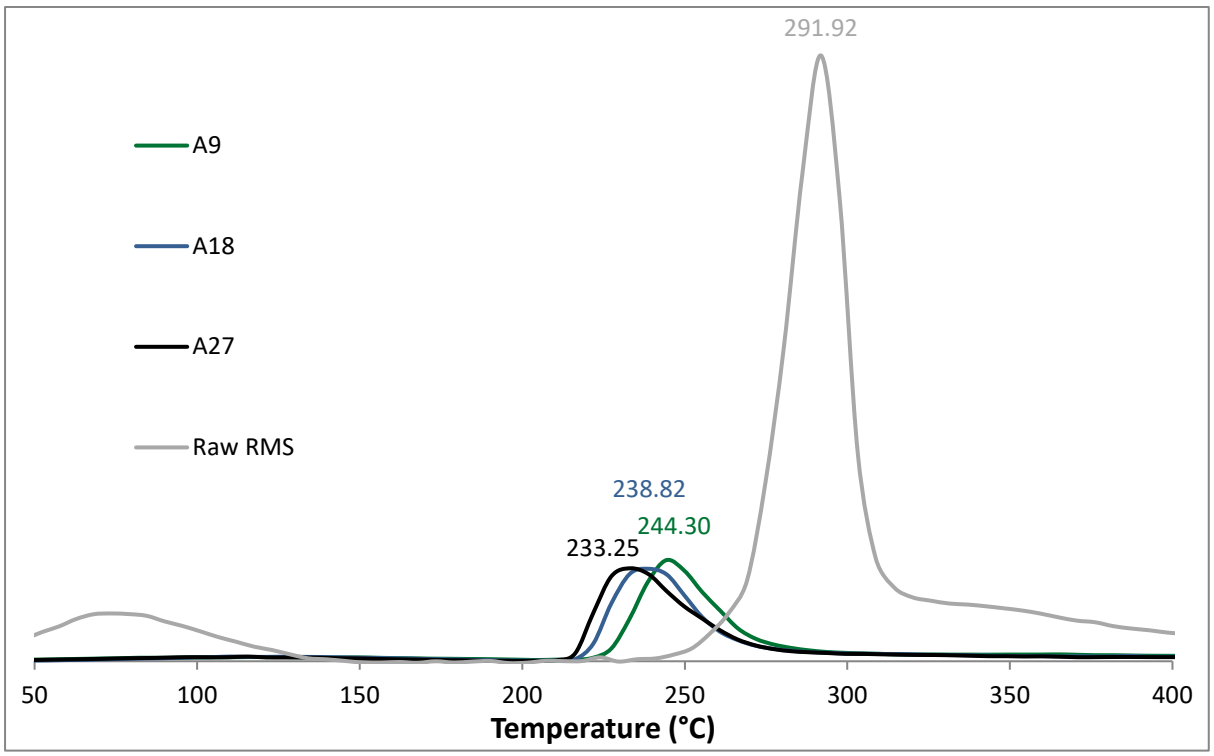

Figure 5-17 First derivative TGA results of RMS-A series compared with raw RMS

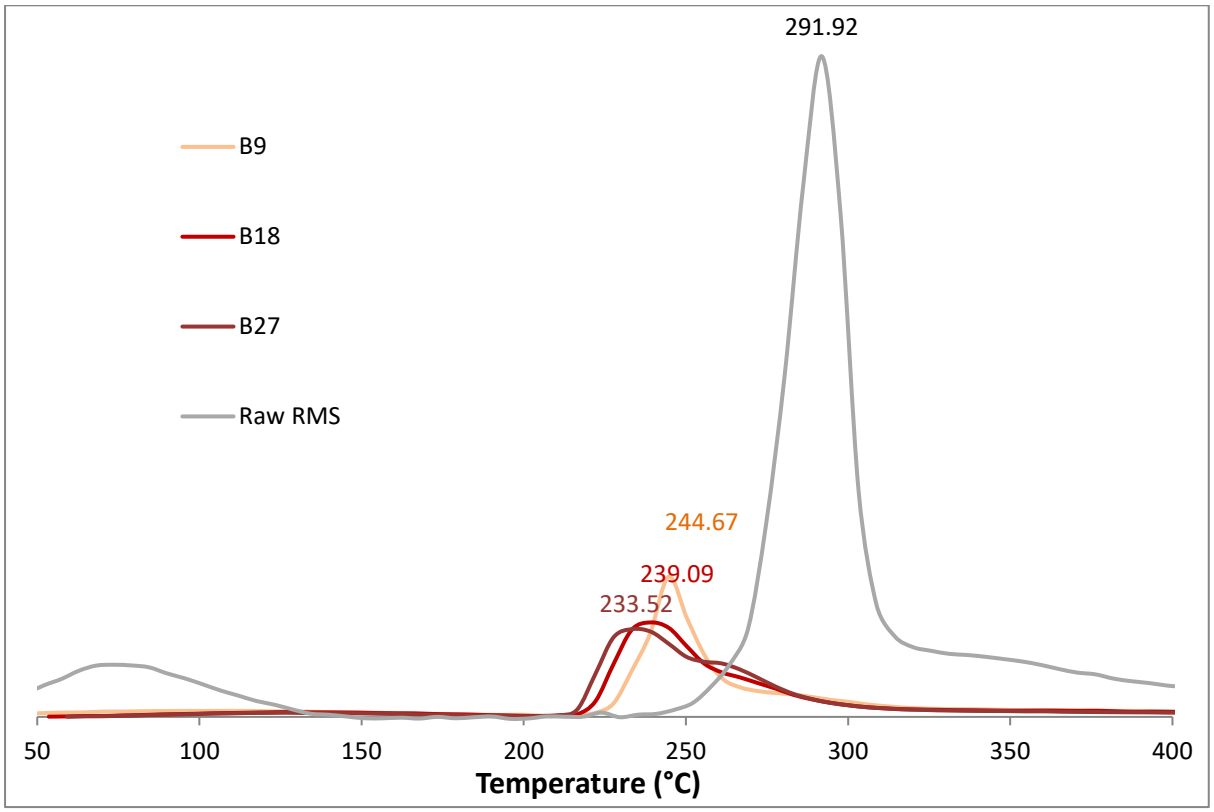

Figure 5-18 First derivative TGA results of RMS-B series compared with raw RMS

As mentioned in chapter 4, raw RMS shows a broad peak at around 80°C which is considered related to water evaporation. Compared to this, neither the RMS-A series samples nor the B series samples show any peak at a similar location. This suggests that in these ILs, water is firmly bound, which is similar to the RMS-G and E series.

The temperatures at peak thermal degradation rate of RMS-A9, A18 and A27 are about 244°C, 239°C and 233°C respectively. In comparison, the same key temperatures of RMS-B9, B18 and B27 are approximately 245°C, 239°C and 234°C respectively, which are almost the same as RMS-A series. The situation is the same regarding degradation onset temperature. Both series have the lowest degradation onset temperature at 212°C for high plasticiser level samples and the highest degradation onset temperature 224°C for low plasticiser level samples. Compared to the raw RMS sample, the peak thermal degradation rate temperature drops by about 60°C, from 292°C to 233°C. However, the onset temperature decreases only from 240°C to 212°C. Although the lowest peak thermal degradation rate temperature of RMS-A and B series samples are lower than RMS E series, the lowest onset temperature is about 10°C higher than RMS E series, suggesting the actual temperature limit of RMS-A and B series is slightly higher.

Similar results have been reported in a study where [Bmim]Cl plasticised cassava starch samples showed a degradation temperature at 255 °C (Ren et al., 2017). It was proposed in the same study that the decrease of thermal degradation temperature is due to starch molecular weight reduction during solution processing. This may be because the imidazole structure of ILs interacts with starch in a different manner to glycerol.

As FTIR and Raman spectroscopy results potentially suggest that the conjugated structure of [Amim]Cl and [Bmim]Cl have stronger abilities to interact with starch compared to [Emim][OAc], the TGA results demonstrate an agreement with the spectra. Considering all three types of ILs studied in this thesis, it is proposed that the peak thermal degradation rate temperature is dominated by the interaction between starch molecules and ILs' conjugated structures.

5.4 Conclusions

In this chapter, the plasticisation effects of [Amim]Cl and [Bmim]Cl on RMS mechanical properties, as well as the interactions between chemical species, have been investigated. The results of FTIR and Raman spectroscopy have demonstrated that strong molecular interaction,

which heavily depends on ILs' conjugated structure, is the key to lower processing torques. Both [Amim]Cl and [Bmim]Cl have shown stronger molecular interaction abilities and effects on RMS processing compared to glycerol and [Emim][OAc]. In detail, [Amim]Cl and [Bmim]Cl are much stronger plasticisers than glycerol. [Emim][OAc] is slightly weaker than the other two ILs. Hence, starch samples plasticised by [Amim]Cl and [Bmim]Cl have achieved lower torques compared to those with [Emim][OAc] and glycerol.

However, the TGA results suggest that such strong molecular interactions with ILs' conjugated structure may also lower the thermal degradation temperature. As compared to the extreme examples of RMS-E27, the peak degradation rate temperatures of RMS-A27 and RMS-B27 are approximately 29 °C lower. It is worth noticing that since the chemical structure of [Amim]Cl and [Bmim]Cl are very similar to each other, their difference in TGA results are generally less than 0.4 °C.

The XRD experiments have also shown that the crystallisation behaviour of RMS plasticized by [Amim]Cl and [Bmim]Cl are very similar to each other. Crystallites tend to transform from A-type toward B-type as the conditioning RH increases, which is different from glycerol and [Emim][OAc]. The variation of crystallinity and crystalline structures has also been shown to be the key factors affecting tensile properties and water uptake results. Similar to the RMS-G and E series, the recrystallisation during conditioning might be the reason for water uptake fluctuation at equilibrium level. However, the chosen plasticiser is still the predominant factor of tensile properties. The effects of crystallinity and water uptake are less prominent.

By using [Amim]Cl and [Bmim]Cl as plasticisers of starch, the Young's modulus is further decreased to 16 MPa and 1.7 MPa, respectively, with a plasticiser level of 27 and conditioning RH of 75%. Under the same conditions, the Young's modulus of samples plasticised with glycerol and [Emim][OAc] were 28 MPa and 24MPa, respectively. Hence, by summarising the facts above, it can be concluded that [Amim]Cl and [Bmim]Cl are more efficient plasticisers than [Emim][OAc] and glycerol.

Since all the ILs have been found to lower Young's modulus and tensile strength of TPS, in order to maintain reasonable mechanical properties of TPS, it is important to investigate the promising strengthening effects of CNTs on TPS processing.

6 EFFECTS OF CNTS ON RMS PROCESSING AND MECHANICAL PROPERTIES

6.1 Introduction

Experiments have been performed to compare the plasticisation effects of glycerol and three different types of ILs in chapter 4 and 5. It has been suggested that ILs have stronger plasticisation effects on TPS processing which can lower processing and torques, lower thermal degradation temperatures, tensile strength and even Young's modulus. The decrease in processing and torque might be beneficial to industrial production. However, the extreme low tensile properties caused by strong plasticisation might potentially limit the material application.

In order to enhance the mechanical properties of TPS, MWCNTs have been investigated in this chapter as a strengthening material. Water uptake and tensile tests have been performed to attain fundamental knowledge of CNTs reinforced TPS. XRD and FTIR/Raman spectroscopy have been analysed to understand the crystallisation and mechanism of the molecular interactions. Results will be compared to previous results in order to understand the CNTs strengthening effects on TPS mechanical properties.

6.2 Experimental

6.2.1 Materials

The starch used in this experiment was RMS. Glycerol, [Emim][OAc], [Amim]Cl and [Bmim]Cl were used as plasticisers. Multi-walled CNTs were added as a strengthening material. Details are outlined in Chapter 3.2.

6.2.2 Experimental Methods

As previous study found that the high level of plasticisers and high level of conditioning humidity can lead to very low mechanical properties, this study focused only on the effect of adding CNTs to starch samples plasticized by one level of plasticisers. Four types (table 6-1) of samples were produced and compression moulded following the methods mentioned in chapter 3.3.1.

Table 6-1 Sample formulation design

Code	RMS Amount	Water	Glycerol	[Emim][OAc]	[Amim]Cl	[Bmim]Cl	CNT
RMS-G18	100	12	18	-	-	-	-
RMS-E18	100	12	-	18	-	-	-
RMS-A18	100	12	-	-	18	-	-
RMS-B18	100	12	-	-	-	18	-
RMS-G18C	100	12	18	-	-	-	1
RMS-E18C	100	12	-	18	-	-	1
RMS-A18C	100	12	-	-	18	-	1
RMS-B18C	100	12	-	-	-	18	1

The sample sheets produced by compression moulding were then conditioned at RH52% and characterised over time using the following techniques:

Water absorption — Water uptake measurement (section 3.3.2.1)

After conditioning was completed, (as indicated by no further weight change in the water uptake measurement) the samples were characterised by the following methods:

Mechanical properties — Tensile testing (section 3.3.3.1)

Molecular Structure — FTIR spectroscopy (section3.3.3.3)

Raman spectroscopy (section 3.3.3.4)

Crystal structure — XRD (section3.3.3.5)

Thermal stability — TGA (section3.3.3.2)

These tests were performed according to the schedule given in table 6-2. Note that the samples are very brittle at the beginning of conditioning, and also this chapter is focusing on comparing the final tensile properties of different samples. Therefore, the tensile tests were only tested at 42 days after conditioning. Also by definition, water uptake at time zero is zero. Therefore, there is no time zero measurement for either of the tests. Only material properties at equilibrium were of interest, hence, tensile testing was only performed at the last stage.

Table 6-2 Conditioning schedule

Time (days)	0.25	1	3	7	14	28	42
Water uptake measurement	×	×	×	×	×	×	×
Tensile testing							×

6.3 Results and Discussion

6.3.1 Water Uptake

As discussed in chapter 4 and chapter 5, water uptake is an important influence on TPS mechanical properties.

Table 6-3 Water uptake percentage at equilibrium level in RH 52%

	RMS-G18C	RMS-E18C	RMS-A18C	RMS-B18C
Average	5.23%	5.93%	5.63%	4.96%
SD	0.19%	0.24%	0.06%	0.09%
	RMS-G18	RMS-E18	RMS-A18	RMS-B18
Average	1.01%	3.38%	7.08%	6.17%
SD	0.16%	0.08%	0.07%	0.21%

Table 6-3 shows the water uptake percentage at the end of the conditioning period (42 days), with data from the samples without CNTs (chapter 4 and 5) added for comparison. As shown in figure 6-1, the water uptake percentage varies in a certain range once equilibrium has been reached, in a similar fashion to all previous water uptake measurements. According to previous discussion in chapter 4 and chapter 5, this phenomenon may be due to the crystal variation in TPS which will be discussed in 6.3.2.3 XRD analysis.

However, it can still be seen that the order from highest water uptake to lowest is RMS-E18C, RMS-A18C, RMS-G18C and RMS-B18C. For RMS-A and B series, water uptake percentage at this condition decreases with the addition of CNTs. In contrast, water uptake percentage increase with the addition of CNTs at the same condition for RMS-G and E series. It is interesting to note that all four samples with CNTs differ in their final water uptake by no more 1%. In terms of water uptake percentage, it seems like the addition of CNTs eliminates the differences between different samples to some extent.

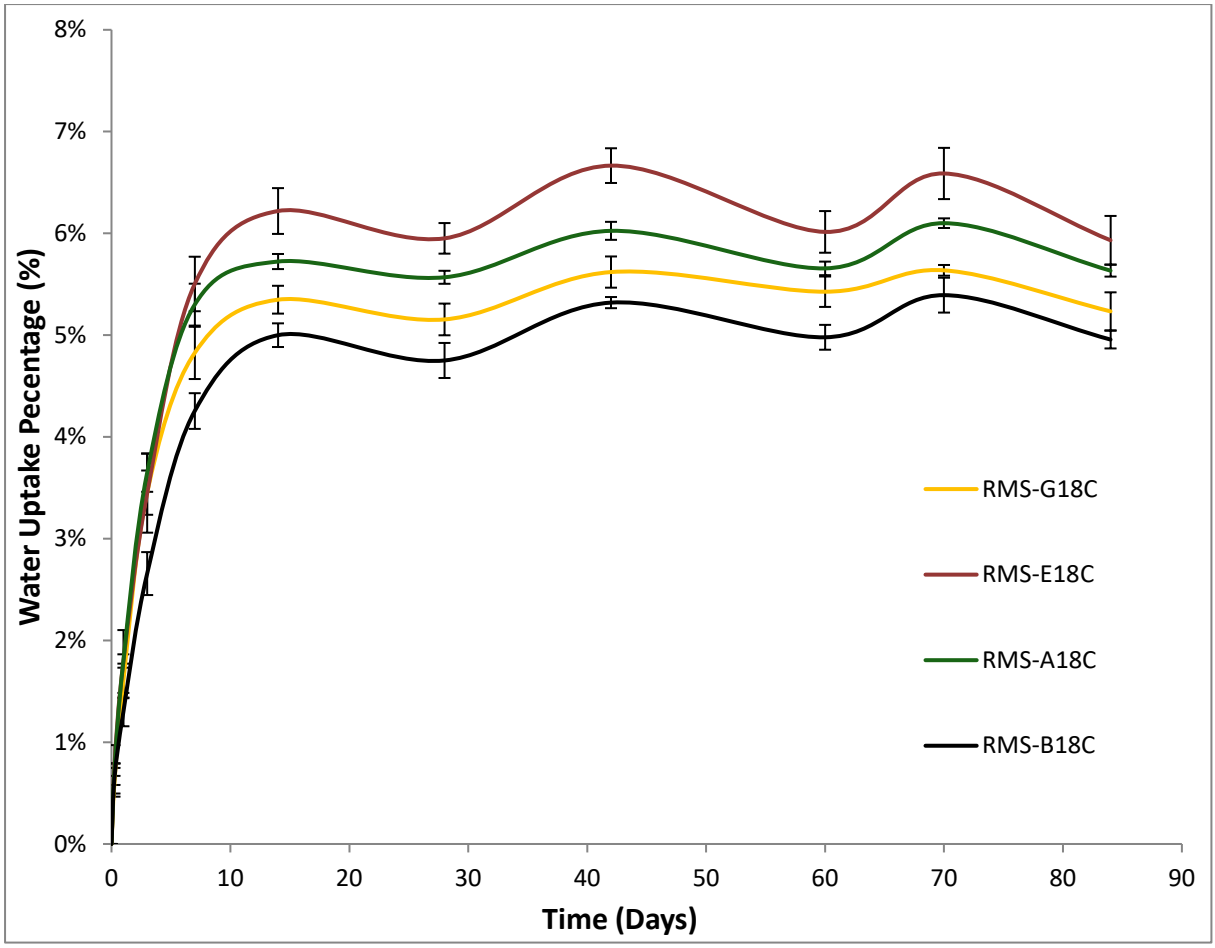

Figure 6-1 Water uptake trend over time of RMS-CNT series samples in RH52%

6.3.2 Characterisation after Sample Conditioning

6.3.2.1 Tensile Test

The tensile strength, Young's modulus and elongation at break are displayed in figure 6-2 (a), 6-2 (b) and 6-2 (c) respectively. The data are summarized in table 6-4.

It was found that CNTs have potential stiffening effects on RMS-G and E series samples, as the mean Young's modulus of both series is increased, and the elongation at break is decreased (although note that the standard deviation error bars for the Young's modulus data overlap so the strengthening effect is not certain). The mean elongation at break of RMS-G18C is 33% of RMS-G18, RMS-E18C is 26% of RMS-E18 whilst the mean Young's modulus of RMS-G18C is approximately 146% of RMS-G18, and RMS-E18C is 148% of RMS-E18.

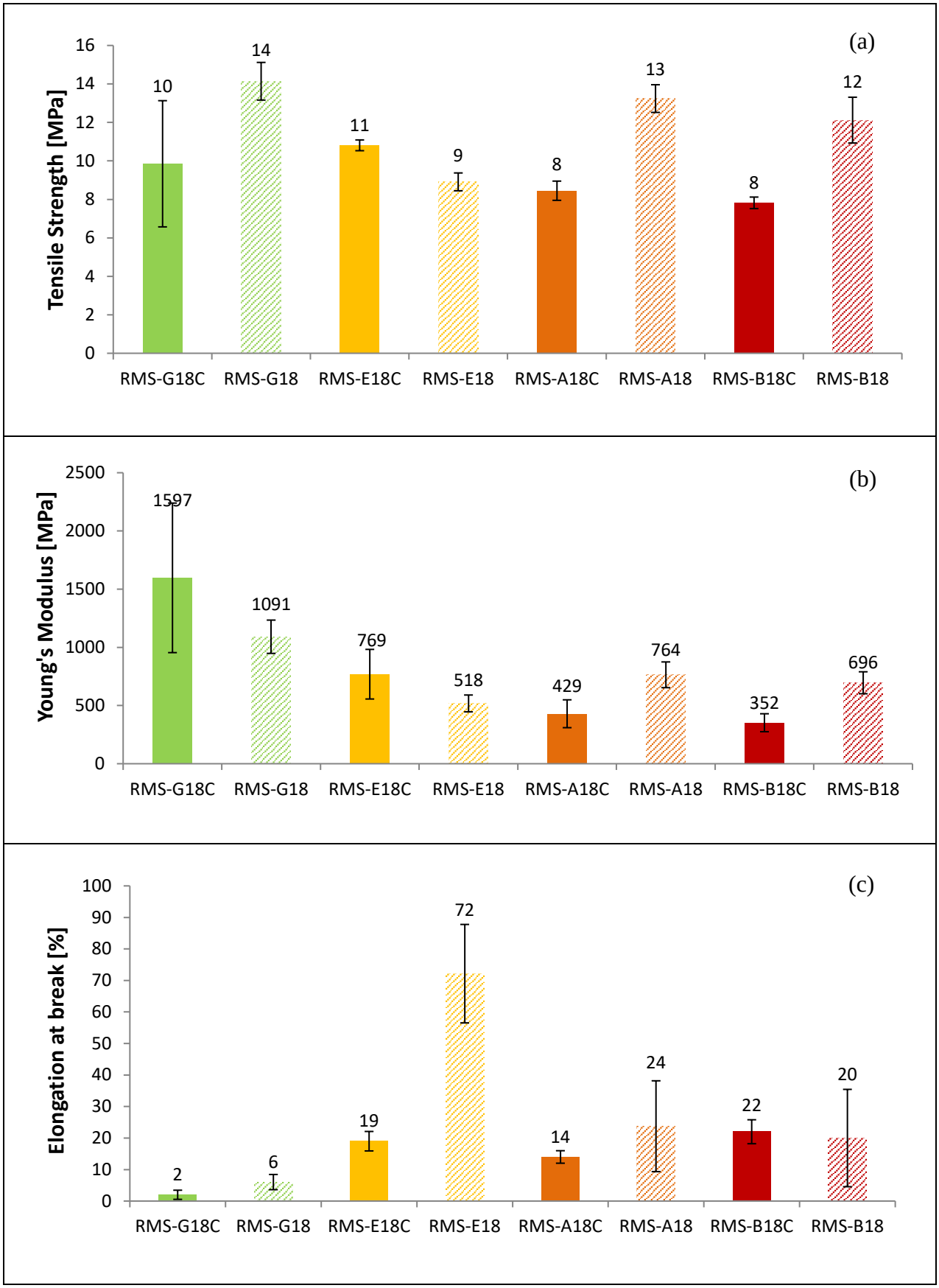

Figure 6-2 Tensile data of all RMS-CNT series samples conditioned in RH52% with standard devidation error bars. (a) Tensile strength; (b) Young's modulus; (c) Elongation at break

Considering the RMS-A and B series, adding CNTs lowers the mean values of both Young's modulus and tensile strength. The mean Young's modulus of RMS-A18 is decreased by 44% when added CNTs, and tensile strength is decreased by 38%. Those of RMS-B18 are decreased by 49% and 33% respectively. The error bars for the elongation at break of both samples shows overlap, which means it is not significantly different. However, it is interesting to note that in the case of all the ILs, adding CNTs decreased the relative error for elongation at break which might suggest a more reproducible structure is being formed

In figure 6-3, which shows typical raw tensile test data for all the samples, the CNTs samples show a lower yield pattern, which indicates the micromorphology of the samples might have changed by the addition of the CNTs.

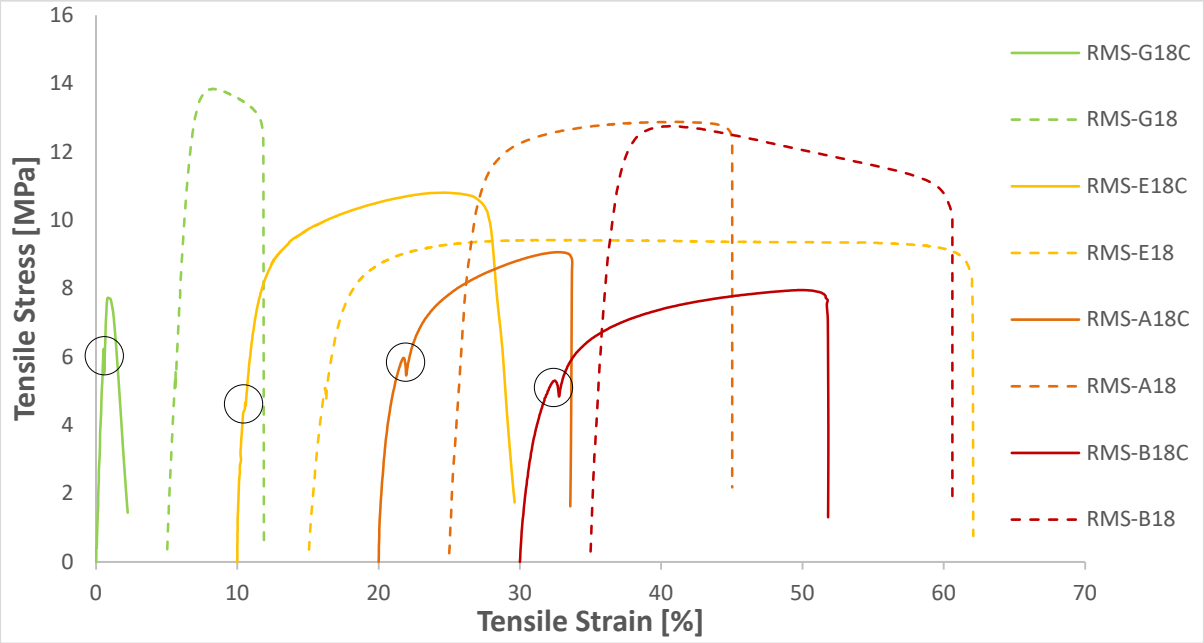

Figure 6-3 Typical tensile testing curve examples of RMS-CNT series samples conditioned at RH 52%. Potential yielding points in the CNT samples are indicated by circles. (The starting point of each subsequent curve is shifted by 5% to aid clarity.)

As discussed in previous chapters, the tensile properties are significantly affected by water uptake, plasticiser interaction and crystallisation behaviour. When CNTs are introduced into these material systems, the complexity of the factors affecting tensile properties increase. In particular, the distribution and dispersion of CNTs can significantly influence the tensile properties as mentioned 2.4.3 (Liu et al., 2011b, Cao et al., 2007, Famá et al., 2011). Also, as a nanofiller, CNTs are very likely to have an effect on crystallisation behaviour, either facilitating the crystallisation due to their nucleating role or slowing the crystal growth, introducing lamellar defects (Taghizadeh and Favis, 2013), and hence in turn affecting water

uptake percentages. The complexity of the CNT nano-composites introduces a myriad of unfamiliar factors which affect the morphology and physical properties of the starch polymer product. It is thus difficult at this point to draw conclusions on the effects of adding CNTs to the TPS system. Further experiments are therefore necessary to investigate the underlying mechanism.

Table 6-4 Tensile properties comparison between CNTs-added samples and original samples conditioned in RH52%

Code	Tensile Strength [MPa]		Young's modulus [MPa]		Elongation at Break [%]	
	Mean	RE	Mean	RE	Mean	RE
RMS-G18C	9.9	0.33	1600	0.40	2.0	0.75
RMS-G18	14	0.07	1100	0.13	6.0	0.40
RMS-E18C	10.8	0.03	770	0.27	19	0.16
RMS-E18	8.9	0.05	520	0.14	72.0	0.22
RMS-A18C	8.5	0.06	430	0.28	14	0.14
RMS-A18	13	0.06	760	0.14	24.0	0.58
RMS-B18C	7.8	0.04	350	0.22	22	0.17
RMS-B18	12	0.10	700	0.13	20	0.75

6.3.2.2 FTIR and Raman Spectroscopy

The CNTs included in the TPS matrix potentially interact with the other ingredients of TPS composites. Hence, FTIR and Raman spectroscopy of the CNTs-added samples have been obtained (table 6-5) and compared to their individual original samples.

Table 6-5 Band assignment for FTIR and Raman spectroscopy for RMS and CNTs

Material	Band assignment	Infrared	Raman	
RMS	Skeletal modes of pyranose ring		480-490	(Cael et al., 1975, Cael et al., 1973, Dhital et al., 2011, Kizil et al., 2002)
	CH2 deformation		872,1470	
	COC α-1,4 glycosidic linkage	930	941-949	
	CH_2OH side chain related mode		1263	
	COH deformation	993, 1014		
	CH deformation of all ring hydrogens		1306	
CNTs	D band		1317-1316	(Brown et al., 2001, Jorio et al., 2002)
	G band		1606	
	D' band		2665	

Figure 6-4 and 6-5 summarize the results of these experiments. In the FTIR spectra, bands of CNTs are not obvious due to the symmetry of the carbon network. However, all samples with CNTs have a growing peak at 995 cm^{-1} compared to 1014 cm^{-1}, indicating interaction

potentially affects COH deformation of starch. This also suggests a possible starch molecular order change, as the absorbance ratio of these two peaks has been associated with ordered and amorphous structures in starch, and can be used as an index to characterise the short-range alignment of helices (Dhital et al., 2011, Vansoest et al., 1995). Specifically, the decrease in the 1014/995 cm^{-1} ratio indicates a decrease in the molecular order, which is likely to be associated with the disruption of double helices (Dhital et al., 2011). Therefore, the introduction of CNTs may influence the crystallisation behaviour as discussed in 6.3.2.1, this will be discussed with XRD results in 6.3.2.3.

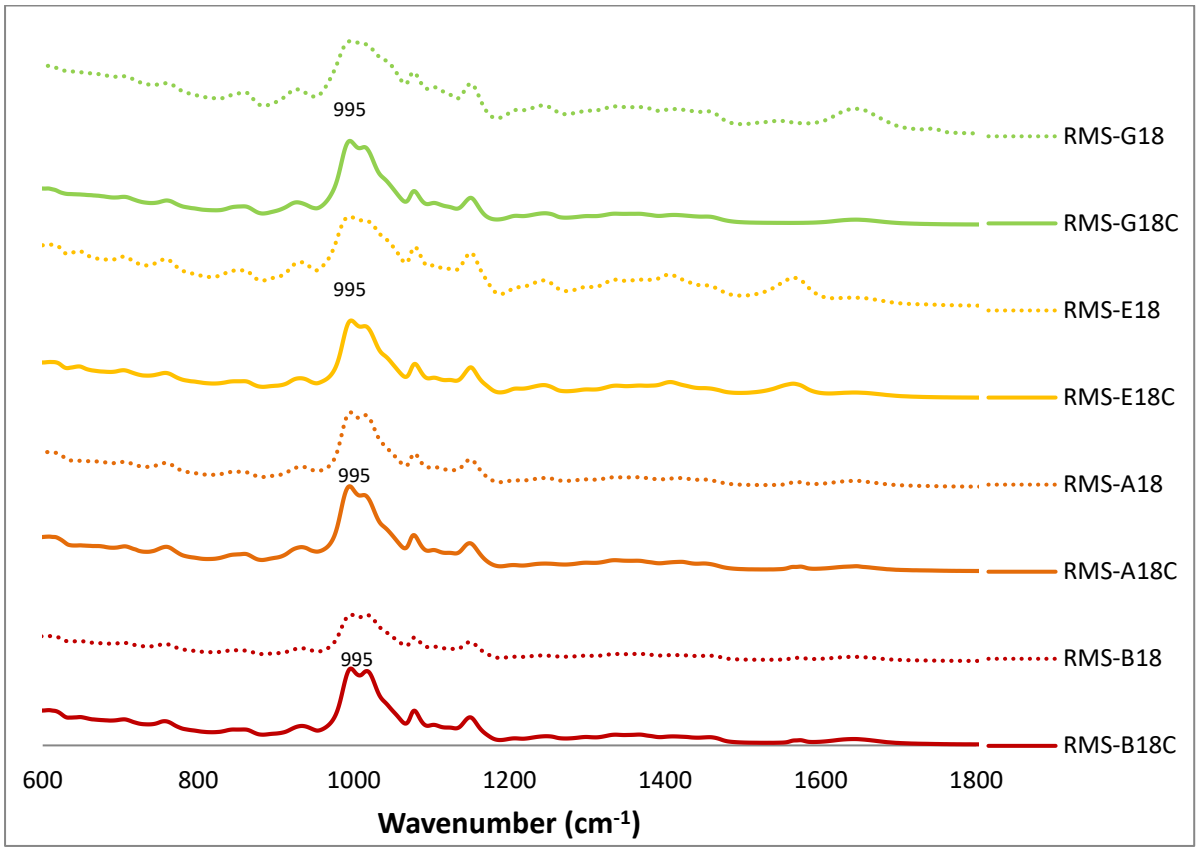

Figure 6-4 FTIR fingerprint region spectra of RMS samples

The FTIR result is supported by Raman spectra. All samples with CNTs have an up-shift of pyranose ring skeletal modes at about 488 cm^{-1}, indicating the interaction between CNTs and starch. Bands at approximately 941 cm-1 show a-1,4 glycosidic linkage of starch molecules which is affected by the appearance of CNTs as well. As for CNTs, most of the diagnostic bands are revealed in Raman spectroscopy. The band of radial breathing mode (RBM) which is usually around 200 cm-1 provides an easy and quick determination of the tube diameter distribution (Jorio et al., 2002). Since this character is not significantly relevant to this study and not obvious in the spectra, the discussion will not be focused on this topic. A very important

feature called the tangential mode vibrations which is the high-frequency E_{2g} first-order mode (Antunes et al., 2006), also widely known as G band, appears at about 1610 cm^{-1} in this study. Another significant feature, known as the D band, usually can be observed between 1250 cm^{-1} and 1450 cm^{-1}. The D band is activated in the first-order scattering process of sp^2 carbons by the presence of in-plane substitutional hetero-atoms, vacancies, grain boundaries or other defects, as well as finite size effects, all of which lower the crystalline symmetry of the quasi-infinite lattice (Brown et al., 2001). Namely, this D band is related to the defects of CNTs. Also, a small second-order harmonic D' band related to the defects is observed at 2665 cm^{-1}. A relatively strong absorption (compared to the G band) of D and D' band indicates less perfect structure of the CNTs embedded in TPS samples (Antunes et al., 2006, Nemanich and Solin, 1979). In figure 6-4, it can be found that the D and D' band become the largest bands (compared to the pyranose ring skeletal mode of starch) in RMS-B18C while the RMS-G18C has the smallest D band. Potentially the CNTs interaction with RMS-B18C is the strongest, RMS-E18C and RMS-A18C are in between while RMS-G18C is the weakest.

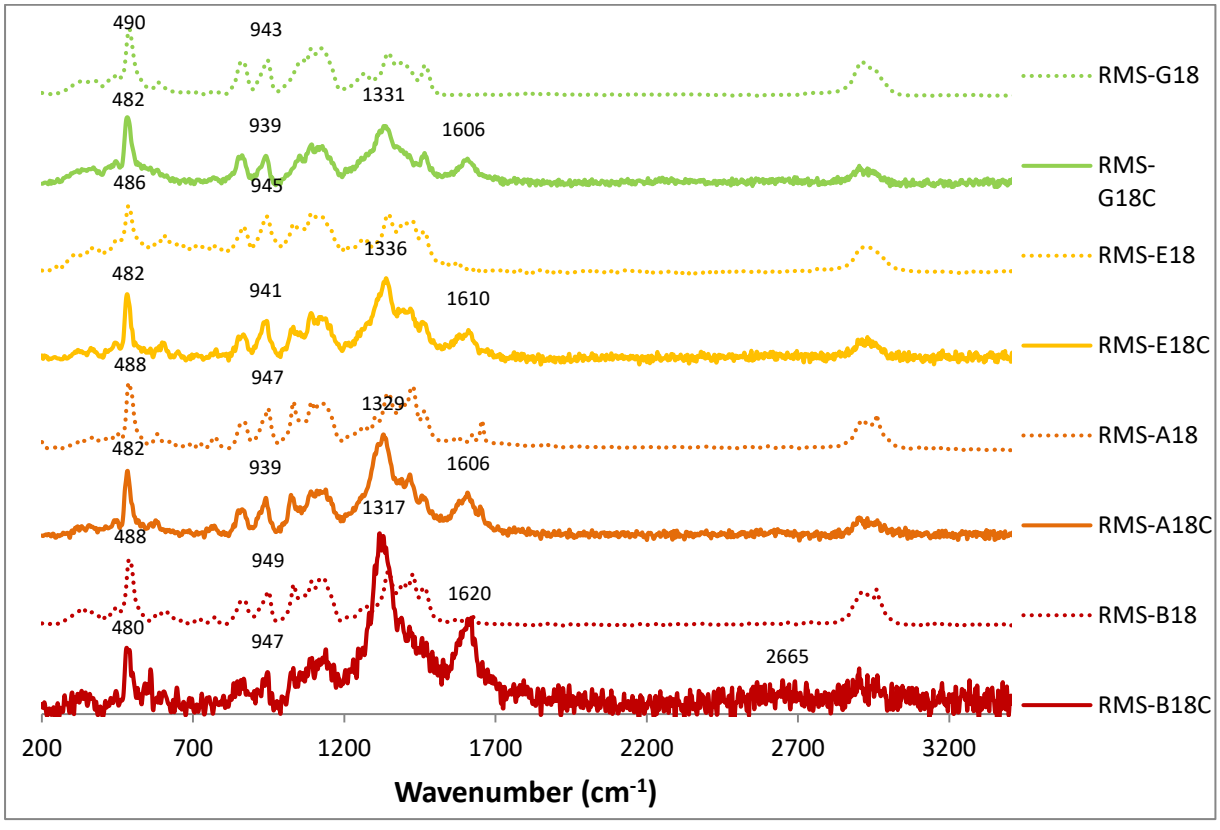

Figure 6-5 Raman spectra of RMS samples

The interactions between CNTs and TPS should have some influences on CNTs dispersion and distribution. Since it has been reported (Zhao et al., 2012, Hameed et al., 2013) that ILs are

effective in dispersing CNTs, the results of FTIR and Raman spectroscopy might have suggested the CNTs dispersion effectiveness of these different plasticisers. According to the analysis, the strongest adhesion between CNTs and TPS samples should be RMS-B18C. Conversely, the weakest might be RMS-G18C.

6.3.2.3 XRD

The diffractogram of RMS samples strengthened by CNTs are displayed in figure 6-6 and figure 6-7. Specifically, figure 6-6 compares the samples plasticized by glycerol with those by [Emim][OAc]. Figure 6-7 compares the [Amim]Cl plasticized samples with those plasticised using [Bmim]Cl. Similar to the previous studies, samples tested before conditioning are labelled with RH0 and samples tested after conditioning are labelled RH52. In figure 6-6, all the curves display an obvious sharp peak at 2θ of 20° with a smaller peak at 2θ of 13°. Some of them have a small tip at 2θ of 7°. These signals are typical V-type crystallite characters which are induced after processing. RMS-G18C-RH0 does not have the small tip at 2θ of 7° which presents in RMS-G18C-RH52, indicating the growth or refinement of V-type crystallites from dry conditions to comparatively humid conditions. This assumption is supported by the peak sharpening at 2θ of 13° from RH0 to RH52. The sharpening of this peak implies either the growth or the refinement of the crystallites. In fact, peaks at 2θ of 15°, 17° and 18° also become slightly sharper and clearer in RMS-G18C-RH52 which represents the refinement of A-type crystalline structure in these samples.

Considering the RMS-E18C samples, the A-type characters also exist in their diffraction patterns. However, a small peak at 2θ of 5° shows the existence of B-type crystallites. Thus, the crystalline structures of RMS-E18C samples are classified as C-type. Similar to the RMS-G18C samples, the diffraction pattern of RMS-E18C-RH52 displays more distinct peaks than RMS-E18C-RH0, suggesting either less defects or larger size of crystallites. The refinement of all types of crystallites may affect the water uptake and the tensile properties, as A and B-type crystallites have open space which can be filled with water molecules (Imberty et al., 1991, Imberty et al., 1987, Imberty et al., 1988, Imberty and Perez, 1988) and V-type crystallites are associated with elastic modulus and yield stress (Liu et al., 2009, Yurdakul et al., 2013).

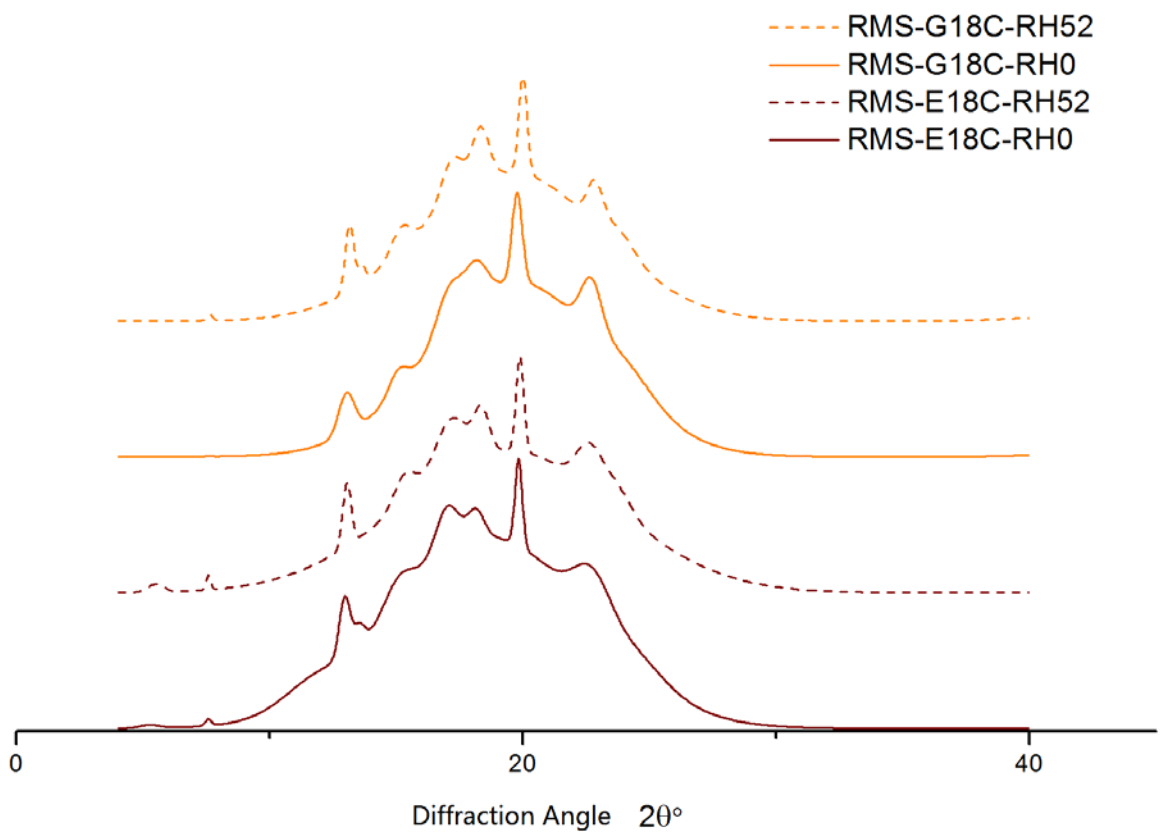

Figure 6-6 RMS-CNT-G and E Series XRD diffractogram

Table 6-6 and 6-7 summarizes the details of XRD analysis. It can be found that the type of crystalline structure does not change in RMS-G18C and RMS-E18C samples after conditioning. Though the humidity change can lower the total crystallinity, the variation is quite small. When, however, comparing samples with and without CNTs, the introduction of CNTs leads to a dramatic drop of crystallinity.

In terms of the RMS-A18C and B18C samples, the crystallisation behaviour is quite similar. First of all, the V-type crystalline structure is indicated by the peaks at 2θ of 7°, 13° and 20° in all samples (figure 6-7). Secondly, all samples have a single peak at 2θ of 15° and a doublet at 2θ of 17°, 18° suggesting the existence of A-type crystalline structure. After conditioning, the crystal type has not been changed in all these samples.

For RMS-A18C samples, the V-type diagnostic peaks seem to be sharper when conditioning RH has been increased to 52%. To the contrary, the A-type crystalline characters in RH52% do not seem to be very different from RH0%. In the case of RMS-B18C, it can be observed

that V-type crystalline characters are weaker in higher RH conditions as the small peak at 2θ of 7° has gone. Similarly, the A-type crystalline characters are little changed.

Comparing the detailed data of RMS-A18C and RMS-B18C in table 6-6, it can be seen that the total crystallinity has decreased after conditioning while the V-type crystallinity has increased. Contrasting these results to the RMS-A18 and RMS-B18 samples in table 6-7, it is apparent that, except for RMS-B18-RH0, the introduction of CNTs in the composite matrix can lead to a decrease in total crystallinity.

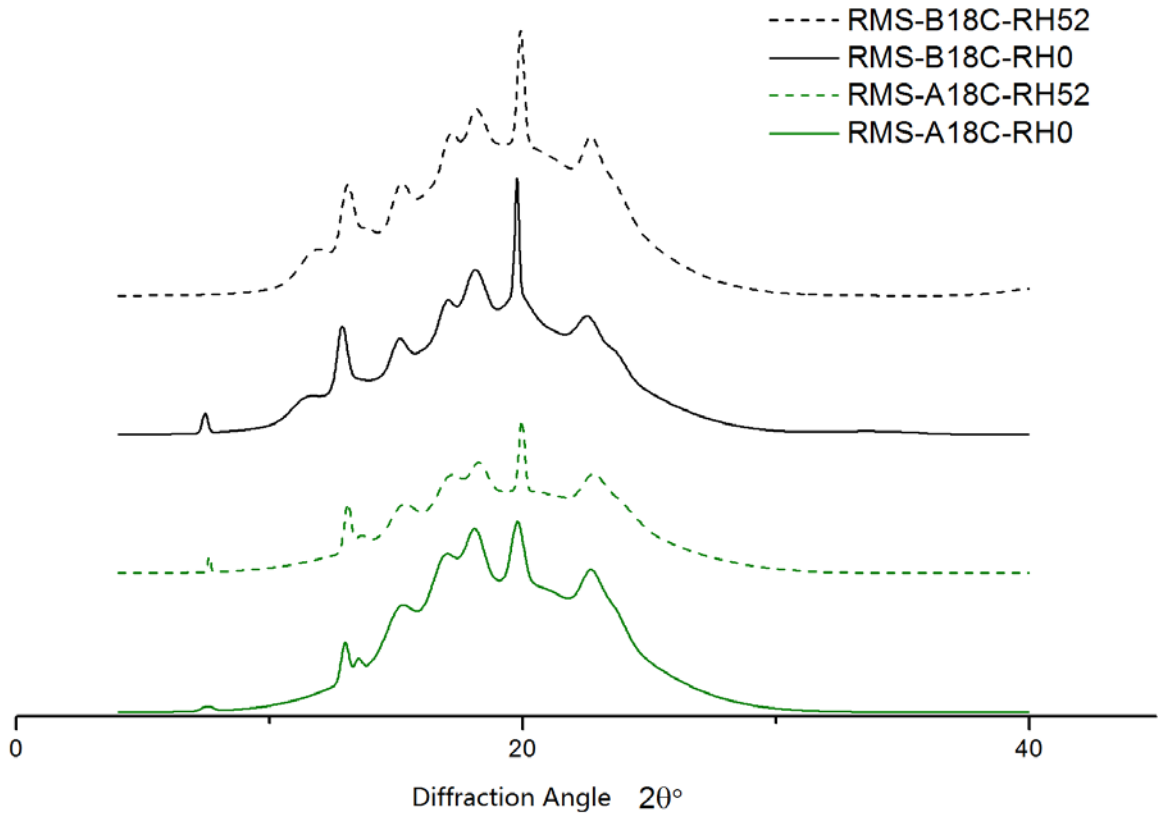

Figure 6-7 RMS-CNT-A and B Series XRD diffractogram

To summarize, the existence of CNTs in plasticized RMS does not alter the crystallite structures as the crystal type has not been changed. It instead has the effect of decreasing total crystallinity. Compared to each formulation without CNTs, the crystallinity of RMS-CNT series samples seems to be less sensitive to RH variations. Moreover, it seems that CNTs are able to reduce the differences of total crystallinity and crystallite structure between different IL-plasticized samples overall. It appears that the introduction of CNTs slow the crystal growth, which introduces lamellar defects (Taghizadeh and Favis, 2013).

Previous chapters have discussed the relationship between crystallinity, water uptake and mechanical properties. In the case of CNT series samples, it is very similar. As crystallites are found growing during conditioning, this suggests that crystallisation behaviour is relevant to water uptake results such as equilibrium level uptake percentage and their oscillating uptake pattern. Crystallisation behaviour is also found to have influences on tensile properties. Similar to another study (Yurdakul et al., 2013), it is observed that the V-type crystallite structure relates heavily to the tensile properties. In detail, the V-type crystallinity of all CNT series samples is decreased compared to those without adding CNTs. This results in lower yield stress, as well as lower or equivalent Young's modulus, of all CNT series samples, which are also subject to other factors such as CNTs dispersion and distribution. It is evident, however, that the variable of which plasticiser is used is still the predominant factor of tensile properties.

Table 6-6 Crystalline pattern and crystallinity of RMS CNT series samples

Code	RH0			Pattern	RH52			Pattern
	Degree of crystallinity [%]				Degree of crystallinity [%]			
	Double Helices	V-type	Total		Double Helices	V-type	Total	
RMS-G18C	12.82	4.32	17.14	A	12.35	4.44	16.79	A
RMS-E18C	14.36	2.91	17.27	C	12.76	3.66	16.42	C
RMS-A18C	15.24	3.28	18.52	A	14.63	3.52	18.15	A
RMS-B18C	16.71	3.79	20.50	A	13.95	4.60	18.55	A

Table 6-7 Crystalline pattern and crystallinity of RMS samples

Code	RH0			Pattern	RH52			Pattern
	Degree of crystallinity [%]				Degree of crystallinity [%]			
	Double Helices	V-type	Total		Double Helices	V-type	Total	
RMS-G18	23.25	6.47	29.72	C	21.57	5.26	26.83	A
RMS-E18	22.09	4.62	26.71	C	21.32	4.31	25.63	C
RMS-A18	18.46	3.13	21.59	A	14.60	6.10	20.70	A
RMS-B18	5.22	2.91	8.13	A	13.99	5.21	19.20	A

6.3.2.4 TGA

Figure 6-8 show and compare the TGA results of TPS samples in terms of both percentage of mass loss and its derivative value. It is clearly seen that adding CNTs to TPS matrix does not greatly affect the thermal stability of the samples. It does not significantly change the thermal degradation onset temperature. Neither does it significantly change the peak temperature of the derivative mass percentage. This is similar to other nano-composites studies involving CNTs which demonstrate that CNTs do not significantly alter the material decomposition temperature (Ferreira et al., 2016, Liu et al., 2017), except in the case of modified CNTs, where the decomposition temperature can be significantly improved (Baishya and Maji, 2016). For RMS-G18C and RMS-E18C, however, CNTs allow samples to degrade more steadily, behaving more like RMS-A18C and RMS-B18C. This may be affected by the similar crystallisation behaviour analysed above.

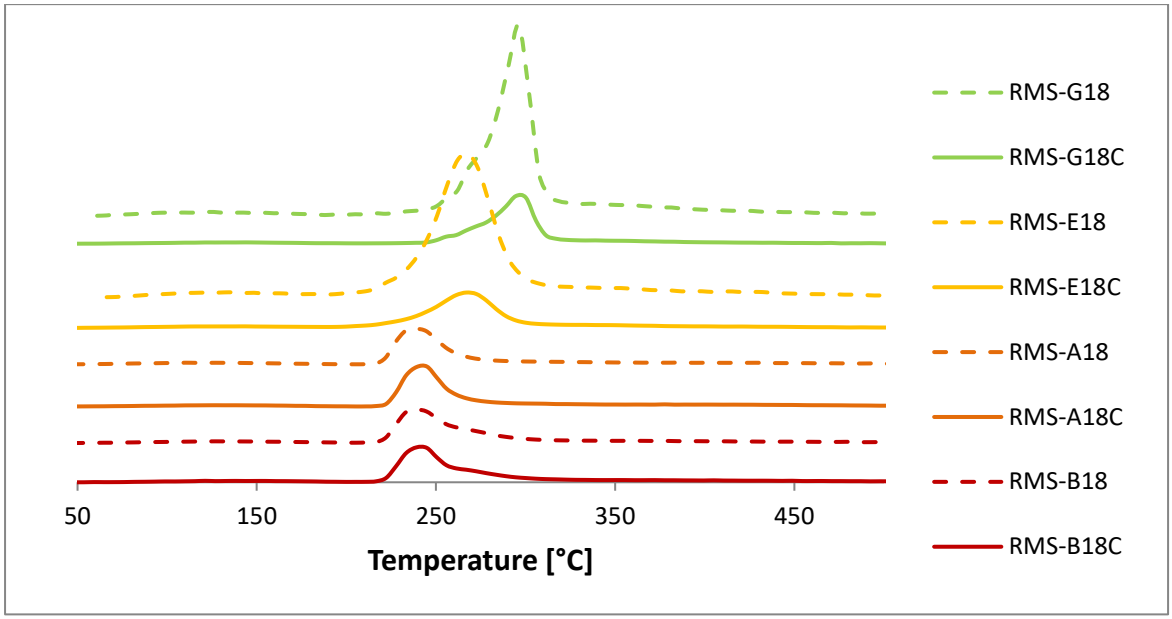

Figure 6-8 First derivative TGA results of RMS samples

6.3.2.5 TEM

To investigate whether our sample preparation methodology had been successful in both distributing and dispersing the CNTs in the TPS matrix as well as to observe the micro morphology of TPS material, a TEM analysis was performed on a representative sample of RMS-B18C.

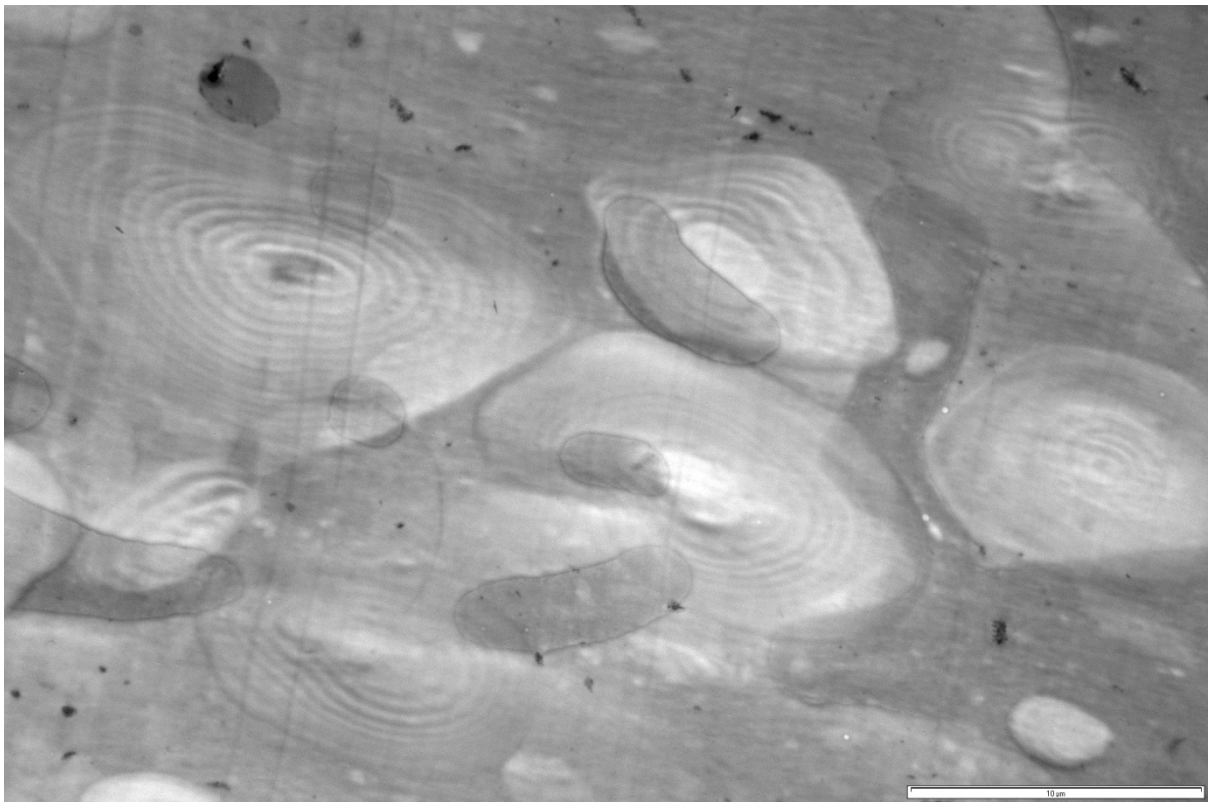

Figure 6-9 The morphology of RMS-B18C sample under 5000 magnification (scale bar - 10µm)

Both amorphous and natural crystalized regions can be observed from figure 6-9. Potentially, the concentric rings are the cross sectional area of starch granules, as describe in chapter 2. The other uniformed regions around the concentric rings are considered amorphous regions. Black aggregated objects which are believed to be CNTs bundles can be found distributed in the amorphous region. However, the distribution is not homogeneous.

Figure 6-10 shows greater magnification levels of the amorphous regions and aggregates. In the amorphous region, a lot of dispersed CNTs can be found (figure 6-10a) indicating the material compounding was quite successful. However, the large aggregates (figure 6-10b) also show that poorly dispersed CNTs still exist in the amorphous region. By observing figure 6-10c and figure 6-10d, the concentric multi-layer morphology (similar to figure 2-6) of MWCNTs becomes much more clear.

In all, the distribution of CNTs in RMS-B18C is achieved in all regions except the natural starch granule region. However, parts of the CNTs are still in aggregated state. This demonstrates that a more effective compounding methodology is needed to achieve homogeneous dispersion and distribution.

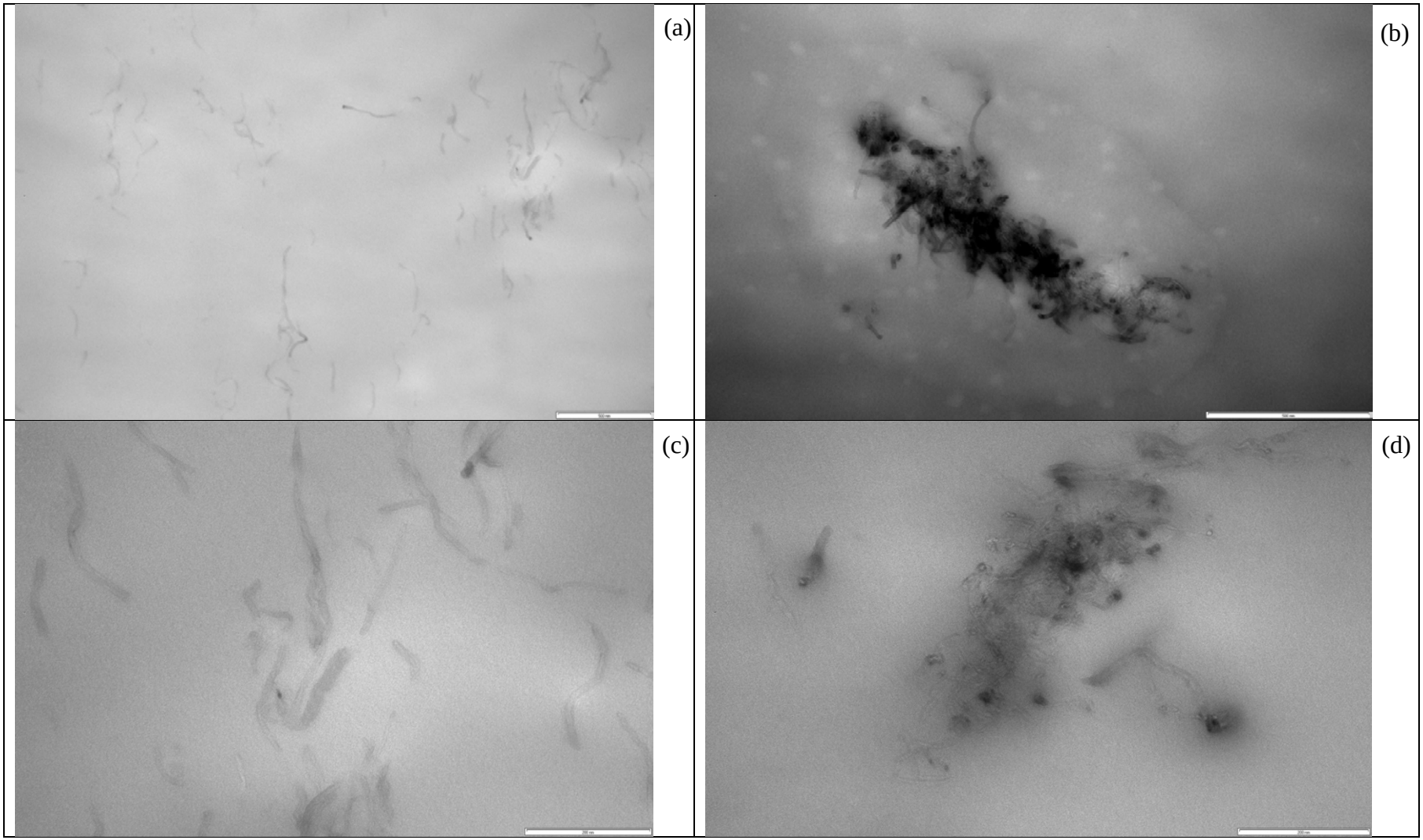

Figure 6-10 amorphous region captured under 60k× magnification (scale bar 500 nm); (b) black aggregate captured under 100k× magnification (scale 500 nm); (c) captured amorphous region photo under 200k× magnification (scale 200 nm); (d) black aggregate captured under 200k× magnification (scale 200 nm).

6.4 Conclusions

CNTs/TPS nano-composites have been investigated in terms of mechanical properties, water uptake ability, thermal degradation temperature, crystallisation behaviour and molecular interactions. Overall, the CNTs strengthening effects on TPS material properties are more complicated than expected.

Firstly, CNTs behave differently in different types of samples. Usually, the same type of strengthening material is expected to affect the same material-based samples in a similar way. However, as discussed previously in session 6.3.2.1 (tensile properties), CNTs show strengthening material characteristics in RMS-G and RMS-E series by increasing the stiffness and rigidness of the materials, but not in the other series. CNTs appear to act more like plasticizing material in RMS-A and RMS-B series samples as the addition of CNTs results in a decline of Young's modulus and tensile strength while elongation at break remains at the same level. Another example would be water uptake experiments. Compared to the earlier results, it can be found that the addition of CNTs has increased the water uptake percentage of RMS-G and RMS-E samples but decreased the RMS-A and RMS-B series slightly.

Secondly, in another aspect, the existence of CNTs reduces the differences between the material properties of the samples. In other words, the differences between the plasticisers used become less obvious, and only some individual characteristics remain to be distinguished. For example, the water uptake percentages of CNT series samples all tend towards about 5% at equilibrium level while previously they were scattered approximately between 1% and 7%. In terms of the crystallisation behaviour, CNTs tends to turn crystallite structures of all kinds into the A-type and hence minimize the crystallinity differences. In addition, the thermal degradation pattern of each CNT series sample also become more similar.

The reasons for these behaviours are complicated. One of the possible explanations is that the number of affecting factors has increased. For example, when comparing the tensile properties, water uptake percentage and crystallinity are not the only relevant factors anymore. CNTs dispersion and distribution as well as the adhesion abilities of CNTs can also affect the tensile properties. When considering the property unifying effects of CNTs mentioned above, the reason might be that the effect of adding the CNTs is the predominant factor for crystallisation behaviour. Hence, it only affects the results such as water uptake, thermal degradation rate but not tensile properties. Further experiments are needed to examine this assumption.

TEM analysis provides some hints for the poor strengthening effects in RMS-B18C. Potentially, the loading amount of CNTs is not large enough to reach a critical value, namely the percolation threshold above which the mechanical properties will be dominated by CNTs. Also, it is assumed that better dispersion of CNTs is required to refine the results as acceptable distribution had been achieved. A more effective methodology to disperse CNTs needs to be developed in the future for this reason. In the meanwhile, it is also significant to obtain the TEM photos of other samples for results comparison.

7 CONDUCTIVITY OF RMS STRENGTHENED BY CNTS

7.1 Introduction

As well as the mechanical strengthening potential of CNTs, they also have an electrical conductivity up to 10^4-10^5 S/cm (Marinho et al., 2012). In addition, ILs are reported to be conductive as mentioned in chapter 2. Hence, the RMS/ILs/CNTs composites might be electrically conductive as well. Consequently, relatively high electrical conductivity will add value to the RMS/ILs/CNTs composites since they can be applied as conductive or semi-conductive material. Therefore, it is useful to investigate how the electrical conductivity can be increased.

In the last chapter, the strengthening effect of CNTs on TPS material has been studied. It has been found that tensile strength and Young's modulus are not necessarily enhanced by adding CNTs. As discussed in chapter 6, the existence of CNTs might be only one of the multiple factors which contribute to the ultimate material properties and even not the predominant one. In fact, the reinforcing material needs to reach a certain level to make it the predominant factor of mechanical properties contribution (Mikitaev and Kozlov, 2015). This critical value which makes the ultimate mechanical properties dependant on reinforcing filler content is referred as percolation threshold.

Percolation theory is not only applied to mechanical property research, but also very significant in terms of investigating the electrical conductivity of nano-composites. The mechanism of electrical conductivity percolation is quite similar to mechanical properties. There is a certain point when the conductive nano-fillers network is build up and significantly increases the electrical conductivity of ultimate nano-composites. This critical point is identified as the percolation threshold (Alig et al., 2012, Vilgis et al., 2009). The percolation threshold can be identified by rheology tests as when a percolation network is formed this would slightly change the material rheological properties (McClory et al., 2010, McClory et al., 2011, McNally et al., 2005, Hassanabadi et al., 2014). For example, any deviation from a linear relationship between G' and G" is indicative of the formation of a percolated network (McClory et al., 2010).

Although it has been found in the last chapter that in some of the cases, introducing CNTs to TPS matrix is not necessarily beneficial to increase the tensile strength and Young's modulus, it should still be useful to inspect the electrical conductivity of these samples. Hence, in this chapter, a simple comparison is made between carbon nanotube added samples and their

original formulation without carbon nanotubes. The effects on material electrical conductivity given by CNTs will be investigated and discussed.

7.2 Experimental

7.2.1 Materials

The starch used in this experiment was RMS. Glycerol, [Emim][OAc], [Amim]Cl and [Bmim]Cl were used as plasticisers. Multi-walled CNTs were added as strengthening and functional material. Details are outlined in Chapter 3.2.

7.2.2 Experimental Methods

Sixteen types of samples of TPS were produced and compression moulded according to the formulation shown in table 7-1, following the methodology outlined in chapter 3.3.1.

Table 7-1 RMS sample formulation design

Code	RMS Amount	Water	Glycerol	[Emim][OAc]	[Amim]Cl	[Bmim]Cl	CNT
RMS-G18	100	12	18	-	-	-	-
RMS-G27	100	3	27	-	-	-	-
RMS-E18	100	12	-	18	-	-	-
RMS-E27	100	3	-	27	-	-	-
RMS-A18	100	12	-	-	18	-	-
RMS-A27	100	3	-	-	27	-	-
RMS-B18	100	12	-	-	-	18	-
RMS-B27	100	3	-	-	-	27	-
RMS-G18-C	100	12	18	-	-	-	1
RMS-G27-C	100	3	27	-	-	-	1
RMS-E18-C	100	12	-	18	-	-	1
RMS-E27-C	100	3	-	27	-	-	1
RMS-A18-C	100	12	-	-	18	-	1
RMS-A27-C	100	3	-	-	27	-	1
RMS-B18-C	100	12	-	-	-	18	1
RMS-B27-C	100	3	-	-	-	27	1

The sample sheets were then conditioned at RH52% and their conductivity measured using the technique described in section 3.3.3.7:

7.3 Results and Discussion

Figure 7-1 shows the calculated electrical conductivity data of all samples with plasticiser level 18. Table 7-2 shows original electrical conductivity data of all samples. The full details of the sample compositions are displayed in table 7-1.

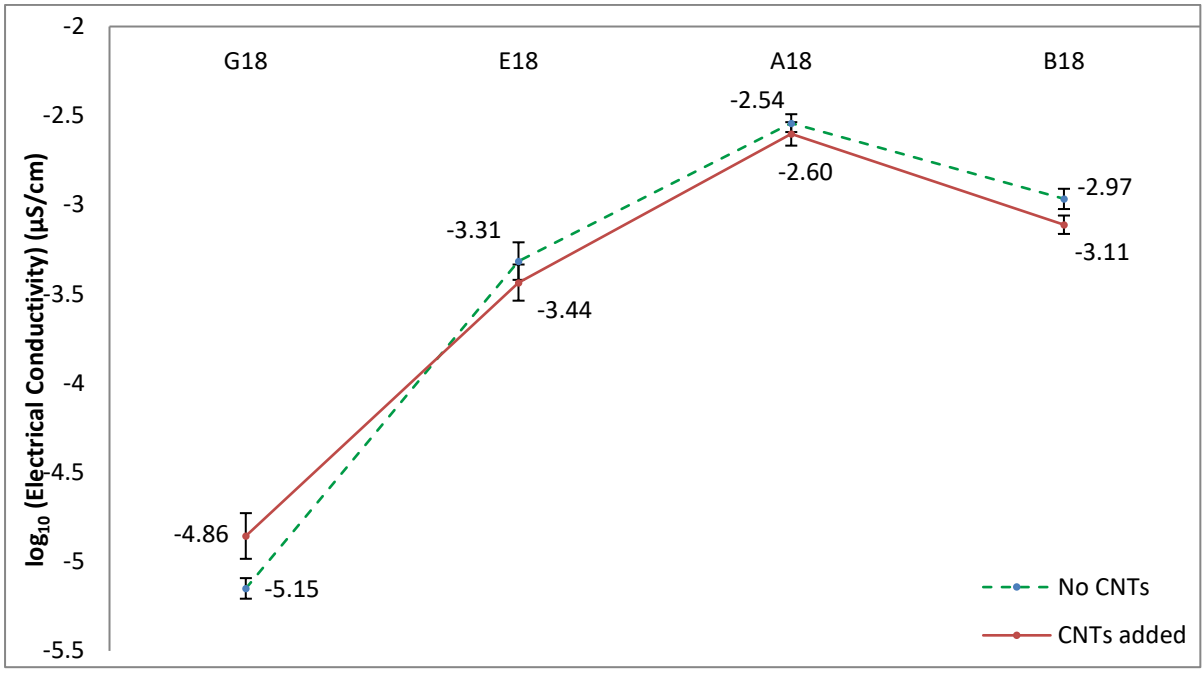

Figure 7-1 Electrical conductivity of plasticiser level 18 RMS samples (µS/cm)

By comparing the plasticisers, the data show that TPS plasticized by [Amim]Cl has the highest electrical conductivity both with or without CNTs. In the case of samples without CNTs, those plasticised by [Bmim]Cl show an average of 1.09×10^{-3} µS/cm conductivity, which is approximately 38% of those plasticised by [Amim]Cl. [Emim][OAc] plasticized samples show an average conductivity of 4.99×10^{-4} µS/cm, which is about 46% of [Bmim]Cl plasticized samples. The mean electrical conductivity of glycerol plasticized samples is 7.15×10^{-6} µS/cm, which is 1.4% of those plasticised by [Emim][OAc], several orders of magnitude lower than the others. It is interesting to note that for the ILs plasticized samples, the addition of CNTs lowered the electrical conductivity by around 25%. Only in the case of glycerol plasticized samples, did it increase from 7.15×10^{-6} µS/cm to 1.46×10^{-5} µS/cm.

Just as was seen in the mechanical properties analysis (chapter 6), it seems that the addition of CNTs does not necessarily improve the electrical conductivity as expected. In all the IL cases, adding CNTs actually decreased the electrical conductivity. However, it cannot be simply concluded that adding CNTs are irrelevant to enhance the electrical conductivity of TPS yet.

The results obtained for the electrical conductivities in these samples are not of the same order of magnitude as that reported for CNTs, which can have low electrical resistivity down to 5.1×10^{-6} Ω·cm (Dervishi et al., 2009, Ebbesen et al., 1996), (i.e. up to approximately 2×10^{11} μS/cm when converted to electrical conductivity). Neither can the results be compared to the values of 2.5×10^{4} μS/cm for [Amim]Cl and 25 μS/cm for [Bmim]Cl as reported in other studies (Ning et al., 2009, Sankri et al., 2010) where solution casting was employed and the TPS were plasticised with twice the level of ILs than used in this thesis, and an overabundance of water. Thus, potentially it indicates that such an amount of CNTs loading is below the percolation threshold. Therefore, the added amount of CNTs might not be the predominant factor which affects material electrical conductivity.

In fact, the existence of CNTs in the matrix is only one of the factors which could influence the ultimate electrical conductivity of product. Obviously, the plasticiser used is another factor. This may be related to the ion mobility of different plasticisers. Compared to the non-conjugated structure of glycerol, and ILs with only a single conjugated imidazole ring such as [Emim][OAc] and [Bmim]Cl, the highly conjugated allyl and imidazole structure of [Amim]Cl is promotes ion delocalisation. Also, as the conductivity is mainly controlled by ion diffusivity and mobility, a smaller anion with delocalised charge is considered a significant factor (Xie et al., 2015). Hence, [Emim][OAc] is only a little less effective as [Bmim]Cl in enhancing the electrical conductivity because [Bmim]Cl has a smaller anion. Compared to the ILs, glycerol does not have conjugated structures or any anions, therefore it does not show any effects in enhancing the electrical conductivity.

However, water uptake percentage might be another relevant factor since water can be advantageous to the transference of the anions and cations in TPS (Ning et al., 2009). Water uptake experiment in chapter 6 has shown that adding CNTs can lead to lower water uptake in RMS plasticized by [Amim]Cl and [Bmim]Cl while higher in the others. Similarly, it is found electrical conductivity decreases in samples plasticized by [Amim]Cl and [Bmim]Cl with CNTs added, while it increases in samples plasticized by glycerol.

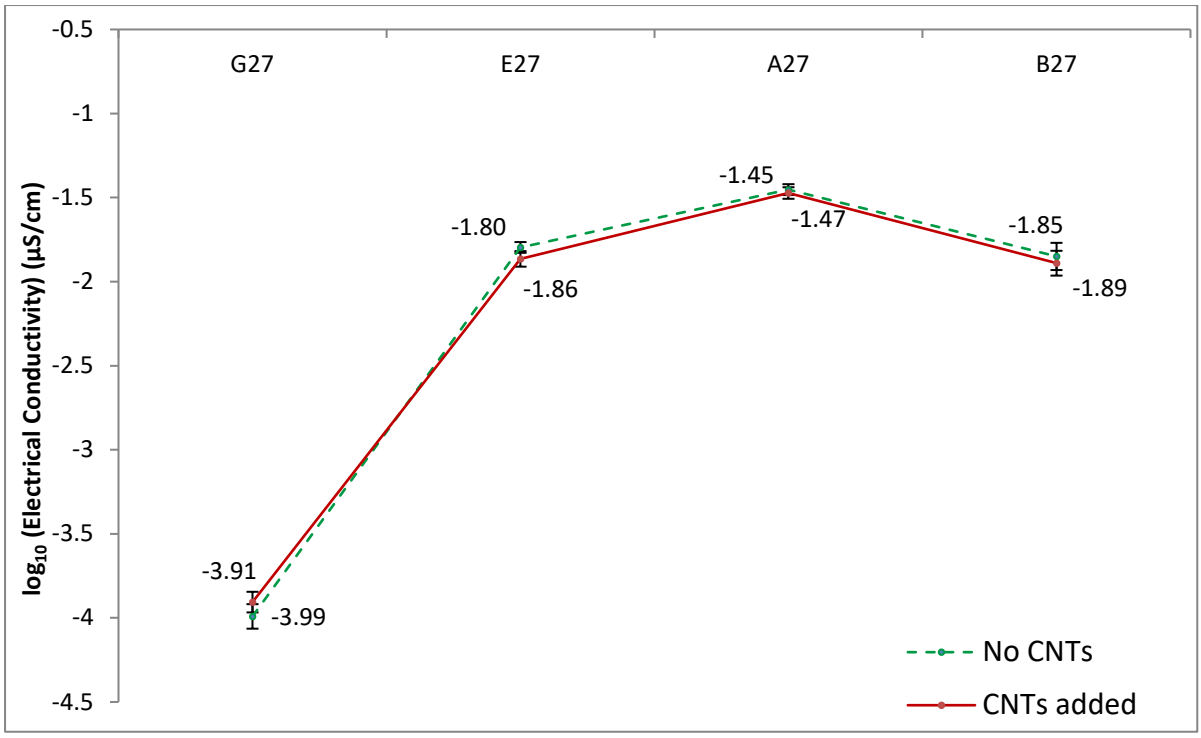

Figure 7-2 Electrical conductivity of plasticiser level 27 RMS samples (µS/cm)

A similar situation can be seen in figure 7-2 for the samples with plasticisers at level 27. For samples without CNTs, those plasticized by [Amim]Cl have the highest electrical conductivity of 3.54×10^{-2} µS/cm. Electrical conductivity of samples plasticised by [Emim][OAc] and [Bmim]Cl are 1.60×10^{-2} µS/cm and 1.44×10^{-2} µS/cm, which are 45% and 41% of [Amim]Cl, respectively. Electrical conductivity of glycerol plasticised samples is still the lowest as 1.03×10^{-4} µS/cm. In this case the addition of CNTs have even less effect that in the case of the level 18 plasticised samples. This corroborates the previous conclusion that in these samples the amount of CNTs added is too small to have an appreciable effect.

When compared to the set of plasticiser level 18 samples, it is obvious that each formulation of plasticiser level 27 has 10-100 times higher electrical conductivity. The reasons of this might be either the extra amount of plasticisers present or the higher water uptake caused by extra amount of plasticisers used, or a combination of both. These results are in agreement with other studies, which have shown that the TPS electrical conductivity is highly dependent on ILs and water contents (Ning et al., 2009, Pongviratchai and Park, 2007). Also, the assumption is supported by another study which suggests the presence of CNTs can weaken the dependence of the electrical conductivity on water content, and even eliminate it when the percolation threshold is reached (Ma et al., 2008).

Table 7-2 Electrical conductivity of RMS samples plasticized by different plasticisers [μS/cm]

	G18	E18	A18	B18
Mean	7.15×10^{-6}	4.99×10^{-4}	2.89×10^{-3}	1.09×10^{-3}
SD	9.69×10^{-7}	1.23×10^{-4}	3.34×10^{-4}	1.41×10^{-4}
	G18-C	E18-C	A18-C	B18-C
Mean	1.46×10^{-5}	3.77×10^{-4}	2.53×10^{-3}	7.80×10^{-4}
SD	4.74×10^{-6}	8.81×10^{-5}	3.79×10^{-4}	9.54×10^{-5}
	G27	E27	A27	B27
Mean	1.03×10^{-4}	1.60×10^{-2}	3.54×10^{-2}	1.44×10^{-2}
SD	1.67×10^{-5}	1.20×10^{-3}	2.70×10^{-3}	2.61×10^{-3}
	G27-C	E27-C	A27-C	B27-C
Mean	1.25×10^{-4}	1.37×10^{-2}	3.38×10^{-2}	1.31×10^{-2}
SD	1.87×10^{-5}	1.58×10^{-3}	2.61×10^{-3}	2.06×10^{-3}

To conclude, there is almost no doubt that the electrical conductivity is highly dependent on the types and amounts of the plasticisers used rather than the amount of added CNTs since the electrical percolation of CNTs has not been achieved yet. Plasticisers with conjugated molecular structure have been proved to be more effective in terms of enhancing electrical conductivity than those without. Basically, plasticisers with more conjugated structure have stronger electrical conductivity enhancing effects. Also, it is suggested that smaller size of the ILs' anion enhances electrical conductivity. In addition, using a larger quantity of plasticiser is also helpful to increase the electrical conductivity as it increases the water uptake which is another significant factor contributing to electrical conductivity.

7.4 Conclusions

In this chapter, the potential electrical conductivity enhancing effects of CNTs have been investigated. The results show similar patterns to the mechanical properties analysis. CNTs, at the levels added in this study, do not necessary improve the electrical conductivity of TPS composites samples. It is suggested by the percolation theory that the added quantity of CNTs is not large enough to be the predominant factor. In this experiment, the final electrical conductivity is determined by the nature of plasticisers with water uptake percentage. CNTs could potentially give enhancing effects on electrical conductivity. However, adding CNTs also decreases the water uptake percentage as reported in chapter 6. Hence, the electrical conductivity result is actually a complicated compromise of multiple factors.

Generally, most of the electrical conductivity results reported in this chapter would be classified as insulating. For some of the best results, they can be hardly defined as semi-conductive. As demonstrated in the introduction of this chapter, to form a proper percolation

is the key to effectively improve the material electrical conductivity. Hence, to successfully enable TPS nano-composites high electrical conductivity, a larger amount of CNTs should be added to the material matrix which would also potentially improve mechanical properties. By reaching the percolation threshold, the other contributed factor might be minimized to a certain level and the electrical conductivity would be much easier to control.

8 CONCLUSIONS AND FUTURE WORK

8.1 Introduction

In order to build on the understandings of starch/IL/CNT nanocomposites to develop practical 'green materials', this thesis has investigated the processing and properties of thermoplastic starch using a variety of ionic liquids as plasticisers, comparing these to the more conventionally used glycerol. The goal was to achieve both ease of processing and mechanical properties that were comparable to conventional polymers. Achieving conductive or semi-conductive characteristics was also desired because it would broaden the material application. The key challenge of achieving these goals lay in designing an optimized formulation of starch/ILs/CNTs composites. In order to achieve this goal, many factors were considered such as material compounding/processing technique, types of ILs to use, amounts of CNTs to add, conditioning method after processing and so on.

This project has focussed on studying the mechanical properties of one particular starch with a relatively low amylose content (RMS). Three different types of ILs have been compared to glycerol as plasticisers and MWCNTs have been investigated as a potential mechanical properties and electrical conductivity strengthening nano-filler.

In order to provide guidelines to aid the development of renewable and biodegradable starch/ILs/CNTs nano-composites, which could potentially substitute conventional petroleum-based polymers this thesis has developed an understanding of the ILs plasticizing effects on starch processing and material properties, and the CNTs strengthening effects on TPS material properties. Any additional functions added to such a nano-composites system would be extra benefit.

Thus, the main objectives of this project were set as follows:

1. To investigate the effects of 1-ethyl-3-methylimidazolium acetate ([Emim][OAc]) on RMS processing and material properties compared to glycerol, and relate these to changes in structure at a nano and micro scale.

2. To compared two other ILs, 1-Allyl-3-methylimidazolium chloride ([Amim]Cl) and 1-Butyl-3-methylimidazolium chloride ([Bmim]Cl), as plasticisers of RMS and their effects on RMS processing and material properties.

3. To investigate the CNTs influences on plasticized RMS mechanical properties and electrical conductivity.

The ultimate thermal mixing torque were used as measures of material processing behaviour. Compared to using glycerol, it was found that using ILs successfully lowered the ultimate mixing torque by a maximum of 34%. Tensile testing was conducted to investigate the mechanical properties of all different samples. It was found that the selection of plasticiser was fundamental to mechanical properties. Also, the quantity of plasticiser used and water uptake were found to significantly affect mechanical properties. FTIR/Raman spectroscopy and TGA were utilised to study the molecular interaction between starch, ILs and CNTs. Crystal structures of TPS were studied by XRD analysis. It was found that the crystalline behaviour was highly dependent on plasticiser options and CNT addition, hence influencing water uptake and tensile properties.

8.2 The Effects of 1-Ethyl-3-Methylimidazolium Acetate ([Emim][OAc]) on RMS Processing and Material Properties Compared to Glycerol

From the results of FTIR/Raman spectroscopy, it was found that the molecular interactions were affected by [Emim][OAc] and glycerol in different ways. [Emim][OAc] tends to weaken the hydrogen bonding between starch molecules by a stronger IL-starch interaction whilst glycerol enhances the hydrogen bonding between starch molecules. Hence, this directly influences the [Emim][OAc] plasticised RMS resulting in a maximum of a 41 °C decrease in temperature of the peak in degradation rate compared to glycerol which may potentially be disadvantageous for the material use. The weakening of the starch-starch OH interaction also leads to a decrease of 19% in processing torque for [Emim][OAc] plasticized starch compared to glycerol plasticized starch.

Different plasticisers can also influence the crystallisation behaviour of plasticized RMS. This crystallisation behaviour has a close relationship with the water uptake of processed RMS. XRD results have shown that [Emim][OAc] tends to form more B-type crystallites which promotes water uptake because of its cavity in crystal structure. However, a higher water uptake leads to a destruction of B-type crystallites and a decline of total crystallinity. Hence, it can be seen that [Emim][OAc] plasticised samples can be up to 3.69% lower in total crystallinity and 4.38% higher in water uptake compared to glycerol plasticised samples. The Young's modulus, tensile strength and the elongation at break of processed RMS samples are predominantly influenced by the choice of plasticiser type and quantity, and also affected by

the total crystallinity and water uptake. Therefore, it was found that the tensile stress and modulus of [Emim][OAc] plasticised samples were generally lower than glycerol plasticised samples although there were some exceptions. With [Emim][OAc], increasing the plasticiser quantity from level 9 to level 18 decreased the tensile stress by 45% and Young's modulus by 91%. Similarly, increasing plasticiser quantity from level 18 to level 27 further decreased the tensile stress by 40% and 61% Young's modulus by 61%. In the case of glycerol, tensile stress and Young's modulus decreased by 55%, and 90% respectively when the plasticiser level increaseed from 9 to 18. They further decreased by 60% and 71% respectively when the plasticiser level further increaseed to 27.

Also, it is worthy of noticing that the crystallite structure change is a dynamic process which occurs during sample conditioning. Water sensitivity is of great significance to TPS material properties because moisture content is relevant to so many material characteristics. It is hard to conclude that whether water uptake is beneficial to material properties since the required material properties depend on the application. However, it is clear that the water uptake of TPS material should be understood and controlled.

As [Emim][OAc] has showed more powerful effects on lowering processing torque, tensile strength, and Young's modulus, is considered a more effective plasticiser than glycerol. Overall, while it achieves lower processing torque to make processing easier, the resulting lower degradation temperature, lower tensile strength and Young's modulus might limit the further application of starch as its mechanical properties are generally lower than the conventional polymers. Therefore, looking at other ILs to increase knowledge of ILs/RMS interaction and reinforcement for RMS is needed.

8.3 The Effects of 1-Allyl-3-Methylimidazolium Chloride ([Amim]Cl)/ 1-Butyl-3-methylimidazolium Chloride ([Bmim]Cl) on RMS Processing and Material Properties

[Amim]Cl and [Bmim]Cl were found to have similar molecular interactions with starch compared to [Emim][OAc]. The reason of this is their similar chemical structures. However, the FTIR/Raman spectroscopy analysis indicated that [Amim]Cl and [Bmim]Cl have stronger interactions with RMS compared to [Emim][OAc], with both spectra indicating that [Bmim]Cl is slightly stronger. This is supported by the TGA analysis s where both [Amim]Cl and [Bmim]Cl showed peak decomposition temperatures of approximately 233°C, which are 29°C lower than [Emim][OAc]. Also, the processing torque further decreases by 9% and 19% respectively compared to [Emim][OAc], and 27% and 34% respectively compared to glycerol.

The crystallisation behaviour of [Amim]Cl and [Bmim]Cl plasticized RMS is very different from the [Emim][OAc] and glycerol plasticized RMS. As indicated by the XRD results, the B-type crystallites firstly grow at the start of sample conditioning and then disappear. The choice of plasticiser is still the predominant factor of water uptake and mechanical properties. Similar to the previous results of using [Emim][OAc], water uptake also results in lower total crystallinity which potentially leads to more ductile and flexible mechanical properties. For instance, samples with a plasticiser level of 27 conditioned in RH75% show an increase of water uptake of approximately 3%, and a decrease of about 2% in total crystallinity, in both ILs cases compared to level 18. Hence, they both show a decrease of over 40% in tensile stress and over 80% in Young's modulus.

Overall, [Amim]Cl and [Bmim]Cl were considered more powerful plasticisers compared to [Emim][OAc] in terms of their effects on lowering degradation temperature, processing torque, tensile strength and Young's modulus.

8.4 The Mechanical Strengthening Effects of CNTs

As the material properties of starch plasticised with ILs were still lower than desired, strengthening by forming nano-composites was investigated. CNTs have shown promise in strengthening other systems such as PP, PE (section 2.4.2) and so it was expected they would also give strong strengthening effects to plasticized RMS. However, the tensile testing results showed that this only occurred in the RMS-G and RMS-E series which showed about 45% to 50% higher Young's modulus whilst in the RMS-A and RMS-B series the Young's modulus actually decreased by about 45% to 50%. Therefore, the CNTs did not significantly show a strengthening effect on the mechanical properties. In the RMS-G and RMS-E series they seemed to act as a kind of strengthening material in the samples whilst they seemed to behave like a plasticizing material in RMS-A and RMS-B.

This evidence indicates that the amount of CNTs added has not reached the percolation threshold so the mechanical properties were not dominated by the CNTs as would be predicted at higher loadings.

FTIR/Raman spectroscopy has showed that CNTs have molecular interactions with other components which therefore affects their dispersion and distribution. The addition of CNTs seems to have a significant effect on the crystallisation behaviour and hence the water uptake and thermal degradation rate. TEM analysis displayed an example of the CNTs dispersion and distribution in sample RMS-B18C. It was found that a reasonable distribution had been

achieved but not a good dispersion. All of these factors have contributions to the ultimate mechanical properties of the RMS/CNTs nano-composites.

Therefore, the mechanical properties are a result of a compromise between all these factors. This study shows that the high strengthening effect of CNTs on TPS have not been achieved by adding 1 wt% of MWCNTs. Potentially, a larger amount of CNTs would be needed to make it the predominant contributing factor for mechanical properties.

8.5 The Electrical Conductivity of CNTs Strengthened RMS

Even though the mechanical properties were not much enhanced by adding CNTs, it was still hoped that electrical conductivity would increase. However, this was not observed in the systems studied. Similarly to the mechanical properties, electrical conductivity enhancing effects only appeared in RMS-G series, not in any of the ILs plasticized cases. The reason is again assumed to be the absence of an effective percolation network.

In this study, it is suggested that the molecular structure and the amount of the plasticisers used are the main factors contributed to the material electrical conductivity. ILs have conjugated molecular structures which are beneficial to ion delocalisation. Hence, the electrical conductivity of ILs plasticized RMS/CNTs nano-composites is always 25 (for E18-C) to 404 (for A18) times higher than the glycerol plasticised samples. Water uptake is also another important factor which contributed to the ultimate electrical conductivity. Therefore, samples with plasticiser level 27 usually showed 10 to 100 times higher electrical conductivity than those with level 18. Finally, in these samples the influence of CNTs is the least powerful contributor to material electrical conductivity. To summarize, the choice of IL is the predominant factor of electrical conductivity in this study because of the low level of CNTs.

Hence, it can be explained that the lower electrical conductivity of CNTs added samples compared to their original formulation is the consequence of the lower water uptake caused by CNTs. To overcome this problem, enough amounts of CNTs to reach the electrical percolation threshold must be ensured.

8.6 Summary and Applications

To conclude, this project has compared the plasticizing effects of three types of ILs and found that [Bmim]Cl is the strongest one. [Emim][OAc] gave the highest values of material tensile strength and Young's modulus. [Amim]Cl gave the strongest influence on electrical conductivity. The differences were mainly caused by the different molecular structures of ILs

which interacted differently with starch and resulted in a variety of micro-structures. Generally, ILs which lower processing torque would also lower tensile strength, Young's modulus and thermal degradation temperature. Stronger molecular interactions were shown to further decrease these characteristics. Therefore, the choice of IL is highly dependent on the requirements of the application. Of the three ILs studied in this project, [Emim][OAc] appears to be the most practical IL to use as it showed much better plasticizing effects than glycerol but could still maintain practical mechanical properties.

CNTs have displayed the potential to effectively strengthen the mechanical properties and enhance electrical properties of starch-based material. However, a larger amount than the 1wt% employed in this work would be needed to achieve an effective mechanical and electrical percolation network. It has been reported that (Hassanabadi et al., 2014) the percolation threshold of MWCNTs in PP and PS is between 1-4 wt% according to individual situations, and it would be expected that a similar amount would be needed to effectively strengthen TPS.

The best Young's modulus of a CNT reinforced RMS was 770 MPa, found in the RMS-E series, and in many cases the addition of CNTs actually decreased the Young's modulus, clearly these results are less than was desired for performance issues. It would be hoped that the materials could be strengthened to higher levels with more CNT added (above the percolation level), to reach levels comparable to conventional polymers. Similarly, once the electrical percolation network has been achieved, the electrical conductivity should also be higher than the current results which were already at the low end of a semi-conductive level. In this case, such a nano-composite could potentially substitute for conventional polymers as an engineering polymer. The electrical conductivity might enable this nano-composite to be a cheap, light weight and biodegradable semi-conductive or conductive material.

This thesis has made a number of advances in the understanding of the processing and properties of IL plasticised starch:

- Most previous work in this area has been performed using solution casting with very limited batch size. In this thesis a thermal processing methodology was successfully used to produce batches of the order of 150g for both starch/IL and starch/IL/CMT systems.

- Detailed spectroscopic analysis of these systems has been performed which has led to an insight into the interactions between the various components.

- X-ray diffraction to monitor the development of different crystal structures has been performed and these results related to the spectroscopic studies.

- The effect of water uptake during conditioning was identified as a key contributor to the ultimate mechanical properties. The differences in the water uptake were related to the changes in crystalline structures and molecular interactions in the systems.

- It was observed that the IL structures have an effect on both the processing behaviour and the properties, usually with ease of processing correlating with lower mechanical properties. Therefore a balance needs to be achieved given a particular application and this work begins to offer some design goals in this area.

- The possibility of using CNTs to reinforce the TPS and also to add useful electrical properties was investigated. Whilst it was possible to successfully incorporate CNTs an adequate level has not been realised.

- Even at the lower level of CNT addition employed, the CNTs did have an effect on the crystallisation behaviour of the systems and reduced the differences observed between the different ILs.

8.7 Future Work

Although this thesis has improved fundamental understandings of starch/IL/CNT nano-composites in several ways, a number of areas still need to be explored. Key to this is to expand the understanding of interactions between the components as this controls both the processing characteristics and the ultimate properties. For instance:

- The little peak at approximately 1624 cm^{-1} of the RMS-A and RMS-B series FT-Raman results has not been identified. Understanding this feature might give additional information on the molecular interaction of the material system.

- NMR can be employed as a further probe of molecular interactions at an atomistic scale.

- Atomistic molecular modelling can be used to gain a fundamental understanding of the relationships between the chemical structure of the ILs and their interactions, and hence guide the choice of suitable ILs for a particular use.

In order to develop a methodology for optimising final properties a number of areas need considering:

- As water uptake has a profound effect on the material properties, further studies of this process, and how it can be controlled is necessary.
- Relationships between the interactions between components, including water taken up during conditioning, and the final properties need to be more fully developed.
- Further material properties characterisation is desirable to determine whether the IL plasticised materials can fulfil engineering design requirements. For instance, Dynamic Mechanical Thermal Analysis should be employed to measure the glass transition temperatures and rheological analysis would assist in understanding the effects of processing.

Reinforcement with CNTs has been shown to have the potential to improve the properties of these systems. Further studies needed in this area include:

- Samples need to be prepared at higher CNT loadings to identify the percolation threshold.
- Further spectroscopic analyses at these higher loadings would show how the interactions change at these levels.
- A systematic study of CNT loading, IL amount and conditioning humidities needs to be performed to investigate the relations between these variables and factors such as water uptake and crystallisation behaviour.
- Further TEM analyses are required to check the dispersion and distribution of the CNTs and relate these to the processing conditions.
- The electrical properties of these systems need fuller analysis to determine if this is a useful additional feature of the nano-composites.

Finally, it would also be important to address issues of toxicity and bio-degradability of the composites for practical applications.

9 REFERENCES

ALIG, I., P TSCHKE, P., LELLINGER, D., SKIPA, T., PEGEL, S., KASALIWAL, G. R. & VILLMOW, T. 2012. Establishment, morphology and properties of carbon nanotube networks in polymer melts. *Polymer*, 53**,** 4-28.

ANDRIANOVA, G.P., BAKEEV, N. F. & KOZLOV, P. V. 1971. STRUCTURAL PLASTICIZATION OF POLYMERS. *Vysokomolekulyarnye Soedineniya Section A*, 13**,** 266-&.

ANTUNES, E. F., LOBO, A. O., CORAT, E. J., TRAVA-AIROLDI, V. J., MARTIN, A. A. & VER SSIMO, C. 2006. Comparative study of first- and second-order Raman spectra of MWCNT at visible and infrared laser excitation. *Carbon*, 44**,** 2202-2211.

ATWELL, W. A., HOOD, L. F., LINEBACK, D. R., VARRIANO-MARSTON, E. & ZOBEL, H. F. 1988. The terminology and methodology associated with basic starch phenomena. *Cereal foods world.*, 33**,** 306.

AVEROUS, L. 2004. Biodegradable multiphase systems based on plasticized starch: A review. *Journal of Macromolecular Science-Polymer Reviews*, C44**,** 231-274.

AVEROUS, L., FRINGANT, C. & MORO, L. 2001. Plasticized starch-cellulose interactions in polysaccharide composites. *Polymer*, 42**,** 6565-6572.

AVEROUS, L. & HALLEY, P. 2009. Biocomposites based on plasticized starch. *Biofuels Bioprod. Biorefining.*

BAISHYA, P. & MAJI, T. K. 2016. Functionalization of MWCNT and their application in properties development of green wood nanocomposite. *Carbohydrate Polymers*, 149**,** 332-339.

BERTIN, E. P. 2012. *Principles and Practice of X-Ray Spectrometric Analysis*, Boston, MA : Springer US.

BOESEL, L. F. 2015. Effect of plasticizers on the barrier and mechanical properties of biomimetic composites of chitosan and clay. *Carbohydrate Polymers*, 115**,** 356-363.

BOOTKLAD, M. & KAEWTATIP, K. 2013. Biodegradation of thermoplastic starch/eggshell powder composites. *Carbohydrate Polymers*, 97**,** 315-320.

BOURTOOM, T. & CHINNAN, M. S. 2008. Preparation and properties of rice starch-chitosan blend biodegradable film. *Food Science and Technology*, 41**,** 1633-1641.

BROWN, S., JORIO, A., DRESSELHAUS, M. S. & DRESSELHAUS, G. 2001. Observations of the D- band feature in the Raman spectra of carbon nanotubes. *Physical Review B*, 64.

BUCKOW, R., JANKOWIAK, L., KNORR, D. & VERSTEEG, C. 2009. Pressure-temperature phase diagrams of maize starches with different amylose contents. *Journal of agricultural and food chemistry*, 57**,** 11510.

BUFFA, F., ABRAHAM, G. A., GRADY, B. P. & RESASCO, D. 2007. Effect of nanotube functionalization on the properties of single ‐ walled carbon nanotube/polyurethane composites. *Journal of Polymer Science Part B: Polymer Physics*, 45**,** 490-501.

CAEL, J. J., KOENIG, J. L. & BLACKWELL, J. 1974. Infrared and Raman spectroscopy of carbohydrates: Part IV. Identification of configuration- and conformation-sensitive modes for D -glucose by normal coordinate analysis. *Carbohydrate Research*, 32**,** 79-91.

CAEL, J. J., KOENIG, J. L. & BLACKWELL, J. 1975. Infrared and Raman spectroscopy of carbohydrates. Part VI: Normal coordinate analysis of V ‐ amylose. *Biopolymers*, 14**,** 1885-1903.

CAEL, S. J., KOENIG, J. L. & BLACKWELL, J. 1973. Infrared and Raman spectroscopy of carbohydrates: Part III: raman spectra of the polymorphic forms of amylose. *Carbohydrate Research*, 29**,** 123-134.

CAO, X., CHEN, Y., CHANG, P. R. & HUNEAULT, M. A. 2007. Preparation and properties of plasticized starch/multiwalled carbon nanotubes composites. *Journal of Applied Polymer Science,* 106**,** 1431-1437.
CHEETHAM, N. W. H. & TAO, L. 1998. Variation in crystalline type with amylose content in maize starch granules: an X-ray powder diffraction study. *Carbohydrate Polymers,* 36**,** 277-284.
CHEN, P., YU, L., KEALY, T., CHEN, L. & LI, L. 2007. Phase transition of starch granules observed by microscope under shearless and shear conditions. *Carbohydrate Polymers,* 68**,** 495-501.
CHENG, J., ZHENG, P., ZHAO, F. & MA, X. 2013. The composites based on plasticized starch and carbon nanotubes. *International Journal of Biological Macromolecules,* 59**,** 13-19.
CHRIS, W., ERIK VAN, S. & BRITTA DENISE, H. 2015. Threat of plastic pollution to seabirds is global, pervasive, and increasing. *Proceedings of the National Academy of Sciences,* 112**,** 11899.
CHUNG, H.-J., LIU, Q., LEE, L. & WEI, D. 2011. Relationship between the structure, physicochemical properties and in vitro digestibility of rice starches with different amylose contents. *Food Hydrocolloids,* 25**,** 968-975.
COLEMAN, D. & GATHERGOOD, N. 2010. Biodegradation studies of ionic liquids. *Chemical Society Reviews,* 39**,** 600-637.
COLEMAN, J. N., KHAN, U., BLAU, W. J. & GUN'KO, Y. K. 2006. Small but strong: A review of the mechanical properties of carbon nanotube–polymer composites. *Carbon,* 44**,** 1624-1652.
COZAR, O., CIOICA, N., FILIP, C., COJA, C. & FILIP, X. 2013. Structural FT-IR and [sup.13]c cp/mas nmr investigation of native starch with plasticizers before and post extrusion process. *Studia Universitatis Babes-Bolyai. Chemia,* 58**,** 275.
CULLITY, B. D. & STOCK, S. R. 2001. Elements of X-ray diffraction / B.D. Cullity, S.R. Stock, Upper Saddle River, N.J. : London, Upper Saddle River, N.J. : Prentice Hall London : Prentice-Hall International.
DAI, H. J. 2002. Carbon nanotubes: opportunities and challenges. *Surface Science,* 500**,** 218-241.
DERVISHI, E., LI, Z., XU, Y., SAINI, V., BIRIS, A. R., LUPU, D. & BIRIS, A. S. 2009. Carbon Nanotubes: Synthesis, Properties, and Applications. *Particulate Science and Technology,* 27**,** 107-125.
DHITAL, S., SHRESTHA, A. K., FLANAGAN, B. M., HASJIM, J. & GIDLEY, M. J. 2011. Cryo-milling of starch granules leads to differential effects on molecular size and conformation. *Carbohydrate Polymers,* 84**,** 1133-1140.
DHUMAL, N. R., KIM, H. J. & KIEFER, J. 2009. Molecular Interactions in 1-Ethyl-3-methylimidazolium Acetate Ion Pair: A Density Functional Study. *The Journal of Physical Chemistry A,* 113**,** 10397-10404.
DIAS, A. B., MUELLER, C. M. O., LAROTONDA, F. D. S. & LAURINDO, J. B. 2010. Biodegradable films based on rice starch and rice flour. *Journal of Cereal Science,* 51**,** 213-219.
DONOVAN, J. W. 1979. Phase transitions of the starch-water system. *Biopolymers,* 18**,** 263-275.
DRESSELHAUS, M. S. 2001. Nanotubes - Burn and interrogate. *Science,* 292**,** 650-651.
EBBESEN, T. W., LEZEC, H. J., HIURA, H., BENNETT, J. W., GHAEMI, H. F. & THIO, T. 1996. Electrical conductivity of individual carbon nanotubes. *Nature,* 382**,** 54.
ELIASSON, A.-C. 2004. *Starch in food: structure, function and applications,* Boca Raton FL, USA : CRC Press.

ESMAEILI, M., PIRCHERAGHI, G. & BAGHERI, R. 2017. Optimizing the mechanical and physical properties of thermoplastic starch via tuning the molecular microstructure through co - plasticization by sorbitol and glycerol. *Polymer International,* 66**,** 809-819.

FAM , L. M., PETTARIN, V., GOYANES, S. N. & BERNAL, C. R. 2011. Starch/multi-walled carbon nanotubes composites with improved mechanical properties. *Carbohydrate Polymers,* 83**,** 1226-1231.

FANG, J. M., FOWLER, P. A., SAYERS, C. & WILLIAMS, P. A. 2004. The chemical modification of a range of starches under aqueous reaction conditions. *Carbohydrate Polymers,* 55**,** 283-289.

FERREIRA, F. V., FRANCISCO, W., MENEZES, B. R. C., BRITO, F. S., COUTINHO, A. S., CIVIDANES, L. S., COUTINHO, A. R. & THIM, G. P. 2016. Correlation of surface treatment, dispersion and mechanical properties of HDPE/CNT nanocomposites. *Applied Surface Science,* 389**,** 921-929.

FERREIRA, T., PAIVA, M. & PONTES, A. 2013. Dispersion of carbon nanotubes in polyamide 6 for microinjection moulding. *Journal of Polymer Research,* 20**,** 1-9.

FISHMAN, M. L., COFFIN, D. R., ONWULATA, C. I. & WILLETT, J. L. 2006. Two stage extrusion of plasticized pectin/poly(vinyl alcohol) blends. *Carbohydrate Polymers,* 65**,** 421-429.

FRENCH, D. 1973. Chemical and physical properties of starch. *Journal of animal science,* 37**,** 1048.

FUNKE, U., BERGTHALLER, W. & LINDHAUER, M. G. 1998. Processing and characterization of biodegradable products based on starch. *Polymer Degradation and Stability,* 59**,** 293-296.

GILFILLAN, W. N., MOGHADDAM, L., BARTLEY, J. & DOHERTY, W. O. S. 2016. Thermal extrusion of starch film with alcohol. *Journal of Food Engineering,* 170**,** 92-99.

GLENN, G. M. & ORTS, W. J. 2001. Properties of starch-based foam formed by compression/explosion processing. *Industrial Crops and Products,* 13**,** 135-143.

GRAZULEVICIENE, V., TREINYTE, J. & ZALECKAS, E. 2012. Film-Forming Starch Composites for Agricultural Applications. *Journal of Polymers and the Environment,* 20**,** 485-491.

HAMAGUCHI, H.-O. & OZAWA, R. 2005. Structure of Ionic Liquids and Ionic Liquid Compounds: Are Ionic Liquids Genuine Liquids in the Conventional Sense? *Advances in Chemical Physics.* John Wiley & Sons, Inc.

HAMEED, N., CHURCH, J. S., SALIM, N. V., HANLEY, T. L., AMINI, A. & FOX, B. L. 2013. Dispersing single-walled carbon nanotubes in ionic liquids: a quantitative analysis. *RSC Adv.*, 3**,** 20034-20039.

HASSANABADI, H., WILHELM, M. & RODRIGUE, D. 2014. A rheological criterion to determine the percolation threshold in polymer nano-composites. *Rheologica Acta,* 53**,** 869-882.

HIZUKURI, S. 1986. Polymodal distribution of the chain lengths of amylopectins, and its significance. *Carbohydrate Research,* 147**,** 342-347.

HUANG, M., YU, J. & MA, X. 2006. High mechanical performance MMT-urea and formamide-plasticized thermoplastic cornstarch biodegradable nanocomposites. *Carbohydrate Polymers,* 63**,** 393-399.

HUSSAIN, F., HOJJATI, M., OKAMOTO, M. & GORGA, R. 2006. Review article: Polymer-matrix Nanocomposites, Processing, Manufacturing, and Application: An Overview. *Journal of Composite Materials,* 40**,** 1511-1575.

IMBERTY, A., BUL ON, A., TRAN, V. & P EREZ, S. 1991. Recent Advances in Knowledge of Starch Structure. *Die Stärke,* 43**,** 375-384.

IMBERTY, A., CHANZY, H., P REZ, S., BUL ON, A. & TRAN, V. 1987. Special issue: 2nd International Workshop on Plant PolysaccharidesThree-dimensional structure analysis of the crystalline moiety of A-starch. *Food Hydrocolloids,* 1**,** 455-459.

IMBERTY, A., CHANZY, H., P REZ, S., BUL ON, A. & TRAN, V. 1988. The double-helical nature of the crystalline part of A-starch. *Journal of Molecular Biology,* 201**,** 365-378.

IMBERTY, A. & PEREZ, S. 1988. A revisit to the three-dimensional structure of B-type starch. *Biopolymers,* 27**,** 1205-1221.

JAMBECK, J. R., GEYER, R., WILCOX, C., SIEGLER, T. R., PERRYMAN, M., ANDRADY, A., NARAYAN, R. & LAW, K. L. 2015. Marine pollution. Plastic waste inputs from land into the ocean. *Science (New York, N.Y.),* 347**,** 768.

JIM NEZ, A., FABRA, M. J., TALENS, P. & CHIRALT, A. 2011. Effect of re-crystallization on tensile, optical and water vapour barrier properties of corn starch films containing fatty acids. *Food Hydrocolloids*.

JIMENEZ, A., JOSE FABRA, M., TALENS, P. & CHIRALT, A. 2012a. Edible and Biodegradable Starch Films: A Review. *Food and Bioprocess Technology,* 5**,** 2058-2076.

JIMENEZ, A., JOSE FABRA, M., TALENS, P. & CHIRALT, A. 2012b. Effect of re-crystallization on tensile, optical and water vapour barrier properties of corn starch films containing fatty acids. *Food Hydrocolloids,* 26**,** 302-310.

JIN, Z., WANG, S., WANG, J. & ZHAO, M. 2012. Effects of plasticization conditions on the structures and properties of cellulose packaging films from ionic liquid [BMIM]Cl. *Journal of Applied Polymer Science,* 125**,** 704-709.

JINHUI, P., XIN, L., XUEMING, Z., YUYING, W. & RUNCANG, S. 2013. Fabrication of Cellulose Film with Enhanced Mechanical Properties in Ionic Liquid 1-Allyl-3-methylimidaxolium Chloride (AmimCl). *Materials,* 6**,** 1270-1284.

JORIO, A., SOUZA FILHO, A., DRESSELHAUS, G., DRESSELHAUS, M., SWAN, A., ÜNL , M., GOLDBERG, B., PIMENTA, M., HAFNER, J. & LIEBER, C. 2002. G-band resonant Raman study of 62 isolated single-wall carbon nanotubes. *Physical Review B,* 65**,** 155412.

K RKK INEN, J., LAPPALAINEN, K., JOENSUU, P. & LAJUNEN, M. 2011. HPLC-ELSD analysis of six starch species heat-dispersed in [BMIM]Cl ionic liquid. *Carbohydrate Polymers,* 84**,** 509-516.

KATHIRGAMANATHAN, K., GRIGSBY, W. J., AL-HAKKAK, J. & EDMONDS, N. R. 2015. Two-Dimensional FTIR as a Tool to Study the Chemical Interactions within Cellulose-Ionic Liquid Solutions. 2015.

KEARNS, J. C. & SHAMBAUGH, R. L. 2002. Polypropylene fibers reinforced with carbon nanotubes. *Journal of Applied Polymer Science,* 86**,** 2079-2084.

KESKIN, S., KAYRAK-TALAY, D., AKMAN, U. & HORTA SU, Ö. 2007. A review of ionic liquids towards supercritical fluid applications. *The Journal of Supercritical Fluids,* 43**,** 150-180.

KHANMIRZAEI, M. H. & RAMESH, S. 2014. Nanocomposite polymer electrolyte based on rice starch/ionic liquid/TiO2 nanoparticles for solar cell application. *Measurement,* 58**,** 68-72.

KIZIL, R., IRUDAYARAJ, J. & SEETHARAMAN, K. 2002. Characterization of irradiated starches by using FT-Raman and FTIR spectroscopy. *Journal of agricultural and food chemistry,* 50**,** 3912.

KOCH, K., GILLGREN, T., STADING, M. & ANDERSSON, R. 2010. Mechanical and structural properties of solution-cast high-amylose maize starch films. *International Journal of Biological Macromolecules,* 46**,** 13-19.

KOTOV, N., ŠTURCOV , A., ZHIGUNOV, A., RAUS, V. & DYBAL, J. 2016. Structural Transitions of 1-Butyl-3-methylimidazolium Chloride/Water Mixtures Studied by

Raman and FTIR Spectroscopy and WAXS. *Crystal Growth and Design,* 16**,** 1958-1967.
KU, H., WANG, H., PATTARACHAIYAKOOP, N. & TRADA, M. 2011b. A review on the tensile properties of natural fiber reinforced polymer composites. *Composites Part B: Engineering,* 42**,** 856-873.
KUPTSOV, A. H. & ZHIZHIN, G. N. Handbook of Fourier Transform Raman and Infrared Spectra of Polymers. Elsevier.
LAI, L. S. & KOKINI, J. L. 1991. Physicochemical changes and rheological properties of starch during extrusion. (A review). *Biotechnology Progress,* 7**,** 251-266.
LELIEVRE, J. 1974. Starch gelatinization. *Journal of Applied Polymer Science,* 18**,** 293-296.
LEROY, E., JACQUET, P., COATIVY, G., REGUERRE, A. L. & LOURDIN, D. 2012. Compatibilization of starch–zein melt processed blends by an ionic liquid used as plasticizer. *Carbohydrate Polymers,* 89**,** 955-963.
LI, M., LIU, P., ZOU, W., YU, L., XIE, F., PU, H., LIU, H. & CHEN, L. 2011. Extrusion processing and characterization of edible starch films with different amylose contents. *Journal of Food Engineering,* 106**,** 95-101.
LIU, H., XIE, F., CHEN, L., YU, L., DEAN, K. & BATEMAN, S. 2005. Thermal Behaviour of High Amylose Cornstarch Studied by DSC. *International Journal of Food Engineering,* 1**,** 3-6.
LIU, H., XIE, F., YU, L., CHEN, L. & LI, L. 2009. Thermal processing of starch-based polymers. *Progress in Polymer Science,* 34**,** 1348-1368.
LIU, H., YU, L., XIE, F. & CHEN, L. 2006. Gelatinization of cornstarch with different amylose/amylopectin content. *Carbohydrate Polymers,* 65**,** 357-363.
LIU, P., XIE, F., LI, M., LIU, X., YU, L., HALLEY, P. J. & CHEN, L. 2011a. Phase transitions of maize starches with different amylose contents in glycerol-water systems. *Carbohydrate Polymers,* 85**,** 180-187.
LIU, P., YU, L., WANG, X., LI, D., CHEN, L. & LI, X. 2010. Glass transition temperature of starches with different amylose/amylopectin ratios. *Journal of Cereal Science,* 51**,** 388-391.
LIU, S., LI, X., CHEN, L., LI, L., LI, B. & ZHU, J. 2017. Understanding physicochemical properties changes from multi-scale structures of starch/CNT nanocomposite films. *International Journal of Biological Macromolecules*.
LIU, W. & BUDTOVA, T. 2013. Dissolution of unmodified waxy starch in ionic liquid and solution rheological properties. *Carbohydrate Polymers,* 93**,** 199-206.
LIU, Z., ZHAO, L., CHEN, M. & YU, J. 2011b. Effect of carboxylate multi-walled carbon nanotubes on the performance of thermoplastic starch nanocomposites. *Carbohydrate Polymers,* 83**,** 447-451.
LOPEZ-RUBIO, A., FLANAGAN, B. M., GILBERT, E. P. & GIDLEY, M. J. 2008. A novel approach for calculating starch crystallinity and its correlation with double helix content: A combined XRD and NMR study. *Biopolymers,* 89**,** 761-768.
LOURDIN, D., COIGNARD, L., BIZOT, H. & COLONNA, P. 1997. Influence of equilibrium relative humidity and plasticizer concentration on the water content and glass transition of starch materials. *Polymer,* 38**,** 5401-5406.
LOURDIN, D., VALLE, G. D. & COLONNA, P. 1995. Influence of amylose content on starch films and foams. *Carbohydrate Polymers,* 27**,** 261-270.
LU, P., ZHANG, M., LIU, Y., LI, J. & XIN, M. 2012. Characteristics of vermiculite-reinforced thermoplastic starch composite films. *Journal of Applied Polymer Science,* 126**,** E116-E122.
LU, X. Y. & JIANG, B. Z. 1991. GLASS-TRANSITION TEMPERATURE AND MOLECULAR-PARAMETERS OF POLYMER. *Polymer,* 32**,** 471-478.

MA, X. & YU, J. 2004. The plastcizers containing amide groups for thermoplastic starch. *Carbohydrate Polymers*, 57**,** 197-203.
MA, X., YU, J. & KENNEDY, J. F. 2005a. Studies on the properties of natural fibers-reinforced thermoplastic starch composites. *Carbohydrate Polymers*, 62**,** 19-24.
MA, X., YU, J. & WANG, N. 2008. Glycerol plasticized-starch/multiwall carbon nanotube composites for electroactive polymers. *Composites Science and Technology*, 68**,** 268-273.
MA, X. F., MA, Y. B. & YU, J. G. 2005b. Urea and formamide as a mixed plasticizer for thermoplastic wheat flour. *Carbohydrate Polymers*, 60**,** 111-116.
MANI, R. & BHATTACHARYA, M. 1998a. Properties of injection moulded starch synthetic polymer blends - IV. Thermal and morphological properties. *European Polymer Journal*, 34**,** 1477-1487.
MANI, R. & BHATTACHARYA, M. 1998b. Properties of injection moulded starch/synthetic polymer blends—III. Effect of amylopectin to amylose ratio in starch. *European Polymer Journal*, 34**,** 1467-1475.
MARINHO, B., GHISLANDI, M., TKALYA, E., KONING, C. E. & DE WITH, G. 2012. Electrical conductivity of compacts of graphene, multi-wall carbon nanotubes, carbon black, and graphite powder. *Electrical conductivity of compacts of graphene, multi-wall carbon nanotubes, carbon black, and graphite powder*, 221**,** 351-358.
MARSH, K. N., BOXALL, J. A. & LICHTENTHALER, R. 2004. Room temperature ionic liquids and their mixtures—a review. *Fluid Phase Equilibria*, 219**,** 93-98.
MATEYAWA, S., XIE, D. F., TRUSS, R. W., HALLEY, P. J., NICHOLSON, T. M., SHAMSHINA, J. L., ROGERS, R. D., BOEHM, M. W. & MCNALLY, T. 2013. Effect of the ionic liquid 1-ethyl-3-methylimidazolium acetate on the phase transition of starch: Dissolution or gelatinization? *Carbohydrate Polymers*, 94**,** 520-530.
MATZINOS, P., TSERKI, V., GIANIKOURIS, C., PAVLIDOU, E. & PANAYIOTOU, C. 2002a. Processing and characterization of LDPE/starch/PCL blends. *European Polymer Journal*, 38**,** 1713-1720.
MATZINOS, P., TSERKI, V., KONTOYIANNIS, A. & PANAYIOTOU, C. 2002b. Processing and characterization of starch/polycaprolactone products. *Polymer Degradation and Stability*, 77**,** 17-24.
MCCLORY, C., MCNALLY, T., BAXENDALE, M., P TSCHKE, P., BLAU, W. & RUETHER, M. 2010. Electrical and rheological percolation of PMMA/MWCNT nanocomposites as a function of CNT geometry and functionality. *European Polymer Journal*, 46**,** 854-868.
MCCLORY, C., MCNALLY, T. & P TSCHKE, P. 2011. Influence of screw speed on electrical and rheological percolation of melt-mixed high-impact polystyrene/MWCNT nanocomposites. *Macromolecular Materials and Engineering*, 296**,** 59-69.
MCNALLY, T., P TSCHKE, P., HALLEY, P., MURPHY, M., MARTIN, D., BELL, S. E. J., BRENNAN, G. P., BEIN, D., LEMOINE, P. & QUINN, J. P. 2005. Polyethylene multiwalled carbon nanotube composites. *Polymer*, 46**,** 8222-8232.
MENDELOVICI, E., FROST, R. L. & KLOPROGGE, T. 2000. Cryogenic Raman spectroscopy of glycerol. *Journal of Raman Spectroscopy*, 31**,** 1121-1126.
MIKITAEV, A. K. & KOZLOV, G. V. 2015. Description of the degree of reinforcement of polymer/carbon nanotube nanocomposites in the framework of percolation models. *Physics of the Solid State*, 57**,** 974-977.
MITCHELL, C. A., BAHR, J. L., AREPALLI, S., TOUR, J. M. & KRISHNAMOORTI, R. 2002. Dispersion of Functionalized Carbon Nanotubes in Polystyrene. *Macromolecules*, 35**,** 8825-8830.
MITRUS, M. 2005. Glass transition temperature of thermoplastic starches. *International Agrophysics*, 19**,** 237-241.

MIZUNO, A., MITSUIKI, M. & MOTOKI, M. 1998. Effect of Crystallinity on the Glass Transition Temperature of Starch. *Journal of Agricultural and Food Chemistry,* 46**,** 98-103.
MOATES, G. K., NOEL, T. R., PARKER, R. & RING, S. G. 2001. Dynamic mechanical and dielectric characterisation of amylose–glycerol films. *Carbohydrate Polymers,* 44**,** 247-253.
MONDRAGON, M., HERNANDEZ, E. M., RIVERA-ARMENTA, J. L. & RODRIGUEZ-GONZALEZ, F. J. 2009. Injection molded thermoplastic starch/natural rubber/clay nanocomposites: Morphology and mechanical properties. *Carbohydrate Polymers,* 77**,** 80-86.
NEMANICH, R. J. & SOLIN, S. A. 1979. First- and second- order Raman scattering from finite-size crystals of graphite. *Physical Review B,* 20**,** 392-401.
NING, W., XINGXIANG, Z., HAIHUI, L. & BENQIAO, H. 2009. 1-Allyl-3-methylimidazolium chloride plasticized-corn starch as solid biopolymer electrolytes. *Carbohydrate Polymers,* 76**,** 482-484.
P REZ, S., BALDWIN, P. M. & GALLANT, D. J. 2009. Structural Features of Starch Granules I-Chapter 5. Elsevier Inc.
PETTY, M. C. 2007. *Electrical Conductivity,* Chichester, UK, Chichester, UK: John Wiley & Sons, Ltd.
PONGVIRATCHAI, P. & PARK, J. W. 2007. Electrical conductivity and physical properties of surimi-potato starch under ohmic heating. *Journal of food science,* 72**,** E503.
POUCHERT, C. J. 1981. *The Aldrich library of infrared spectra / Charles J. Pouchert,* Milwaukee, Wis., Milwaukee, Wis. : Aldrich Chemical Co.
PUSHPADASS, H. A., MARX, D. B. & HANNA, M. A. 2008. Effects of Extrusion Temperature and Plasticizers on the Physical and Functional Properties of Starch Films. *Starch - Stärke,* 60**,** 527-538.
RAHMAN, M. & BRAZEL, C. S. 2006. Ionic liquids: New generation stable plasticizers for poly(vinyl chloride). *Polymer Degradation and Stability,* 91**,** 3371-3382.
RAHMAT, M. & HUBERT, P. 2011. Carbon nanotube–polymer interactions in nanocomposites: A review. *Composites Science and Technology,* 72**,** 72-84.
RAMKUMAR, D. & BHATTACHARYA, M. 1997. Effect of crystallinity on the mechanical properties of starch/synthetic polymer blends. *Journal of Materials Science,* 32**,** 2565-2572.
RAMKUMAR, D., VAIDYA, U. R., BHATTACHARYA, M., HAKKARAINEN, M., ALBERTSSON, A. C. & KARLSSON, S. 1996. Properties of injection moulded starch synthetic polymer blends .1. Effect of processing parameters on physical properties. *European Polymer Journal,* 32**,** 999-1010.
RAMKUMAR, D. H. S., BHATTACHARYA, M. & VAIDYA, U. R. 1997. Properties of injection moulded starch/synthetic polymer blends .2. Evaluation of mechanical properties. *European Polymer Journal,* 33**,** 729-742.
RATNAYAKE, W. S. & JACKSON, D. S. 2008. Chapter 5 Starch Gelatinization. *In:* STEVE, L. T. (ed.) *Advances in Food and Nutrition Research.* Academic Press.
RATNAYAKE, W. S. & JACKSON, D. S. 2009. Starch gelatinization. *Advances in food and nutrition research,* 55**,** 221.
REN, J., ZHANG, W., LOU, F., WANG, Y. & GUO, W. 2017. Characteristics of starch‐based films produced using glycerol and 1‐butyl‐3‐methylimidazolium chloride as combined plasticizers. *Starch ‐ Stärke,* 69**,** n/a-n/a.
RODRIGUEZ-GONZALEZ, F. J., RAMSAY, B. A. & FAVIS, B. D. 2004. Rheological and thermal properties of thermoplastic starch with high glycerol content. *Carbohydrate Polymers,* 58**,** 139-147.

SABETZADEH, M., BAGHERI, R. & MASOOMI, M. 2012. Effect of corn starch content in thermoplastic starch/low - density polyethylene blends on their mechanical and flow properties. *Journal of Applied Polymer Science*, 126**,** E63-E69.
SADEGH-HASSANI, F. & MOHAMMADI NAFCHI, A. 2014. Preparation and characterization of bionanocomposite films based on potato starch/halloysite nanoclay. *International Journal of Biological Macromolecules,* 67**,** 458-462.
SANKRI, A., ARHALIASS, A., DEZ, I., GAUMONT, A. C., GROHENS, Y., LOURDIN, D., PILLIN, I., ROLLAND-SABATE, A. & LEROY, E. 2010b. Thermoplastic starch plasticized by an ionic liquid. *Carbohydrate Polymers,* 82**,** 256-263.
SCOTT, M. P., RAHMAN, M. & BRAZEL, C. S. 2003. Application of ionic liquids as low-volatility plasticizers for PMMA. *European Polymer Journal,* 39**,** 1947-1953.
SHAMSUDIN, I. J., AHMAD, A., HASSAN, N. H. & KADDAMI, H. 2015. Bifunctional ionic liquid in conductive biopolymer based on chitosan for electrochemical devices application. *Solid State Ionics*, 278**,** 11-19.
SHARMA, S., SINGH, N. & SINGH, B. 2015. Effect of extrusion on morphology, structural, functional properties and in vitro digestibility of corn, field pea and kidney bean starches. *Die Stärke*, 67**,** 721-728.
SHOGREN, R. L. & JASBERG, B. K. 1994. Aging properties of extruded high-amylose starch. *Journal of Environmental Polymer Degradation,* 2**,** 99-109.
SHOGREN, R. L., LAWTON, J. W., DOANE, W. M. & TIEFENBACHER, K. F. 1998. Structure and morphology of baked starch foams. *Polymer,* 39**,** 6649-6655.
SIMONS, W. W. 1978. *The Sadtler handbook of infrared spectra / editor, William W. Simons*, Philadelphia, Philadelphia : Sadtler Research Laboratories.
SINNOTT, S. B. & ANDREWS, R. 2001. Carbon nanotubes: Synthesis, properties, and applications. *Critical Reviews in Solid State and Materials Sciences*, 26**,** 145-249.
SOUZA, R. C. R. & ANDRADE, C. T. 2002. Investigation of the gelatinization and extrusion processes of corn starch. *Advances in Polymer Technology,* 21**,** 17-24.
STEPTO, R. F. T. 2003. The processing of starch as a thermoplastic. *Macromolecular Symposia,* 201**,** 203-212.
STEVENSON, D. G., BISWAS, A., JANE, J.-L. & INGLETT, G. E. 2007. Changes in structure and properties of starch of four botanical sources dispersed in the ionic liquid, 1-butyl-3-methylimidazolium chloride. *Carbohydrate Polymers*, 67**,** 21-31.
SUMIO, I. 1991. Helical microtubules of graphitic carbon. *Nature,* 354**,** 56.
SUZUKI, T., KONO, K., SHIMOMURA, K. & MINAMI, H. 2014. Preparation of cellulose particles using an ionic liquid. *Journal of Colloid and Interface Science*, 418**,** 126-131.
SWATLOSKI, R. P., SPEAR, S. K., HOLBREY, J. D. & ROGERS, R. D. 2002. Dissolution of Cellose with Ionic Liquids. *Journal of the American Chemical Society,* 124**,** 4974-4975.
TAGHIZADEH, A. & FAVIS, B. D. 2013. Carbon nanotubes in blends of polycaprolactone/thermoplastic starch. *Carbohydrate Polymers*, 98**,** 189-198.
TAN, I., FLANAGAN, B. M., HALLEY, P. J., WHITTAKER, A. K. & GIDLEY, M. J. 2007. A method for estimating the nature and relative proportions of amorphous, single, and double-helical components in starch granules by (13)C CP/MAS NMR. *Biomacromolecules,* 8**,** 885-891.
TERRONES, M. 2003. Science and technology of the twenty-first century: Synthesis, properties and applications of carbon nanotubes. *Annual Review of Materials Research,* 33**,** 419-501.
TESTER, R. F., KARKALAS, J. & QI, X. 2004. Starch—composition, fine structure and architecture. Elsevier Ltd.

THUNWALL, M., BOLDIZAR, A. & RIGDAHL, M. 2006. Compression Molding and Tensile Properties of Thermoplastic Potato Starch Materials. *Biomacromolecules,* 7**,** 981-986.
THUWALL, M., BOLDIZAR, A. & RIGDAHL, M. 2006. Extrusion processing of high amylose potato starch materials. *Carbohydrate Polymers,* 65**,** 441-446.
TIEFENBACHER, K. F. 1993. Starch-Based Foamed Materials—Use and Degradation Properties. *Journal of Macromolecular Science, Part A,* 30**,** 727-731.
VAN SOEST, J. J. G., HULLEMAN, S. H. D., DE WIT, D. & VLIEGENTHART, J. F. G. 1996a. Changes in the mechanical properties of thermoplastic potato starch in relation with changes in B-type crystallinity. *Carbohydrate Polymers,* 29**,** 225-232.
VAN SOEST, J. J. G., HULLEMAN, S. H. D., DE WIT, D. & VLIEGENTHART, J. F. G. 1996b. Crystallinity in starch bioplastics. *Industrial Crops and Products,* 5**,** 11-22.
VANSOEST, J., TOURNOIS, H., DEWIT, D. & VLIEGENTHART, J. 1995. Short-range structure in (partially) crystalline potato starch determined with attenuated total reflectance Fourier-transform IR spectroscopy. *Carbohydr. Res.,* 279**,** 201-214.
VILGIS, T. A., HEINRICH, G. & KLÜPPEL, M. 2009. *Reinforcement of Polymer Nano-Composites Theory, Experiments and Applications,* Cambridge, Cambridge : Cambridge University Press.
VOSKRESENSKII, V. A., ORLOVA, E. M., ABRAMOVA, E. I. & PROKHOROVA, N. S. 1971. Plasticisation of Polymers. *Russian Chemical Reviews,* 40**,** 78.
WANG, J., YU, L., XIE, F., CHEN, L., LI, X. & LIU, H. 2010. Rheological properties and phase transition of cornstarches with different amylose/amylopectin ratios under shear stress. *Starch - Stärke,* 62**,** 667-675.
WANG, N., YU, J., CHANG, P. R. & MA, X. 2008. Influence of formamide and water on the properties of thermoplastic starch/poly(lactic acid) blends. *Carbohydrate Polymers,* 71**,** 109-118.
WANG, S. & HOU, L. X. 2011. Application of Four Ionic Liquids as Plasticizers for PVC Paste Resin. *Iran. Polym. J.,* 20**,** 989-997.
WANG, X., LI, H., CAO, Y. & TANG, Q. 2011. Cellulose extraction from wood chip in an ionic liquid 1-allyl-3-methylimidazolium chloride (AmimCl). *Bioresource Technology,* 102**,** 7959-7965.
WERNER, S., HAUMANN, M. & WASSERSCHEID, P. 2010. Ionic Liquids in Chemical Engineering. *Annual Review of Chemical and Biomolecular Engineering,* 1**,** 203-230.
WILLETT, J. L., MILLARD, M. M. & JASBERG, B. K. 1997. Extrusion of waxy maize starch: melt rheology and molecular weight degradation of amylopectin. *Polymer,* 38**,** 5983-5989.
WILPISZEWSKA, K. & SPYCHAJ, T. 2011. Ionic liquids: Media for starch dissolution, plasticization and modification. *Carbohydrate Polymers,* 86**,** 424-428.
WU, J., BAI, J., XUE, Z., LIAO, Y., ZHOU, X. & XIE, X. 2015. Insight into glass transition of cellulose based on direct thermal processing after plasticization by ionic liquid. *Cellulose,* 22**,** 89-99.
WU, Q. X. & ZHANG, L. N. 2001. Structure and properties of casting films blended with starch and waterborne polyurethane. *Journal of Applied Polymer Science,* 79**,** 2006-2013.
XIE, F., FLANAGAN, B. M., LI, M., SANGWAN, P., TRUSS, R. W., HALLEY, P. J., STROUNINA, E. V., WHITTAKER, A. K., GIDLEY, M. J., DEAN, K. M., SHAMSHINA, J. L., ROGERS, R. D. & MCNALLY, T. 2014. Characteristics of starch-based films plasticised by glycerol and by the ionic liquid 1-ethyl-3-methylimidazolium acetate: A comparative study. *Carbohydrate Polymers,* 111**,** 841-848.

XIE, F., FLANAGAN, B. M., LI, M., TRUSS, R. W., HALLEY, P. J., GIDLEY, M. J., MCNALLY, T., SHAMSHINA, J. L. & ROGERS, R. D. 2015. Characteristics of starch-based films with different amylose contents plasticised by 1-ethyl-3-methylimidazolium acetate. *Carbohydrate Polymers,* 122**,** 160-168.

XIE, F., POLLET, E., HALLEY, P. J. & AV ROUS, L. 2013. Starch-based nano-biocomposites. *Progress in Polymer Science,* 38**,** 1590-1628.

XIE, F., YU, L., CHEN, L. & LI, L. 2008. A new study of starch gelatinization under shear stress using dynamic mechanical analysis. *Carbohydrate Polymers,* 72**,** 229-234.

XUAN, X., GUO, M., PEI, Y. & ZHENG, Y. 2011. Theoretical study on cation–anion interaction and vibrational spectra of 1-allyl-3-methylimidazolium-based ionic liquids. *Spectrochimica Acta Part A: Molecular and Biomolecular Spectroscopy,* 78**,** 1492-1499.

XUE, T., YU, L., XIE, F., CHEN, L. & LI, L. 2008. Rheological properties and phase transition of starch under shear stress. *Food Hydrocolloids,* 22**,** 973-978.

YANG, B. X., PRAMODA, K. P., XU, G. Q. & GOH, S. H. 2007. Mechanical Reinforcement of Polyethylene Using Polyethylene-Grafted Multiwalled Carbon Nanotubes. *Advanced Functional Materials,* 17**,** 2062-2069.

YANG, J.-H., YU, J.-G. & MA, X.-F. 2006a. Preparation and properties of ethylenebisformamide plasticized potato starch (EPTPS). *Carbohydrate Polymers,* 63**,** 218-223.

YANG, J.-H., YU, J.-G. & MA, X.-F. 2006b. Study on the properties of ethylenebisformamide and sorbitol plasticized corn starch (ESPTPS). *Carbohydrate Polymers,* 66**,** 110-116.

YANG, Q. & DIONYSIOU, D. D. 2004. Photolytic degradation of chlorinated phenols in room temperature ionic liquids. *Journal of Photochemistry and Photobiology A: Chemistry,* 165**,** 229-240.

YOUNG, R. J. & LOVELL, P. A. 2011. *Introduction to polymers / Robert J. Young and Peter A. Lovell,* Boca Raton, Boca Raton : CRC Press.

YU, L., KEALY, T. & CHEN, P. 2006. Study of Starch Gelatinization in a Flow Field Using Simultaneous Rheometric Data Collection and Microscopic Observation. *International Polymer Processing,* 21**,** 283-289.

YURDAKUL, H., DURUKAN, O., SEYHAN, A. T., CELEBI, H., OKSUZOGLU, M. & TURAN, S. 2013. Microstructural characterization of corn starch‐based porous thermoplastic composites filled with multiwalled carbon nanotubes. *Journal of Applied Polymer Science,* 127**,** 812-820.

ZHANG, B., CHEN, L., XIE, F., LI, X., TRUSS, R. W., HALLEY, P. J., SHAMSHINA, J. L., ROGERS, R. D. & MCNALLY, T. 2015. Understanding the structural disorganization of starch in water-ionic liquid solutions. *Physical Chemistry Chemical Physics,* 17**,** 13860-13871.

ZHANG, B., XIE, F., ZHANG, T., CHEN, L., LI, X., TRUSS, R. W., HALLEY, P. J., SHAMSHINA, J. L., MCNALLY, T. & ROGERS, R. D. 2016. Different characteristic effects of ageing on starch-based films plasticised by 1-ethyl-3-methylimidazolium acetate and by glycerol. *Carbohydrate Polymers,* 146**,** 67-79.

ZHANG, H., WU, J., ZHANG, J. & HE, J. 2005. 1-Allyl-3-methylimidazolium Chloride Room Temperature Ionic Liquid: A New and Powerful Nonderivatizing Solvent for Cellulose. *Macromolecules,* 38**,** 8272-8277.

ZHANG, W. D., SHEN, L., PHANG, I. Y. & LIU, T. 2003. Carbon Nanotubes Reinforced Nylon-6 Composite Prepared by Simple Melt-Compounding. *Macromolecules,* 37**,** 256-259.

ZHANG, Y. & HAN, J. H. 2006a. Mechanical and Thermal Characteristics of Pea Starch Films Plasticized with Monosaccharides and Polyols. *Journal of Food Science,* 71**,** E109-E118.

ZHANG, Y. & HAN, J. H. 2006b. Plasticization of Pea Starch Films with Monosaccharides and Polyols. *Journal of Food Science*, 71**,** E253-E261.
ZHANG, Y., REMPEL, C. & LIU, Q. 2014. Thermoplastic Starch Processing and Characteristics-A Review. *Critical Reviews in Food Science and Nutrition*, 54**,** 1353-1370.
ZHAO, D., PALAPARTHI, A. D., HUANG, Q., FU, X., LIU, H. & YU, L. 2015. Effects of ionic liquid 1-allyl-3-methylimidazolium chloride treatment on the microstructure and phase transition of cornstarch. *Industrial Crops & Products*, 77**,** 139-145.
ZHAO, L., LI, Y., CAO, X., YOU, J. & DONG, W. 2012. Multifunctional role of an ionic liquid in melt-blended poly(methyl methacrylate)/multi-walled carbon nanotube nanocomposites. *Nanotechnology*, 23**,** 255702.
ZHOU, J., SONG, J. & PARKER, R. 2006. Structure and properties of starch-based foams prepared by microwave heating from extruded pellets. *Carbohydrate Polymers*, 63**,** 466-475.

10 APPENDICES

10.1 Appendix A (Preliminary Experiments)

10.1.1 Introduction

There are various types of starches existing in the market, and with a wide diversity of properties. Varying the amylose and amylopectin content affects the properties of starches a great deal and, in general, better mechanical performance often comes with higher amylose content in starch. However, advanced mechanical properties mean to increase the processing difficulties at the same time. It is thus desirable to study a higher performance starch as possible and so initial experiments were conducted to find out a set of parameters to process a type of high performance starch.

Before RMS was chosen as the focus for this thesis, G50 was initially investigated because it has an amylose content of 50% which is a middle value and can be a good reference for further experiments. An attempt to process samples of G50 was made with 15mins at temperatures from 100°C to 180°C, and rotor speeds of 30rpm or 50rpm. However, none of the results was able to show that G50 could be stably processed under such conditions. Due to technical issues with the equipment, neither digital nor printed data was able to be obtained from these experiments.

Therefore, G50 was considered too difficult to obtain good results and a lower amylose content starch, RMS, was instead selected. This appendix describes from preliminary experiments performed, which guided the development of the methodology described in chapter 3.

10.1.2 Experimental

10.1.3 Material

The starches studied in this chapter were RMS and G50. The plasticiser was glycerol.

10.1.4 Experimental Methods

To investigate suitable processing parameter for RMS, preliminary experiments were carried out according to the table 10-1.

Table 10-1 Experimental formulation

Code	Starch type	Starch amount	Water	Glycerol	Set Temperature [°C]	Rotor speed [rpm]
RMS30-T90-R30	RMS	100	15	15	90	30
RMS30-T90-R50	RMS	100	15	15	90	50
RMS30-T100-R30	RMS	100	15	15	100	30
RMS30-T100-R50	RMS	100	15	15	100	50
RMS30-T110-R30	RMS	100	15	15	110	30

10.1.5 Results and Discussion

Torque-time curves are shown as following figures. Note that the places showed on the figures as 'A', 'X1', 'X2' etc are machine automatic check points hence not relevant to the discussion. The upper line represents the temperature while the lower line represents the torque value.

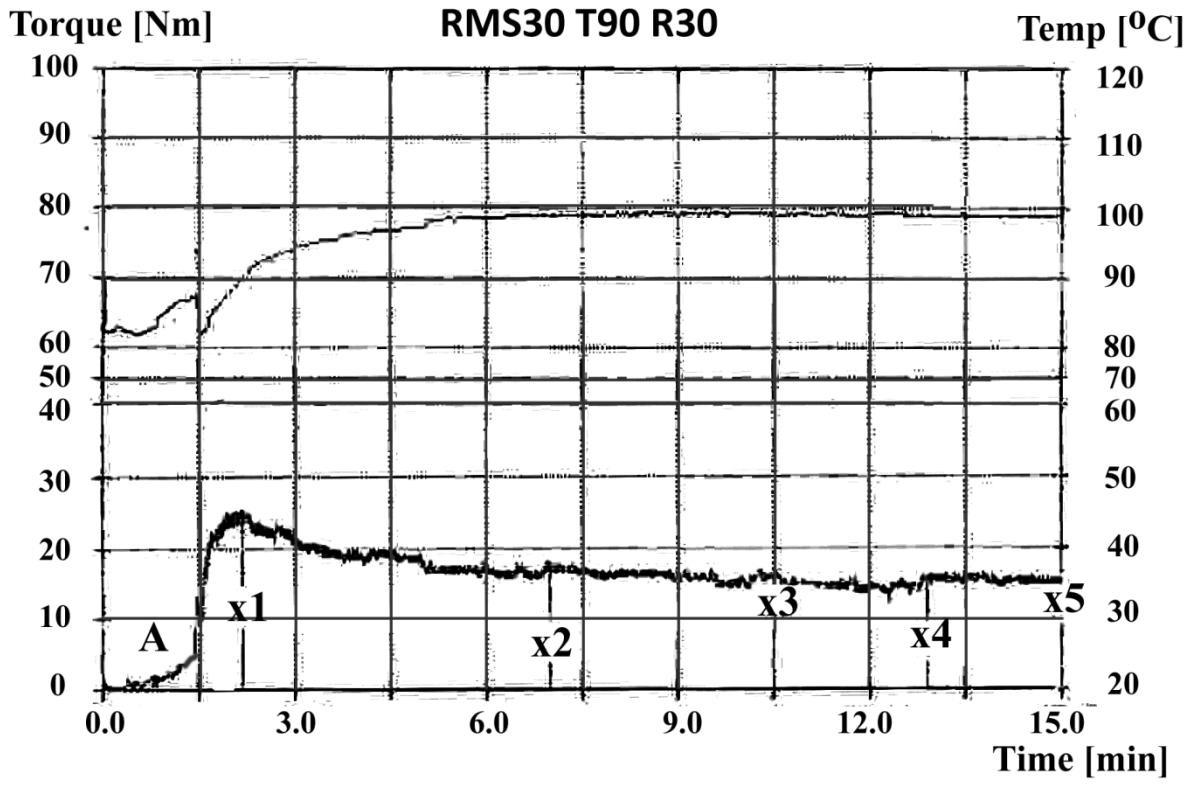

Figure 10-1 Processing torque over time of RMS30-T90-R30

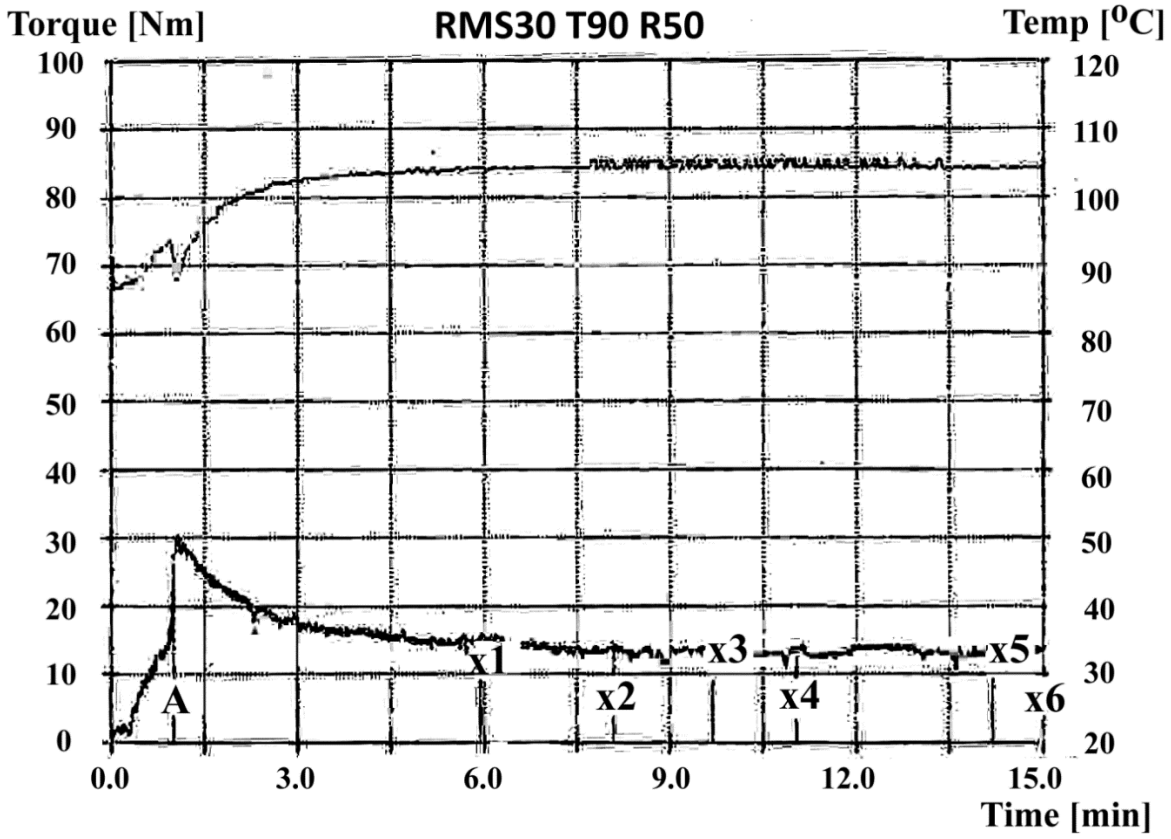

Figure 10-2 Processing torque over time of RMS30-T90-R50

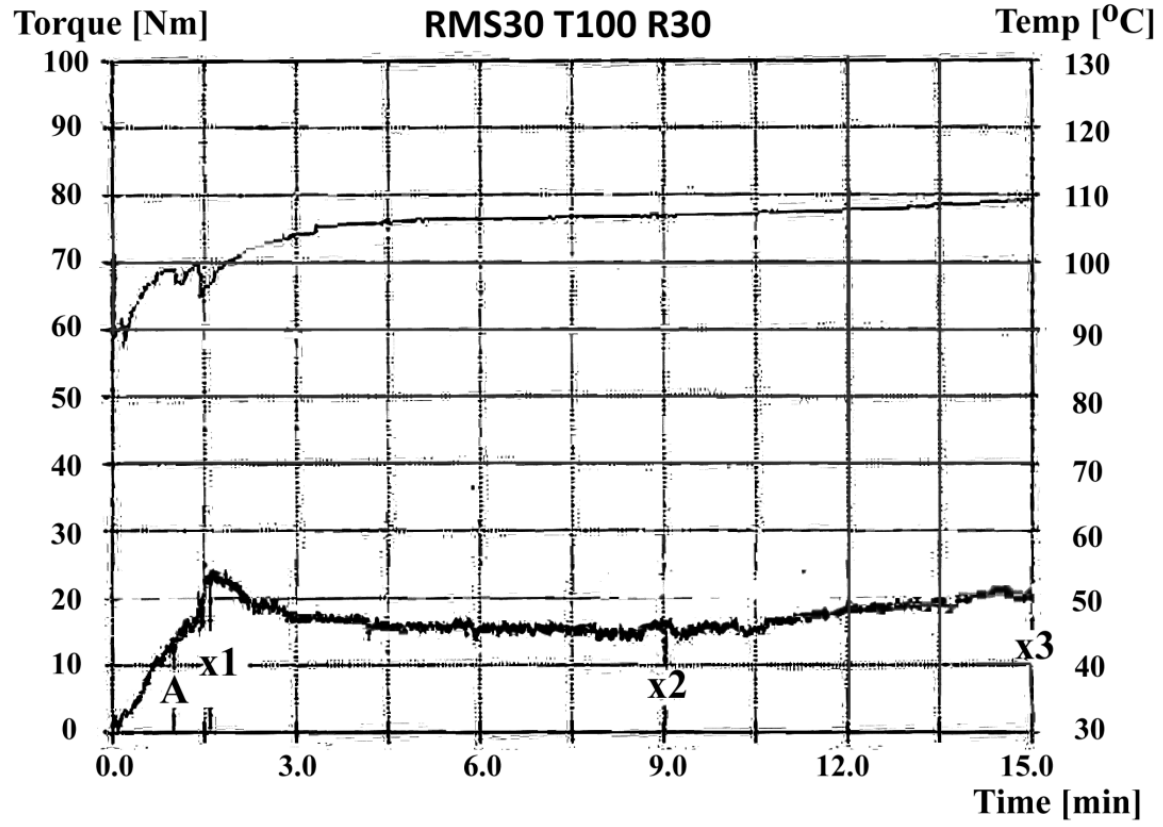

Figure 10-3 Processing torque over time of RMS30-T100-R30

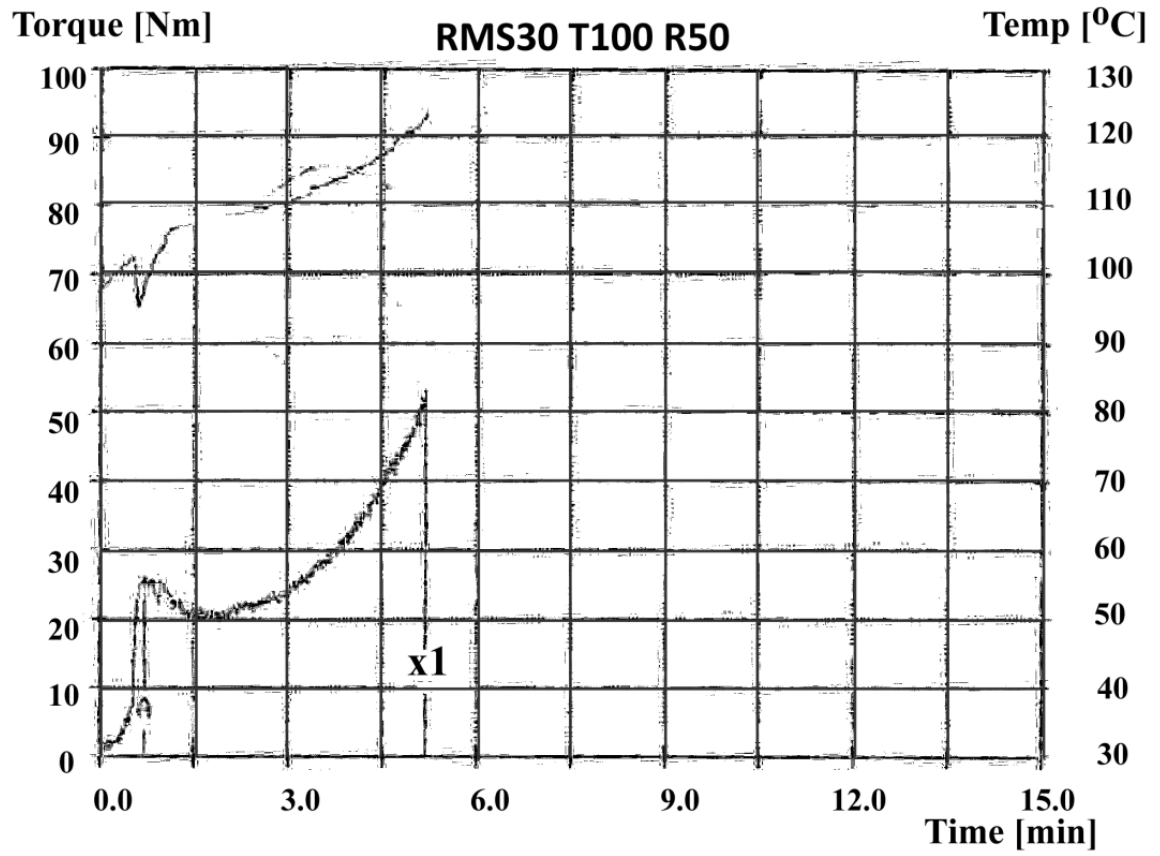

Figure 10-4 Processing torque over time of RMS30-T100-R50

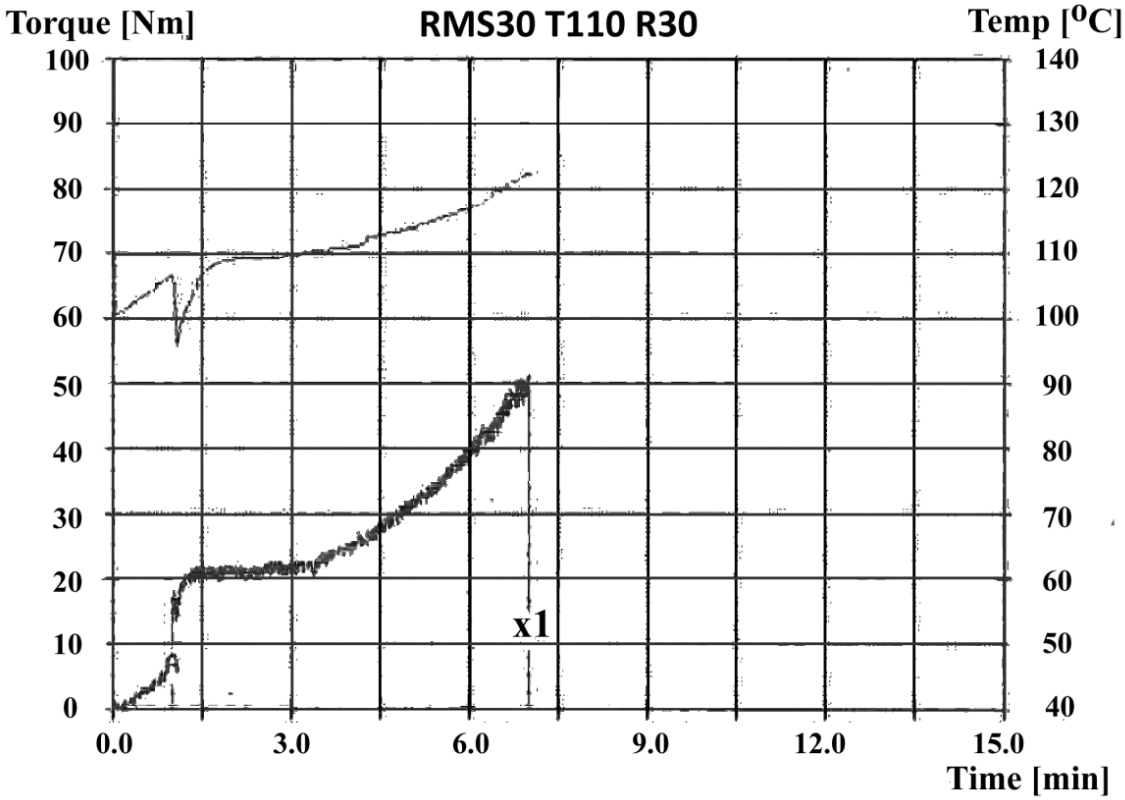

Figure 10-5 Processing torque over time of RMS30-T110-R30

The thermal processing of TPS in the mixer was stable with the set temperature of 90°C. The situation with set temperature 100°C and rotor speed 30rpm was also stable (table 10-2). The torque-time diagram showed no difference in those samples.

For RMS30-T90-R50, the chamber temperature had a sudden drop when the material was fed in. Then, as the mixing proceeded, the temperature gradually rose up to equilibrium at approximately 100°C. The torque value was low initially, then a sudden increase appeared at a temperature of around 70°C at 1.5 minutes after mixing had started which showed that gelatinisation happened at that time. After the peak appeared in the gelatinisation process, the torque went downward steadily and equilibrated to approximatly 16 N·m by the end. A similar trend was seen in RMS30-T100-R30, with the temperature and torque ending around, 110°C and 20 N·m compared to 100°C and 16 N·m respectively.

Table 10-2 Processing outcomes of preliminary experiments

Set Temperature (°C)	90	100	110
Rotor speed 30rpm	Stable	Stable	Unstable
Rotor speed 50rpm	Stable	Unstable	

However, it was observed that the samples recovered from the mixer became increasingly stiff and more transparent when the temperature was higher. Samples processed at lower temperatures tended to be softer and stickier. Higher rotor speed made no difference except to increase the measured temperature in the chamber. Because of the effect of shear stress while kneading in the mixer, when the actual temperature in the chamber was higher than 110°C, the processing ultimately became unstable. The mixing machine had to be stopped before overloading. Therefore, it could be concluded that around actual processing temperature in the chamber of 110°C and rotor speed of 30rpm, the outcome was the most ideal one.

10.1.6 Conclusion

The preliminary work shows that compared to G50 which has 56.3% amylose content, RMS, a starch with 24.4% amylose content, is more accessible to thermal processing by a mixer. It was therefore decided to focus on RMS alone in the remainder of this thesis.

Results displayed in this appendix have showed the critical condition of RMS processing is at a temperature of 110°C and with a rotor speed of 30rpm. Any processing temperature above this point will finally result in unstable outcomes. Compared to a rotor speed of 30rpm, the effect of having a rotor speed of 50rpm only increased the actual processing temperature. Therefore, in order to achieve good mixing outcomes, starch processing temperature should be kept between the gelatinisation temperature and 110°C with a rotor speed of 30rpm. The results obtained in this preliminary experiment were a very significant reference for sample preparation for the further studies.

10.2 Appendix B (Effects of Glycerol/[Emim][OAc] on RMS processing)

This appendix contain the full results for water uptake measurements for the RMS-G and RMS-E series (section 4.3.2). The experimental methodology was described in section 3.3.2.1.

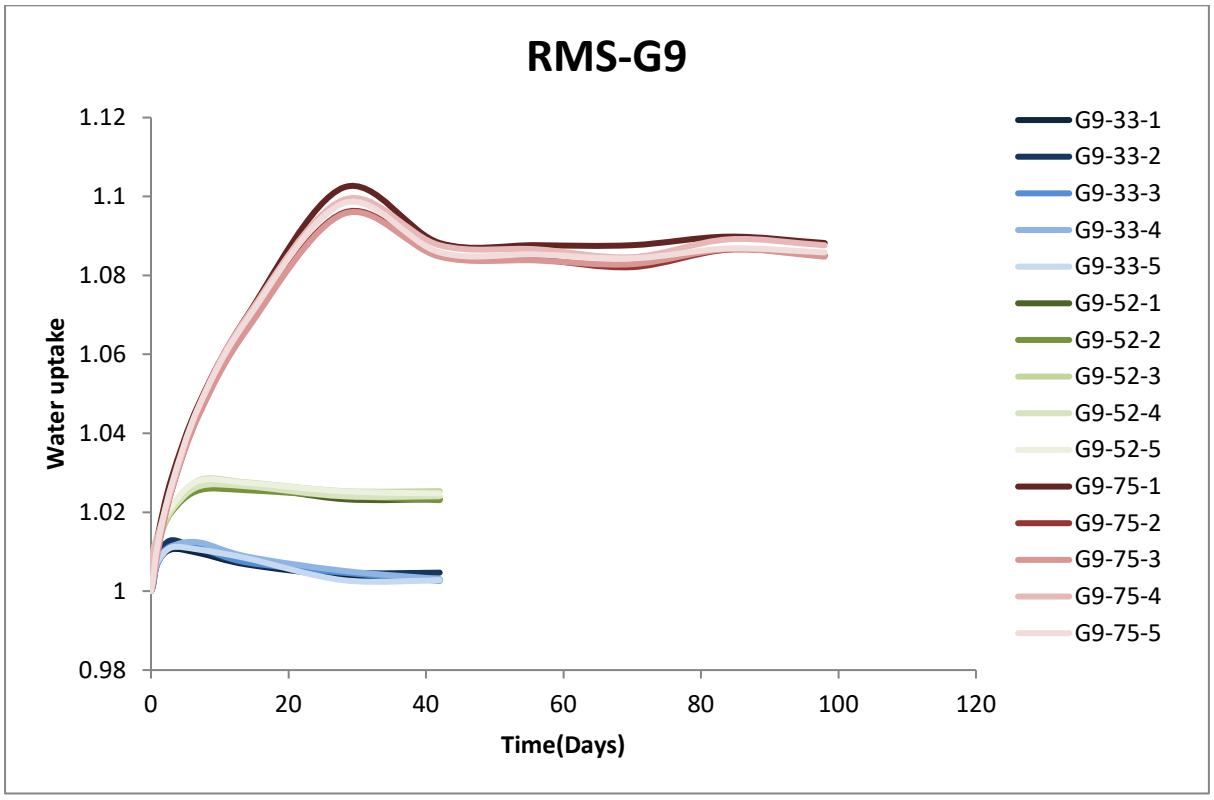

Figure 10-6 Water uptake ratio of RMS-G9 in different relative humidity levels over time

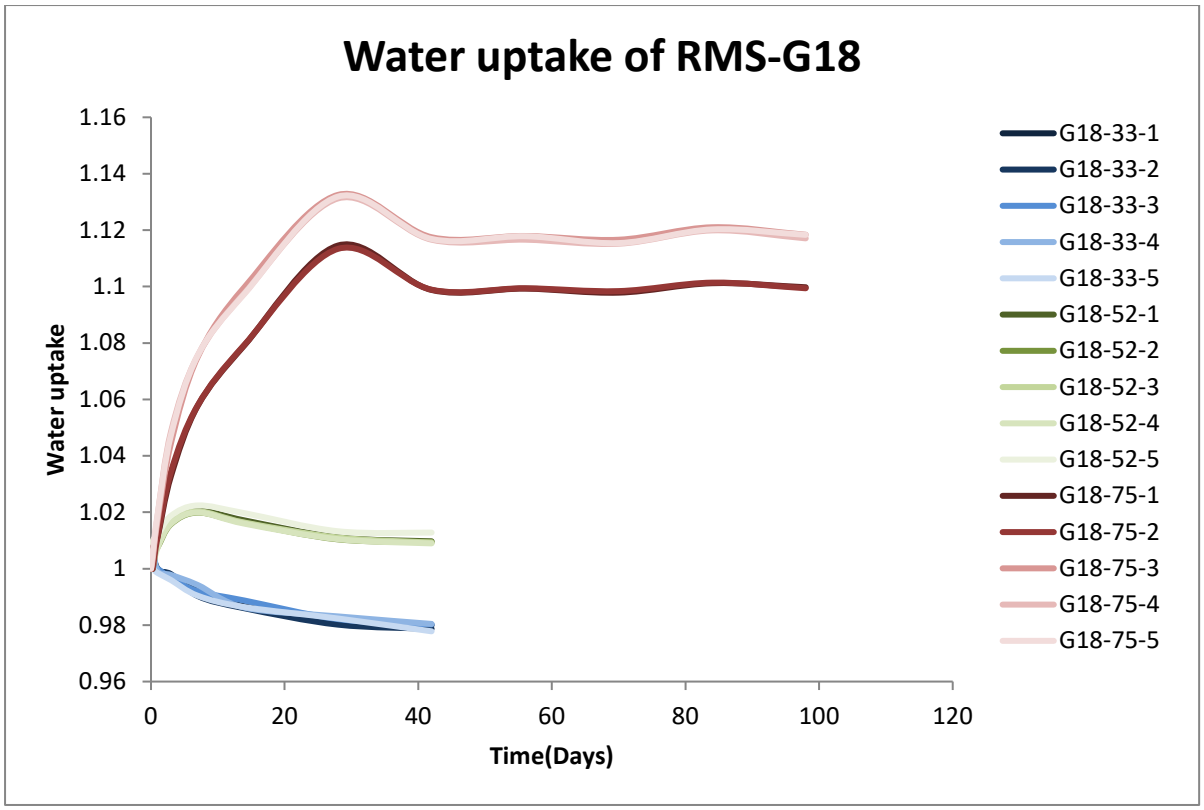

Figure 10-7 Water uptake ratio of RMS-G18 in different relative humidity levels over time

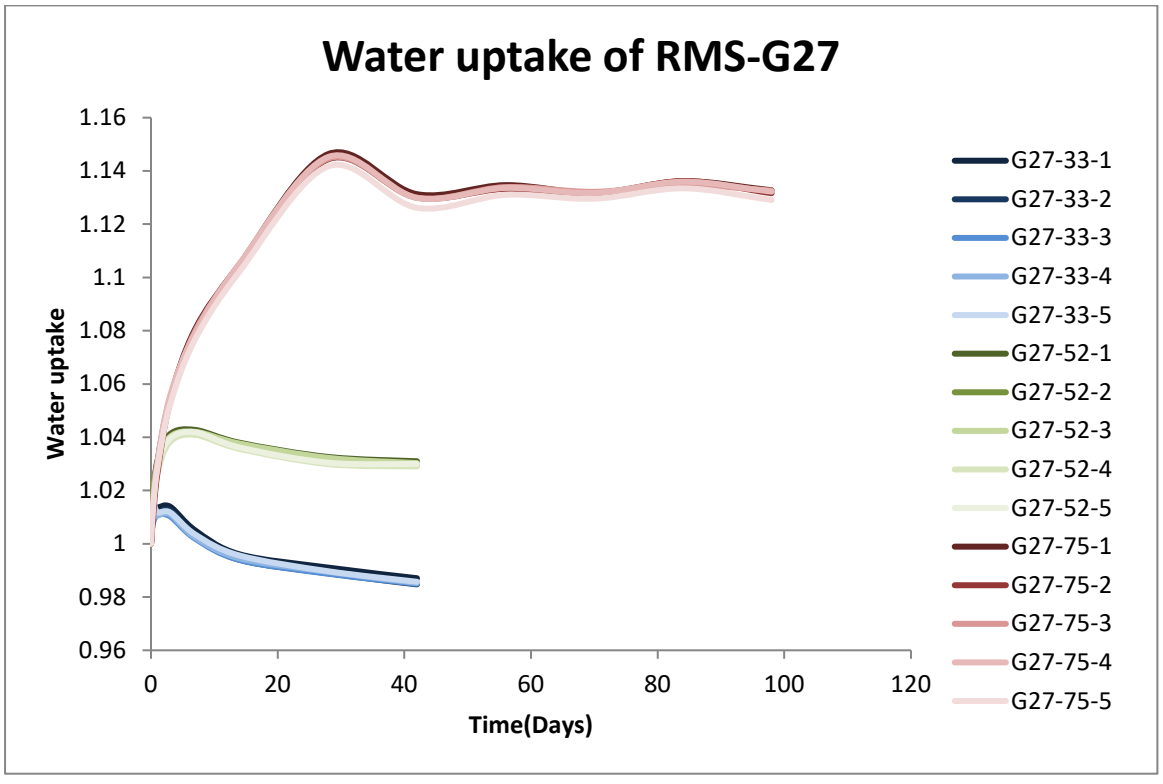

Figure 10-8 Water uptake ratio of RMS-G27 in different relative humidity levels over time

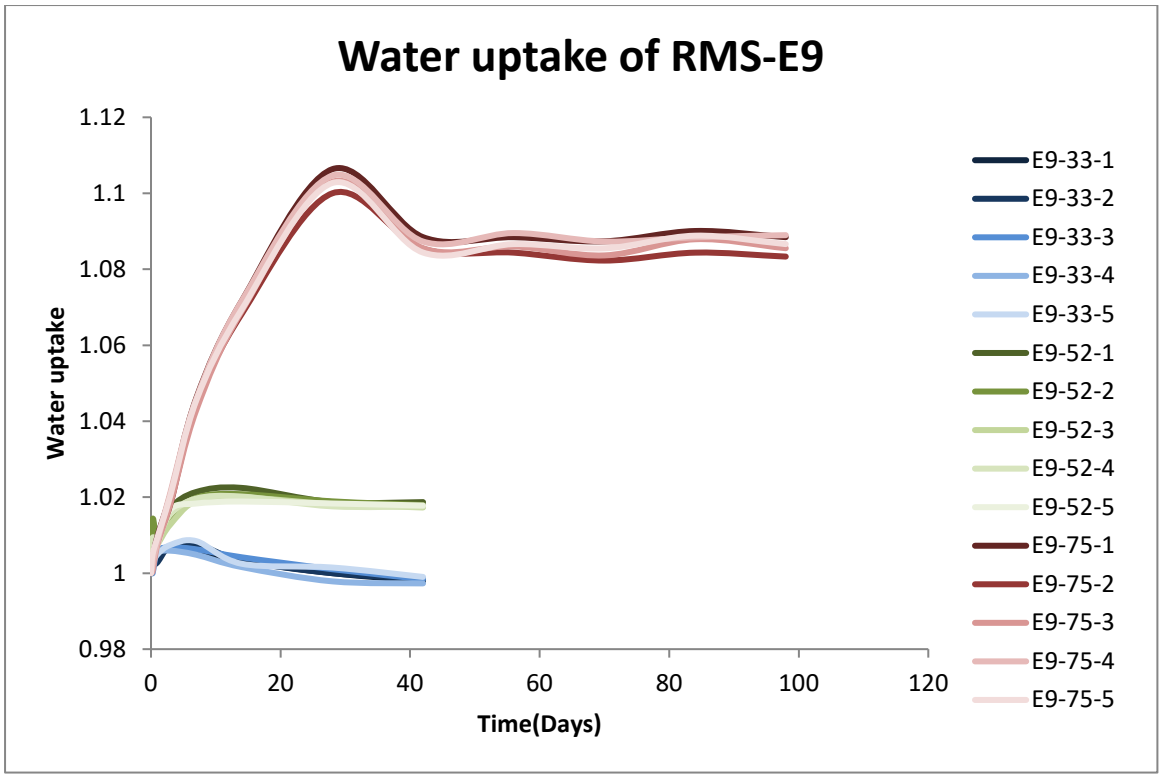

Figure 10-9 Water uptake ratio of RMS-E9 in different relative humidity levels over time

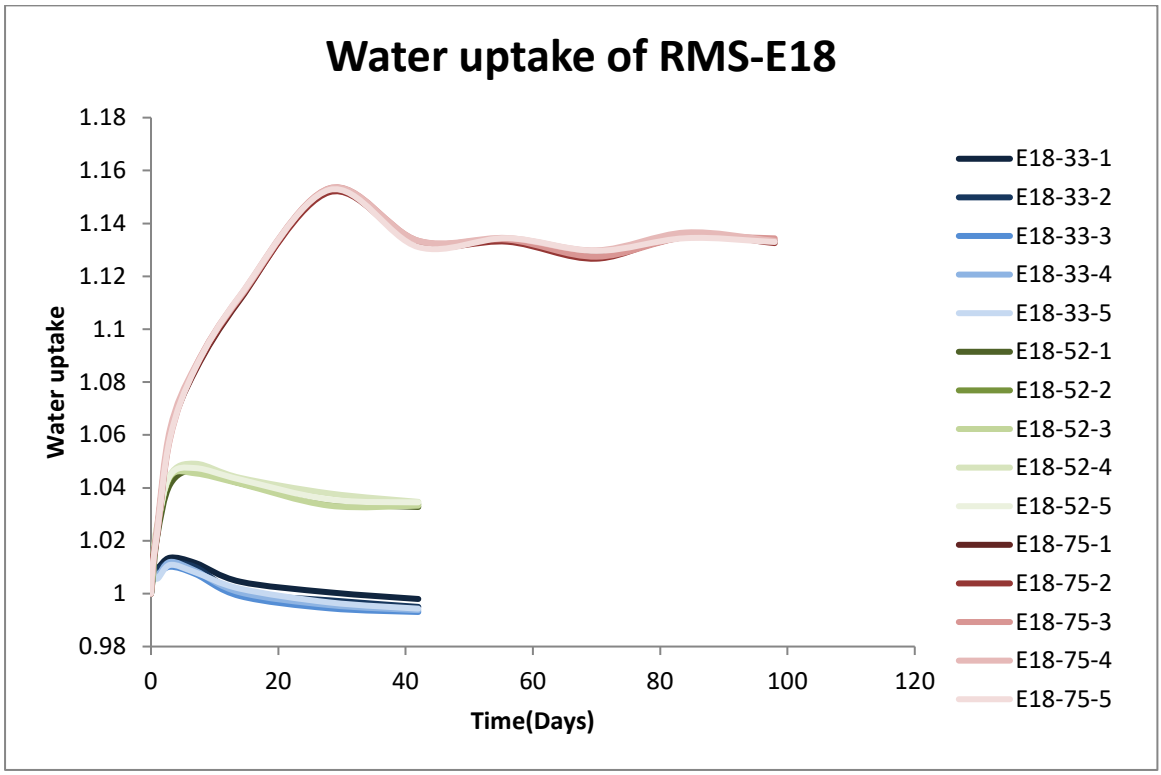

Figure 10-10 Water uptake ratio of RMS-E18 in different relative humidity levels over time

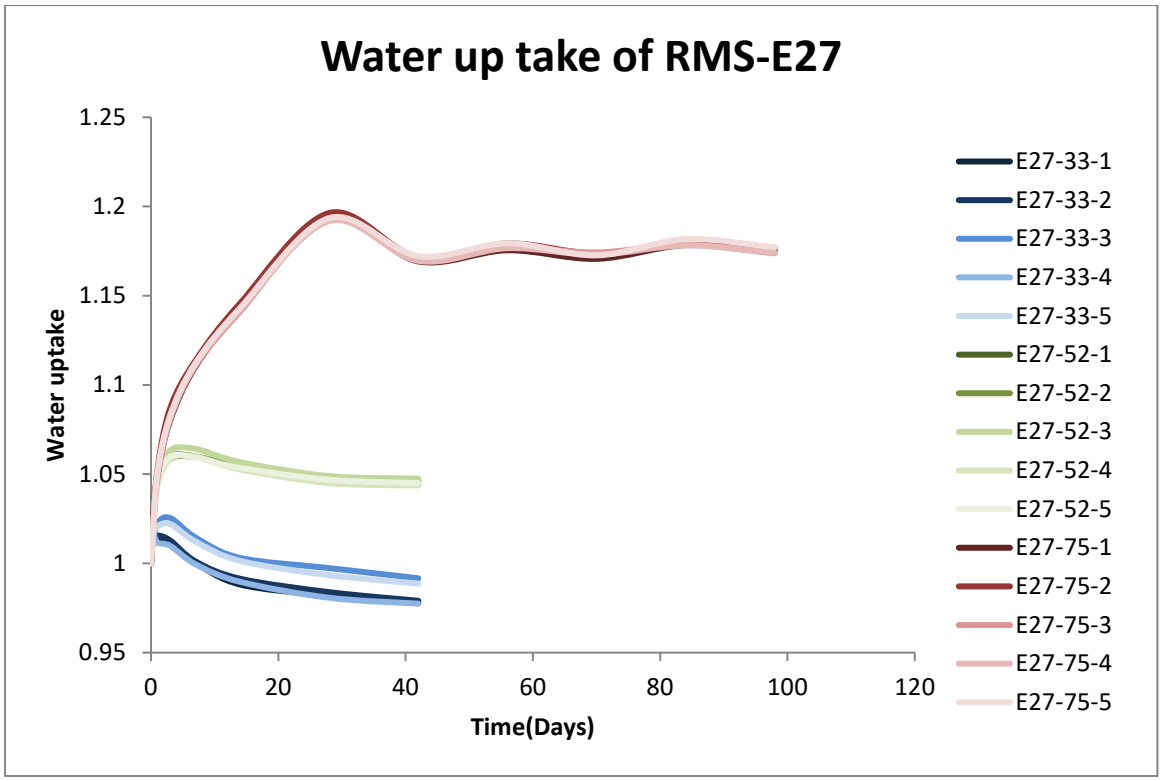

Figure 10-11 Water uptake ratio of RMS-E27 in different relative humidity levels over time